

ATOMIC FLUORESCENCE SPECTROSCOPIC METHODS FOR ULTRATRACE
ELEMENTAL ANALYSIS USING A HIGH-REPETITION RATE TUNABLE DYE
LASER AND FURNACE SAMPLE ATOMIZATION

By

RICARDO Q. AUCÉLIO

A DISSERTATION PRESENTED TO THE GRADUATE SCHOOL
OF THE UNIVERSITY OF FLORIDA IN PARTIAL FULFILLMENT
OF THE REQUIREMENTS FOR THE DEGREE OF
DOCTOR OF PHILOSOPHY

UNIVERSITY OF FLORIDA

1999

ACKNOWLEDGMENTS

I would first like to thank my research advisor, Dr. James D. Winefordner, for accepting me in his group and for all his guidance and support through the past four years. It has been a true learning experience Jim has allowed me to work with freedom and allowed me to interact with postdoctoral researchers from several parts of the world and different cultures and with fellow graduate colleagues. Dr. Benjamin Smith (Ben) was also a fundamental support, providing me important suggestions and background.

Many friendly people participated directly in this work and in other projects in which I had the opportunity to be involved. I am grateful to Dr. Nicolo Omeneto, Dr. Eugene Wagner, Dr. Edison Becerra, Dr. David Powell, Dr. Igor Gornushkin, Dr. Scott Baker, Dr. Brian Castle, Melody Bi, Mark Villoria, Valéria Rubin and Celeste Johnson. I would like to extend these acknowledgments to all other past and present members of the group, specially Dr. Andrea Croslyn, Dr. Leslie King, Dr. Robin Russel, Kris Ingenieri, Mike Shepard, and Gretchen Potts. I also extend thanks Jeanne Karably, Todd Prox, Steve Milles, and the people from the University of Florida Analytical Instrumentation.

I am especially grateful to my family for their support. Andreia Gerk deserves particular and special gratitude. In her I found the love and emotional strength that I needed.

I am immensely thankful to Coordenacao de Aperfeicoamento de Pessoal de Nivel Superior (CAPES, Brasil) for the financial support that allowed me to obtain the degree. Financial support for this work was provided by the United States Department of Energy (DOE) and the Engineering Research Center (ERC) for Particle Science and Technology at the University of Florida.

TABLE OF CONTENTS

	<u>page</u>
ACKNOWLEDGMENTS.....	i
ABSTRACT.....	vii
CHAPTERS	
1 INTRODUCTION.....	1
Need for Ultratrace Analysis.....	1
Laser-excited Atomic Fluorescence.....	2
Intent of Dissertation.....	7
2 LASER-EXCITED FLUORESCENCE SPECTROMETRY.....	10
Introduction.....	10
Fluorescence Excitation-Detection Schemes.....	12
General Fluorescence Flux Equations.....	14
Laser-excited Atomic Fluorescence.....	16
Optical Saturation.....	20
Fluorescence Analytical Curves.....	22
Efficiency of Detection.....	24
Sources of Noise in LEAFS.....	27
Concomitant Scatter.....	27
Stray Light.....	28
Blackbody Emission.....	29
Molecular Fluorescence.....	30
Non-analyte Atomic Fluorescence.....	30
Other Interferences and Noise Sources.....	30
3 SAMPLE ATOMIZATION.....	31
Introduction.....	31
Electrothermal Atomization.....	34
Atomization Mechanisms.....	39

Minimization of Interferences in Electrothermal Atomization.....	41
Optimal Temperature Program.....	42
Stabilized Temperature Platform Furnace.....	42
Chemical Modification.....	44
 4 EXPERIMENTAL.....	 46
Instrumentation.....	46
Excitation Source.....	48
Sample Atomizer.....	55
Detection-signal processing-acquisition System.....	55
Wavelength Tuning.....	58
Cleaning of Glassware.....	58
Procedures.....	58
Analyte Solutions.....	58
Other Solutions.....	59
Samples.....	59
Pre-conditioning of the Graphite.....	61
Microwave Digestion.....	61
Theory.....	62
Instrumentation.....	65
Procedures.....	68
 5 LASER-EXCITED FLUORESCENCE OF Ge, In, AND Pt IN A GRAPHITE FURNACE.....	 72
Brief overview of the importance and current methods to determine ultratrace concentrations of Ge, In and Pt.....	72
Results and Discussion.....	77
Choice of the Laser Repetition Rate.....	77
Optical Saturation Conditions.....	78
Imaging Considerations.....	81
Choice of the Fluorescence Analytical Schemes.....	85
Atomization Techniques and Furnace Parameters.....	86
Limiting Noises.....	100
Influence of Acids and Bases.....	100
Chemical Modification Studies.....	105
Influence of Salts and Potential Interferents.....	112
Analytical Figures of Merit.....	114
Sample Analysis.....	120
Conclusion.....	138

6	FILTER FURNACE LASER-EXCITED ATOMIC FLUORESCENCE SPECTROMETRY FOR THE DETERMINATION OF LEAD IN WHOLE BLOOD.....	140
	Introduction.....	140
	Filter Furnace Atomization.....	142
	Results and Discussion.....	143
	Permeability of the Filter and Fluorescence Time Profile.....	146
	Comparison of Atomization Techniques for Blood Analysis.....	148
	Influence of the Amount of Blood in the Recovery and	
	Reproducibility.....	154
	Conclusion.....	157
7	DETERMINATION OF THULIUM BY LEAFS IN A RHENIUM-LINED TUBE ATOMIZER.....	160
	Ultratrace Determination of Thulium.....	160
	Metallic Atomizers.....	162
	Introduction.....	162
	Atomization Mechanisms.....	164
	Intent of the Chapter.....	165
	Results and Discussion.....	165
	Analytical Scheme and Laser Repetition Rate.....	165
	Atomization and Furnace Parameters: A Comparative Study	
	Between Different Tube Atomizer.....	166
	Sample Analysis.....	185
	Conclusion.....	187
8	FINAL COMMENTS	190
	APPENDIX	193
	LIST OF ACRONYMS.....	193
	REFERENCES.....	195
	BIOGRAPHICAL SKETCH.....	207

Abstract of Dissertation Presented to the Graduate School
of the University of Florida in Partial Fulfillment of the
Requirements for the Degree of Doctor of Philosophy

ATOMIC FLUORESCENCE SPECTROSCOPIC METHODS FOR ULTRATRACE
ELEMENTAL ANALYSIS USING A HIGH REPETITION RATE TUNABLE DYE
LASER AND FURNACE SAMPLE ATOMIZATION

By

Ricardo Q. Aucelio

July 1999

Chairman: James D. Winefordner
Major Department: Chemistry

The goal of this work was to develop ultrasensitive methods based on Electrothermal atomization laser-excited atomic fluorescence (ETA-LEAFS) to determine Ge, In, Pb, Pt and Tm in complex samples such as biological and environmental. The ultimate goal was to achieve high sensitivity and high selectivity with little sample manipulation and simple sample calibration procedures.

For In, Ge, and Pt sensitive determination methods (femtogram limits of detection) using a standard graphite furnace technique were developed. High sensitivity was achieved by the proper choice of experimental parameters and instrumental design. A high repetition rate copper vapor pumped dye laser was employed to probe more efficiently the transient atom population generated in the atomizer. Tube atomizers with front illumination detection scheme was employed to increase the number of fluorescent

atoms detected, improve the dynamic linear range and decrease interferences from the surrounding atmosphere. Experimental parameters were optimized to maximize the signal to noise ratio. Special care concerning imaging and sample atomization conditions was taken to minimize the noise level reaching the detection system. Improvements in the sample atomization efficiency and minimization of interferences were achieved by the choice of the best atomization technique, graphite material, use of matrix modifiers. Efforts are made to improve sensitivity and minimizing interferences by choosing between wall and platform techniques, and optimizing furnace parameters to eliminate sample matrix components.

For Pb, a porous graphite filter was used to develop a filter furnace LEAFS method allowing the determination of this element by simple calibration curve method in whole blood with minimum sample manipulation.

A graphite tube lined with rhenium foil was employed for the determination of Tm. The performance of the rhenium lined tube was compared with pyrolytic graphite, graphite tubes coated with carbide forming elements, and graphite tubes lined with W and Ta foils. A better performance in terms of sensitivity, reproducibility and long term stability was achieved.

CHAPTER 1 INTRODUCTION

Need for Ultratrace Elemental Analysis

Atomic spectrometry holds a central role in the monitoring of biological and environmental samples as well as in the characterization of technologically interesting high purity materials. The impact of trace elements in the environment and consequently on man's health has resulted in both the development of analytical instrumentation and techniques which are sensitive, selective, accurate, reliable and that are applicable to real samples.^{1,2,3} The necessity of the determination of ultratrace levels of elements in these samples often requires highly sensitive state of the art techniques capable of limits of detection between 0.1 pg to 0.1 fg or even lower.⁴ In many cases, especially in biological monitoring, the challenge is even greater since very limited sample sizes are available.⁵

For most of the elements present in trace amounts and certainly for those present in ultratrace amounts, very little is known about their exact biological behavior. The effects of a substance in the human body depend on its relative concentration. This means that a toxic element can certainly be essential at low concentrations; therefore, the analyst must not only monitor the higher concentrations at which a certain elements are toxic, but also learn to determine the often low concentration levels at which these elements are essential.⁶ In biological systems, there is a growing interest in the

distribution of elemental components in tissues and even single cells and membranes. The determination of an element at the concentration of 1 ng g^{-1} in an individual cell weighing $1 \text{ }\mu\text{g}$, for example would require an absolute limit of 1 fg .⁵

Global ecological problems have resulted in an increasing awareness and interest in the analysis of environmental samples. Concentrations no greater than part per billion or lower are of concern in all phases of the environment: air, water, soil and the biosphere, and include indigenous metals as well as those derived from anthropogenic activities. Highly sensitive techniques are especially necessary to establish 'baseline' levels of many elements and to attempt to reconstruct the past natural distribution of toxic pollutants on a global scale.⁷

In material sciences, there is a great demand for highly sensitive techniques since properties of ultrahigh purity metals, high performance ceramics and micro electronic components can be expected to be affected by foreign atoms or impurity concentrations of the order of $10^{-12}\%$.⁵

Laser-excited Atomic Fluorescence

Laser-based techniques are, in many occasions, the only choice for analysis and are especially indicated in two situations. First, for microanalysis, where the absolute detection limit of a technique is the important parameter rather than the concentration detection limit. This is a suitable domain for laser-based techniques due to the ability to detect atoms with a high sensitivity in a small volume during a short time. Second, when the sensitivity, selectivity, and freedom from matrix interferences needs to be enhanced,

when detecting atoms in conventional atom sources for trace elements. As a result, the range of measurable analyte concentrations can be extended, sample preparation can be simplified, contamination can be minimized and, finally, the sample volume or mass required for analysis can be reduced.⁸

Laser-excited atomic fluorescence (LEAFS) has emerged as one of the most effective methods for detection of trace elements at extremely low concentration or minuscule amounts.⁹ First, the high radiant energy of the laser source saturates some atomic transitions ensuring high sensitivity and second, because of both the selective nature of the fluorescence and the narrow band-width of the excitation line, interferences due to other atomic species and most potential molecular interferents are greatly reduced. The merits of laser excitation for atoms can be illustrated by a comparison with emission techniques.¹⁰ Considering that the same atomization process is used for both techniques, the spontaneous emission of radiation from the excited state is detected in both cases. The signal S_A is proportional to the Einstein factor for spontaneous emission, A_{21} , the population of the excited state (i.e. the probability that an atom is in the excited state), n_{exc} , and the duty-cycle of the detection, ϵ :

$$S_A \propto A_{21}n_{\text{exc}}\epsilon \quad (1.1)$$

Assuming that the number density of the analyte atoms is low, *ie*, no self absorption is expected, the main difference between the two techniques is the way in which the excited state is populated, which leads to large differences in magnitude of excited state population. In addition, differences in the duty cycle, as well as the

possibility of choice of the excited state have to be taken into account. In atomic emission spectrometry, the excited state is populated through absorption of thermal energy or by collisions with gas phase constituents, while in atomic fluorescence the selective excitation takes place due to absorption of photons from the laser beam. The probability of the population in the excited state due to thermal and collision excitation is typically 10^{-5} to 10^{-10} while the atom population in the excited state induced by photon absorption can be more than 50 % (>0.5) of the of the total atom population.¹⁰ However, this overwhelmingly large difference in n_{exc} by five to ten orders of magnitude is normally not reflected in the signal to noise ratio (S/N) and consequently in the difference in terms of limits of detection between the two techniques. It is known that in many cases, limits of detection experimentally reported using LEAFS methods are still far from the expected limits of detection (intrinsic detection limit theoretically calculated).¹¹ This is especially true when complex samples are being analyzed. This difference can be accounted by many reasons such as low probe efficiency of the atomic population, high noise levels, and poorly optimized atomization conditions for a specific analyte. In order to achieve a desired better performance of a LEAFS method, the analyst must choose intelligently the appropriate instrumental components such as laser excitation source, atomizer and detection design as well as experimental parameters like temperature, laser repetition rate, atomization conditions and analytical scheme.

The low duty-cycle of the pulsed laser source (product of the pulse duration and the repetition rate of the laser) is one of the main reasons why the expected limits of detection are not achieved. The large excited state population is maintained roughly

during the laser pulse, therefore improvements are expected if the duty cycle is increased by increasing the repetition rate of the laser excitation source.¹⁰

Bolshov *et al.*¹² predicted and proposed that by increasing the repetition rate of the laser source, improvement in the detection limit of LEAFS would be achieved. According to them, the value of the repetition rate should be increased up to values of the order of τ .⁻¹ The value τ (approximately 10^{-5} s) is the time window that one atom can be probed by the laser beam and is limited by either the life time of the excited atom or the residence time of the atom in the analytical volume. In both cases, the probability of the atoms interacting with the laser beam producing the analytical signal is increased. They expected, by theoretical calculations, an improvement of one and a half orders of magnitude in the limit of detection when a copper vapor laser operating at 10^4 Hz is employed to probe a system with a transient population of atoms. In addition, since the signal to noise ratio improves approximately as the square root of the repetition rate, it is advantageous to use a laser capable of high repetition rate.¹⁰

A copper vapor laser operating at ten's of kHz with a sufficient power level to achieve a reasonable conversion efficiency (the ratio between the output energy of the dye laser and the pump laser) can be successfully used to bridge the gap between continuous wave (cw) and high energy low repetition rate lasers as a dye pump laser. Continuous wave lasers can be used as dye pump lasers, however, an extremely unfavorable overall conversion efficiency is achieved. Pulsed lasers, such as NdYAG, N₂ and excimer lasers, operate more efficiently and provide power levels in the MW range; however many experiments, which require more efficient probing efficiency, are

handicapped by the extremely low duty cycle caused by low repetition rates (10–100 Hz).¹³

Comparative studies made by the Winefordner's group¹⁴ have shown experimentally the advantages of employing the high repetition rate copper vapor pumped dye laser (operating at 6000 Hz) as the source for LEAFS. They found that for lead, atomized in a graphite furnace, the limit of detection using the copper vapor pumped dye laser was at least 6 times better than the ones obtained with a nitrogen pumped dye laser (operating at 20 Hz) or a NdYAG pumped dye laser (operating at 30 Hz).

Among all the atomization techniques, electrothermal atomization (ETA) is most commonly employed for LEAFS.^{10,15} ETA-LEAFS is a successful combination of the analytical performance of the graphite furnace atomizer with the extreme sensitivity and selectivity of laser induced fluorescence.¹⁶ According to Omenetto,¹¹ if the analytical power of detection has to be pushed to limits as low as 1 part in 10^{13} or (0.1 pg g^{-1} in the original sample), then ETA-LEAFS is the only choice. This technique has allowed extremely low detection limits, in the femtogram and even sub-femtogram range, to be obtained for many elements.^{10,15} It has not only been applied to metals and semi-metals but also to non-metals such as phosphorous,¹⁷ chloride,¹⁸ fluoride,^{18,19} and bromide.^{19,20} For most non-metal measurements, the analyte is indirectly measured using the molecular fluorescence of diatomic molecules generated in the furnace involving the analyte and a reagent. Electrothermal atomizers are especially recommended when the sample amount is restricted and when the analysis calls for slurry solutions, solid samples and solutions with a high content of organic matter.⁹ Semi-enclosed furnace (tubes) have the

atomization efficiencies at least 10 times better than those in flame atomization.²¹ Furnaces allow a fast, high atom density build up in a relatively low interference environment when the right experimental conditions are chosen. An improved linear dynamic range results by the elimination of pre and post filter effects and further minimization of vapor phase interferences, caused by the temperature gradient between the atom formation and excitation zones, can be achieved when tube furnaces with a proper excitation scheme are employed.²¹

Intent of Dissertation

Laser techniques cannot be considered mature as techniques.⁸ Although excellent performance and in certain cases unchallenged results have been reported, ETA-LEAFS is highly demanding rather than routine at this time. Among the disadvantages include the need for experienced personnel and for single element measurements although sequential multi-element determinations using a optical parametric oscillator have been successfully performed.²² According to Slavin,²³ the introduction of a new technique for trace element analysis requires an enormous amount of development and testing, comparable to the amount that was necessary to make furnace atomic absorption spectrometry (FAAS), inductively coupled plasma optical emission spectrometry (ICP-OES) and inductively coupled plasma mass spectrometry (ICP-MS) useful and successful techniques. In addition, it has been pointed out that refinements leading to femtogram detection limits not only for a few but also for a large number of elements, will constitute a landmark in the analytical development of ETA-LEAFS and will increase both the

number of laboratories involved in this application and the attractiveness of the method for medical and environmental monitoring and applications in industry.¹¹

The main objective of this dissertation work was to develop ultrasensitive methods based on ETA-LEAFS to determine Ge, In, Pb, Pt and Tm in biological and environmental samples. High sensitivity is achieved by the choice of experimental parameters and instrumental design. A high repetition rate copper vapor pumped dye laser was employed to probe more efficiently the transient atom population generated in the tube atomizer. Tube atomizers with a front illumination detection scheme were employed to increase the number of fluorescent atoms detected, improve the dynamic linear range and decrease interferences from the surrounding atmosphere. Experimental parameters were optimized to maximize the signal to noise ratio. Special care concerning imaging and sample atomization conditions was taken to minimize the noise level reaching the detection system. Improvements in the sample atomization efficiency and minimization of interferences were achieved by the choice of the best atomization technique, use of matrix modifiers and coating of the surface of the atomizer. The ultimate goal was to achieve high sensitivity and high selectivity with little sample manipulation and simple sample calibration procedures.

A brief overview of the fundamentals of laser-excited atomic fluorescence and atomization techniques for LEAFS is given in chapters 2 and 3 respectively. In chapter 4, detailed descriptions of the experimental set up as well as the experimental procedures used in this work are given. In chapter 5, In, Ge and Pt are determined using LEAFS with standard graphite furnace techniques. Efforts are made to improve sensitivity and to minimize interferences by choosing between wall and platform techniques, choosing a

proper graphite material, and optimizing furnace parameters to eliminate sample matrix components. In some cases, matrix modifiers are tested in order to stabilize the analyte during the atomization step ensuring high sensitivity. In chapter 6, a Katskov type graphite filter is used to develop a filter furnace laser-excited atomic fluorescence method allowing the determination of lead by simple calibration curve interpolation technique in whole blood with minimum sample manipulation. A graphite tube lined with rhenium foil was employed for the determination of a rare earth element (thulium) in chapter 7. The performance in terms of reproducibility, signal to noise ratio and long term stability of the rhenium foil was compared with a pyrolytic graphite tube, graphite tubes coated with carbide forming elements, and graphite tubes lined with tungsten and tantalum foils. Finally in the last chapter, general conclusions will be given and possibilities for future work will be proposed.

CHAPTER 2

LASER-EXCITED ATOMIC FLUORESCENCE SPECTROMETRY

Introduction

In laser-excited atomic fluorescence spectrometry, atoms are selectively promoted from a lower state to an excited state after the absorption of incident photons from the characteristic radiation of a laser source. The subsequent relaxation is caused by a loss of excess energy through radiational deactivation in which photons are emitted from the excited state producing fluorescence.²⁴ According to the two level resonance fluorescence scheme (Figure 2.1a), the absorption occurs at a rate $B_{12}E_v$ ($10^8 - 10^9 \text{ s}^{-1}$), where B_{12} is Einstein coefficient of stimulated absorption ($\text{cm}^3 \text{ J}^{-1} \text{ s}^{-1} \text{ Hz}$) and E_v is the spectral energy density (power per unit area and frequency interval) ($\text{J cm}^{-3} \text{ Hz}^{-1}$) of the laser radiation. The lower level is usually the ground or a low lying excited state. The relative population of an excited state, N_{exc} , in relation to the total population N_t , is given by:

$$N_{\text{exc}} = \frac{g_{\text{exc}}}{Z(T)} N_t e\left(-\frac{E}{kT}\right) \quad - (2.1)$$

where E is the energy difference between the excited and the ground states and g_{exc} is the degeneracy of the excited level, k is the Boltzmann constant, $Z(T)$ is the electronic partition function and T is the temperature.¹⁰

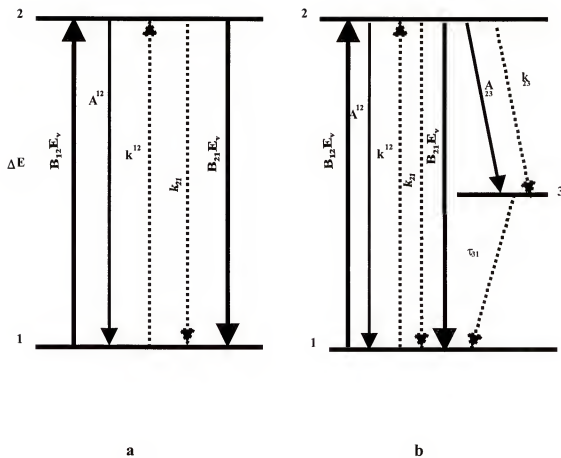


Figure 2.1. a) Two level and b) Three level atomic levels diagrams

Several physical and chemical processes can take place when an atom is in the excited state. The most important physical processes are fluorescence or spontaneous emission, stimulated emission and inelastic collisions. Considering the two-level energy diagram, fluorescence can occur to lower lying states with a rate A_{21} (typically 10^7 – 10^8 s^{-1}). Stimulated emission can force the atoms to ground state with a rate $B_{21}E_\nu$. Finally, inelastic collisions can transfer atoms to lower lying states (collisional deexcitation) or higher lying states (collisional excitation) with rates of k_{21} and k_{12} respectively. Collisional deexcitation (quenching) rates are of the order of 10^6 – 10^7 s^{-1} under argon atmosphere in a graphite furnace.¹⁰ Argon atoms, free electrons, and molecular impurities such as CO or nitrogen compounds and matrix components of the sample can be the main collision partners in a graphite furnace. Blackbody radiation might also be important in the redistribution of the population of excited states and can be included as collisions.¹⁰ In addition to the physical processes described before, molecule formation can cause a loss of free analyte atoms. Since the activation energy for a reaction is supplied by the excitation energy, molecular formation rates are typically much larger from excited states than from the ground state.¹⁰

Fluorescence excitation-detection schemes

There are several types of fluorescence²⁴ and they can be categorized under resonance and non-resonance fluorescence. Resonance fluorescence (Figure 2.2a) results when the same lower and upper levels are involved in the excitation-deactivation process. Since wavelengths of excitation and fluorescence are the same, this scheme is usually avoided due to high levels of background noise due to scattered laser light. Several

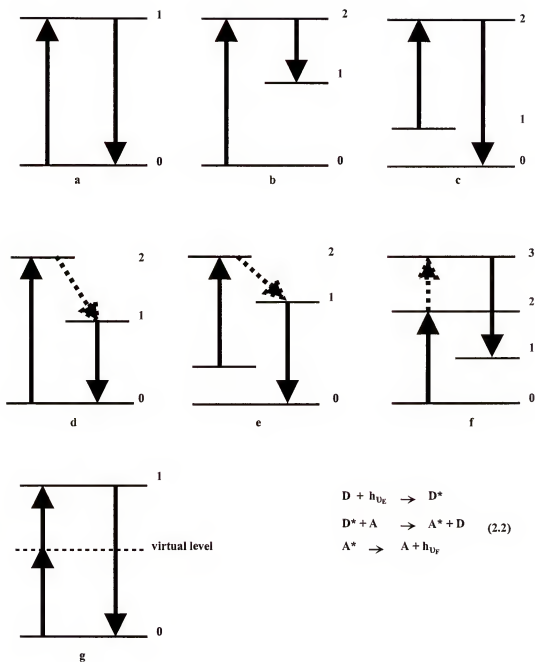


Figure 2.2. Types of atomic fluorescence transitions (solid arrows represent radiative excitation and deexcitation and dashed arrows represent non-radiative excitation and deexcitation)

different schemes result for non-resonance fluorescence. Non-resonant Stokes and anti-Stokes denote that the excitation wavelength is less than or greater than the fluorescence wavelength, respectively. They both yield high sensitivity, and high rejection of both stray and scattered light can be achieved. For both Stokes and anti-Stokes fluorescence, if the same upper level is involved in the excitation-emission scheme, they are denoted as direct line fluorescence (Figure 2.2b and 2.2c). On the other hand, the fluorescence is called stepwise-line when the upper levels involved in the excitation and emission are different (Figure 2.2d and 2.2e). When the excitation process involves a radiative component followed by a further thermal excitation, the process is designated as thermally assisted (Figure 2.2f).

Multiphoton fluorescence involves the absorption of two or more photons exciting an atom to the excited state followed by the emission of one photon (Figure 2.2f). This scheme results in low noise levels but it is also normally accompanied by a decrease of analytical signal. Finally, sensitized fluorescence occurs when a donor species (D) excited by a photon ($h\nu_E$) transfers energy to a acceptor atom (A) which deactivates radiatively ($h\nu_F$) (Equations 2.2).²⁴

General fluorescence flux equations

For atomic fluorescence with a conventional line source, the absorption rate B_{12} generally exceeds the collisional excitation rate. Stimulated emission is also considered negligible. With these assumptions, the efficiency of the fluorescence process can be related to atomic parameters of the absorbing species.^{24,25}

For a low atom concentration (optically thin conditions) the total fluorescence power, Φ_F , in a given volume, V , by an absorption length, l , is given by:

$$\Phi_F = \Phi_{\lambda 0} Y \alpha_L \quad (2.3)$$

where Φ_0 is the incident spectral radiant power ($\text{J s}^{-1} \text{m}^{-1}$), α_L is the absorption factor for a line source and Y is the fluorescence power yield (dimensionless).

The fluorescence power yield, Y , is expressed by:

$$Y = \frac{A_{ji}}{A_{ji} + k_j} \quad (2.4)$$

where A_{ji} is the Einstein coefficient of spontaneous emission (s^{-1}) and k_j is the collisional de-excitation rate (s^{-1}).

The absorption factor under optically thin conditions can be expressed as

$$\alpha = k_m l \quad (2.5)$$

where l is the pathlength (m), and k_m is the maximum absorption coefficient (m^{-1}) and can be expressed as:

$$k_m = \frac{e^2 \lambda_m^2 n_i f_{ij}}{4 \epsilon_0 m_e c^2 \Delta \lambda_{eff}} \quad (2.6)$$

where e is the electron charge (C), λ_m is the wavelength of the transition involved (m), f_{ij} is the absorption oscillator strength (dimensionless), ϵ_0 is the permittivity of free space ($J^{-1} C^2 m^{-1}$), m_e is the electron mass (kg), c is the speed of light ($m s^{-1}$) and $\Delta\lambda_{eff}$ is the effective width of the absorption line (m). $\Delta\lambda_{eff}$ is defined as the width of an equivalent rectangular profile with the same peak value and area as the spectral profile.

Substituting 2.5 and 2.6 into 2.3, the total fluorescence produced under optically thin conditions is given by:

$$\Phi_F = \frac{8.82 \times 10^{-13} \lambda_m^2 n_i f_{ij} I \Phi_0 Y}{\Delta\lambda_{eff}} \quad (2.7)$$

The above relationship is the basis of atomic fluorescence spectrometry where Φ_F is the observed radiant power of fluorescence which is directly proportional to the number density of the ground state which can be related to the analyte concentration.

Laser-excited Atomic Fluorescence

A non-resonant fluorescence excitation-detection scheme can be described approximately by a three level system (Figure 2.1b). The rate equations which describe the time behavior of the level populations N_i ($i=1,2,3$) are given by equations:

$$\begin{aligned} \frac{dN_1}{dt} &= -N_1 E_\nu B_{12} + N_2 (A_{21} + E_\nu B_{21} + k_{21}) + \frac{N_3}{\tau_{31}} \\ \frac{dN_2}{dt} &= N_1 E_\nu B_{12} - N_2 (A_{21} + E_\nu B_{21} + k_{21} + A_{23} + k_{23}) \\ \frac{dN_3}{dt} &= N_2 (A_{21} + k_{21}) - \frac{N_3}{\tau_{31}} \end{aligned} \quad (2.8)$$

where τ_{31} is the lifetime of level 3 (s).

For the solution of the system of equations described by 2.8, two limiting cases will be considered: the metastable case, where the lifetime of the intermediate level 3 is large (large τ_{13}) and the fast decay case, where the lifetime of the level 3 is small ($\tau_{13} \rightarrow 0$).²⁵⁻²⁷

The metastable case

In a three level system, there is a distinguishing characteristic which can considerably influence the fluorescence signal under laser excitation. For example, if optical transitions between 1-2 and 2-3 levels are allowed, the transition 3-1 is partly forbidden, i.e., level 3 can decay either due to radiationless collisions or due to magnetic dipole and quadrupole radiation. Rather typical is the situation when all the above mentioned decay rates are small and level 3 is metastable. Thus, at sufficient power and duration of the laser pulse, a considerable portion of atoms can accumulate in level 3. The temporal behavior now is determined by N_2 :

$$N_2 = N_T + \frac{k_{13}}{\xi_2 - \xi_1} [\exp(-\xi_1 t) - \exp(\xi_2 t)] \quad (2.9)$$

where N_T is $N_1 + N_2 + N_3$, and ξ_1 and ξ_2 are determined by:

$$\xi_{1,2} = \frac{k_{13} + k_{31} + k_{32} + k_{21}}{2} \pm \left[\left(\frac{k_{13} + k_{31} + k_{32} + k_{21}}{2} \right)^2 - k_{13}k_{32} \right]^{1/2} \quad (2.10)$$

The number of fluorescence photons emitted per atom and laser pulse is given by:

$$N_f = \int_{t_0}^{\tau} A_{23} N_2(t) dt \quad (2.11)$$

The approximate solution of the system is strongly dependent upon parameters of the laser (spectral energy density and pulse width) and upon parameters of the atomic system (transition probabilities and nonradiative deexcitation constants).

At moderate laser intensities N_f is given by:

$$N_f = N_0 A_{23} \tau \frac{E_\nu B_{12}}{A_{21}^\Sigma + A_{23}^\Sigma} \quad (2.12)$$

where N_0 is the total number of atoms: $A_{21}^\Sigma = A_{21} + k_{21}$; and $A_{23}^\Sigma = A_{23} + k_{23}$.

When the laser intensity approaches saturation, the fluorescence from the upper level does not depend any more upon laser energy density but only upon fundamental constants including statistical weights and Einstein coefficients:

$$N_f = N_0 \frac{A_{23} \tau_l}{\varepsilon} \quad (2.13)$$

where $\varepsilon = 1 + g_1/g_2$ and τ_l is the duration of the laser pulse.

It is important to note that when a metastable level is available, the atoms will follow the cycle 1-2-3 only once within the duration τ_l of the laser pulse.

The fast decay case ($\tau_{13} \rightarrow 0$)

In this case, since $N_3(t) \approx 0$, the three level system converges to the two level scheme.

The number of fluorescence photons emitted per atom N_f is given by the time of integration of the excited state population during the laser pulse duration τ , times the spontaneous emission factor A_{21} :

$$N_f = \int_{t_0}^{\tau} A_{21} N_2(t) dt . \quad (2.14)$$

The solution of this system follows exactly the same steps described for the metastable case and the result is equal to equation 2.13.

In this case, $A_{23}\tau_1/\epsilon$ is much greater than 1 so that $N_f \gg N_0$. This means that in a strong laser field, atoms undergo transitions between levels 1 and 2 without being retained in level 3. From the physical viewpoint, it indicates the presence of a cyclic interaction of the low-level system with the resonance field in the saturation regime; as a result of this interaction one atom will repeatedly radiate photons during the interaction with the resonance field radiation.

Optical Saturation

Under saturation conditions the rates of excitation and de-excitation are equal, therefore, maximum fluorescence is observed.¹⁰ For these conditions the fluorescence signal is independent of the quantum efficiency because the source induced radiative

excitation and de-excitation rate coefficients dominate the mechanism of level population. The fluorescence power under saturation conditions is given by:

$$\Phi_F = h\nu A_{ij} n_j V \quad (2.15)$$

where:

$$n_j V = N_j$$

where N is the population of the excited state, n_j is the number density of the excited state (m^{-3}) and V is the volume of collected fluorescence (m^3); h is Planck's constant (J s), ν is the frequency (s^{-1}).

Because both the rate of excitation and rate of de-excitation are equal, the following expression is given for the case of a 2-level atom:

$$\left(\frac{B_{ij}(E_\nu)_i}{c}\right)n_i = [k_{ij} + A_{ij} + \frac{B_{ji}(E_\nu)_i}{c}]n_j \quad (2.16)$$

Where $(E_\nu)_i$ is the spectral irradiance of level i ($\text{W m}^{-2} \text{nm}^{-1}$) and n_i and n_j are the number densities of the ground state and excited state respectively.

The statistical weights of the two levels, g_i and g_j , relate to B_{ij} and B_{ji} by:

$$B_{ij} = \frac{g_j}{g_i} B_{ji} \quad (2.17)$$

Substituting fluorescence power yield equation 2.4 and 2.17 into 2.16 and rearranging, the following expression is obtained:

$$\frac{g_i n_j}{g_j n_i} = \left[1 + \frac{A_{ji} c g_i}{Y B_{ij} (E_\nu)_i g_i} \right]^{-1}. \quad (2.18)$$

The saturation spectral irradiance (the spectral irradiance for which fluorescence signal is 50% of its maximum) in ($\text{W m}^{-2} \text{ nm}^{-1}$), is given by:

$$(E_\nu^s)_i = \frac{A_{ji}}{Y B_{ij}} \frac{g_i}{g_i + g_j}. \quad (2.19)$$

When optical saturation is achieved, n_j is equal to n_i , (assuming $g_i = g_j$) and the total number density, n_t , which is the sum of n_i and n_j , can be related to n_j by the expression:

$$n_j = n_t \left(1 + \frac{n_i}{n_j} \right)^{-1}. \quad (2.20)$$

Using equation 2.20 and combining with equations 2.15 and 2.18, the fluorescence flux expression under saturation conditions Φ_F is achieved and given by:

$$\Phi_F = h \nu A_{ij} V n_m \left(\frac{g_i}{g_i + g_j} \right) \left[1 + \frac{(E_\nu^s)_0}{(E_\nu^s)_i} \right]^{-1} \quad (2.21)$$

however; when a high intensity excitation source, like a laser, is employed, the spectral radiance is much greater than the saturation spectral irradiance, and the bracketed term in equation 2.21 approaches unity. Thus, the total fluorescence flux can be simplified to:

$$\Phi_F = h\nu A_{ij} V' n_m \frac{g_i}{g_i + g_j}. \quad (2.22)$$

The best signal-to-noise ratio in ETA-LEAFS is often obtained when the transition is driven close to saturation, i.e. $E_v \approx E_v^S$. Although the fluorescence signal is independent of the source intensity under saturation conditions, stray light levels are directly proportional to the source intensity even at high spectral radiance; therefore the minimum laser intensity required to saturate the transition should be employed.^{10,21}

Fluorescence Analytical Curves

It has been predicted and later experimentally observed that for a line source, the fluorescence curve of growth can be divided in two regions. At low atomic concentrations (low optical densities) the integrated radiance of the fluorescence signal is linearly related to the atom population, N_0 , in the ground state. As a consequence, a slope of 1 is expected for the plot of log of population of atoms in the ground state (N_0) versus the log of fluorescence signal (S_F). Equation 2.23 describes this relationship. A formal development of 2.23 can be found in Omenetto *et. al.*²⁵ and Butcher *et. al.*²⁹

$$S_F = \frac{\Omega_E G \eta_{\epsilon} z_A Y I}{4\pi \Delta \lambda_{DA}} N_0 \quad (2.23)$$

where, $\Omega_F/4\pi$ is the solid angle, G is a geometric term of the atomization cell, η_c (dimensionless) is the optical efficiency of the fluorescence system (dimensionless), $\Delta\lambda_{DA}$ is the full width at half maximum (FWHM) of the absorption line due to Doppler broadening (nm), l is the absorption path length (cm), z_a is a constant related to the absorption transition at a certain temperature and $I_{\lambda L}$ is the total intensity of the line source integrated over its spectral width ($\text{erg s}^{-1} \text{sr}^{-1} \text{cm}^{-2}$) and Y is the fluorescence yield.

It is only at higher atomic concentrations (high optical densities) that the relationship between integrated radiance and atomic concentration becomes complex. In atomic fluorescence spectrometry, the concentration of atoms outside the optical path of measurement will influence the analytical signal. Therefore, experimental growth curves in atomic fluorescence spectrometry are a direct and complex function of the atom cell geometry and it is dependent upon the method of cell illumination and fluorescence collection.²⁸ Self-absorption is the main reason for the deviation of fluorescence calibration graphs. This is the reduction of the fluorescence due to the re-absorption of atomic fluorescence by analyte atoms in the portion of the atom cell irradiated by the source. Post and pre-filter effects, which are special cases of self-absorption, can be made negligible by using a front illumination scheme of fluorescence detection. In such a case the fluorescence signal is proportional to the negative square $[-(N_0)^{1/2}]$ and the plot $\log(N_0)$ versus $\log(S_F)$ shows a slope of -0.5 . This behavior is described by equation 2.24.^{25,29}

$$S_F = \frac{\Omega_E G \eta_e Y 2 I_{L\lambda}}{4\pi(\pi)^{1/4}} \left[\frac{a_F \Delta\lambda_{DF}}{Lz_F} \right]^{1/2} (N_O)^{-1/2} \quad (2.24)$$

where a_F is the fluorescence damping constant, z_F is a constant related to the fluorescence transition at a certain temperature, $\Delta\lambda_{DF}$ is the full width at half maximum (FWHM) of the absorption line due to Doppler broadening (nm) and L is length of the cell illuminated by the source.

Efficiency of Detection

A few assumptions must be made in order to estimate the efficiency of the detection of atoms with a LEAFS system.²¹ First, the residence time (τ_r) of the atom in the probe volume is assumed to be much larger than the duration of the laser pulse (t_l). Second, it is considered that only one photon can be emitted per atom during each laser pulse, implying that the number of photons detected is equal the number of atoms detected. Third, the atoms are distributed uniformly throughout the atom cell. Finally, the limit of detection (LOD) is limited by intrinsic noise sources. Under these conditions, the number of atoms detected (N_d) during a single laser pulse is given by:

$$N_d = \epsilon_0 N_s \quad (2.25)$$

where N_s is the number of atoms in the cell and ϵ_0 is the overall atomization efficiency.

The overall atomization efficiency (ϵ_0) is equal to the product of three individual efficiency terms:

$$\varepsilon_0 = \varepsilon_a \varepsilon_p \varepsilon_d \quad (2.26)$$

where ε_a is the fraction of atoms atomized in the cell, ε_p is the fraction of atoms probed by the laser and detected by the detector and ε_d is the probability that a given free atom in the probe volume emits a photon during the probing time.

The atomization efficiency (ε_a) is given by:

$$\varepsilon_a = \frac{N_a}{N_s} \quad (2.27)$$

Where N_a is the number of free atoms in the atomizer. Typical atomization efficiencies for a furnace falls in the range of 0.1 to 1 and it depends on the element, type of furnace and temperature.²¹

The spatial probing efficiency (Equation 2.28) is equal to the probe volume, V_p , which is the volume illuminated by the laser and observed by the detector, divided by the total volume occupied by all the free atoms, V_s .

$$\varepsilon_{ps} = \frac{V_p}{V_s} \quad (2.28)$$

The temporal probing efficiency (ε_{pt}) is given by:

$$\varepsilon_{pt} = f\tau_r \leq 1 \quad (2.29)$$

where f is repetition frequency of the laser (Hz) and τ_r is the residence time of atoms in the furnace (s).

The overall probing efficiency (ε_p) is then given by:

$$\varepsilon_p = \varepsilon_{ps} \varepsilon_{p_i} \quad (2.30)$$

The approximate efficiency of detection can be calculated²¹ by:

$$\varepsilon_d = f_c f_d A_{ji} \eta \left(\frac{\Omega}{4\pi} \right) t_i \quad (2.31)$$

where f_c is the fraction of atoms that fluoresce (f_c is related to the probability of fluorescence and can be either calculated or experimentally obtained),²⁶ f_d is the fraction of the photons illuminating the collection optics that are efficiently reflected to the detector (f_d is approximately 0.8 for the front illumination fluorescence scheme with the pierced mirror),²¹ A_{ji} is the Einstein transition coefficient (s^{-1}), η is the quantum efficiency of the detector (dimensionless), t_i is the laser pulse duration (s) and $\Omega/4\pi$ is the fractional solid angle over which fluorescence is collected (typically 0.04 for front illumination scheme).²¹

Substituting equations 2.27, 2.28 into equation 2.31, the expanded general expression for the number of atoms detected during a single laser pulse is obtained:

$$N_d = \frac{N_a V_p f_c f_d A_j \eta \Omega t_l}{N_s V_s 4\pi} \quad (2.32)$$

Since in LEAFS the signal to noise ratio is proportional to the square root of the laser repetition rate, $R^{1/2}$, the detection limit can be improved by using a high repetition rate laser. Equation 2.32 is often modified to include this factor:

$$N_d = \frac{N_a V_p f_c f_d A_j \eta \Omega TR^{1/2}}{N_s V_s 4\pi}. \quad (2.33)$$

Sources of Noise in LEAFS

In order to achieve high sensitivity in an analytical method, the analyst must know of the dominant noise source(s) in order to systematically optimize experimental variables or modify the instrumental design for improved S/N. The relative importance of most noise sources depends on the choice of analyte and excitation scheme. In this section, the potential sources of noise in LEAFS, particularly with electrothermal atomization, are identified and experimental methods to minimize them are discussed.^{10,21,30}

Concomitant Scatter

Concomitant scatter is a result of scattering of laser radiation from concomitant particles introduced into the analytical zone during the atomization of the sample. Concomitant scatter is expected to be most significant for the analysis of matrices with high content of nonvolatile components. For these conditions, concomitant scatter can be the limiting noise source for resonance LEAFS and an important component of noise for

non-resonance LEAFS schemes where the difference between excitation and emission wavelengths are small (less than 5 nm). Concomitant scatter magnitude can be minimized by employing a narrow band width laser whose line is equal or less than that of the absorption line width which will ensure that little unabsorbable radiation is available to be scattered. Tube furnaces are expected to reduce recombination and the associated scattered light because the analytical zone is maintained at high temperature and therefore, less subject to vapor phase interferences from the surrounding atmosphere. Since tube atomizers produce a high density vapor phase, a properly optimized pre-atomization step is very advisable in order to reduce concomitant particles released during atomization of the analyte.

Stray Light

Scattered radiation that does not originate from the sample itself is called stray light. It may be caused by scatter of radiation from parts of the atomizer such as windows and walls of the atom cell. Just as for concomitant scatter the use of a narrow-band laser can minimize stray light levels reaching the detector. It is the limiting noise in resonance fluorescence schemes and it also can be the limiting noise when detecting fluorescence in the UV in non-resonance schemes because of poor rejection of stray radiation caused by the use of monochromators with wide spectral band pass. Particularly for tube furnaces with front illumination detection scheme, significant stray light levels are caused by the furnace windows. Minimization of stray light is achieved using windows mounted at an angle close to the Brewster's angle (typically 56°) and positioning them as far away as possible from the center of the tube in order to defocus the stray light from the window while the analyte fluorescence is focused in the entrance

slit. For the front illumination scheme, particular attention must be paid when focusing the laser beam in order to avoid scatter at the edge of the hole in the pierced mirror and on the walls of platform the tube.

Blackbody Emission

It is recognized that blackbody radiation generated at the walls of the tube furnace is of primary importance in LEAFS. The magnitude of the blackbody radiation increases with detection wavelength and is also strongly dependent on the temperature; therefore, if experimental conditions are not chosen carefully, limits of detection are degraded. In order to ensure good S/N ratios, atomization temperatures are optimized and kept as low as possible. For more volatile elements, which are atomized at lower temperatures, detection wavelengths below 400 nm can be used, while for elements with higher boiling points, schemes with detection wavelengths below 320 nm generally allow improved limits of detection. Procedures to minimize blackbody radiation levels reaching the detector must also be taken. Computer modeling of collection efficiency of tube furnace LEAFS has shown that an efficient rejection of background is achieved with careful imaging the center of the tube furnace onto the slit of the monochromator.³¹ The slit is generally adjusted not only in width but also in height in order to improve the blocking of blackbody radiation. Pulsed excitation sources (with high peak intensities) together with gated detection systems, so that noise is measured only during the short "on" time of the detector, are expected to generate better results.³²

Molecular Fluorescence

Unlike furnace AAS, where molecular signals can be a serious interference, in furnace LEAFS, this type of interference is not common, even though there exists the

possibility that some of the molecular species generated may fluoresce.²⁸ In a rod or cup furnace significant molecular formation is expected because atomization occurs in a cool environment above the atomizer. In a tube furnace, molecular fluorescence must originate primarily from the sample because atomization occurs in an inert argon atmosphere at high temperatures. An appropriate pre-atomization step may eliminate most of the potential interferents before the atomization of the analyte. A narrow bandwidth laser also minimizes the possibility of molecular fluorescence excitation.³⁰ Smith *et al.*³⁴ have observed a significant fluorescence background generated at the windows of the furnace when determining thallium. Good quality quartz, silica or LiF windows of minimum thickness must be used to minimize this problem.

Non-analyte Atomic Fluorescence.

The extent of spectral overlap with atomic concomitants in LEAFS increases with increasing laser bandwidth. It is very unlikely to occur in furnace LEAFS and has never been reported.²¹

Other Interferences and Noise Sources

Other minor interferences and noise sources in furnace LEAFS include radio frequency generated by pump lasers and electronic noise produced by the boxcar or by the photomultiplier.²¹

CHAPTER 3 SAMPLE ATOMIZATION

Introduction

One common feature among all atomic spectroscopic analytical methods is the necessity to convert the element being investigated into a vapor of neutral atoms or occasionally ions capable of absorbing and/or emitting characteristic radiation. The atomization process occurs in sample containers called atomizers that consist of a hot gas and/or an enclosed furnace. These devices can be continuous atomizers (flames, ICP) or pulsed atomizers (electrothermal atomizer, laser induced plasma and glow discharge). In a continuous atomizer, the atomization conditions (temperature or voltage potential) are constant in time and the introduction of sample, in the form of droplets, dry aerosol or vapor, is constant. In a non-continuous or pulsed atomizer, the atomization conditions vary in a cyclic way in time with introduction of discrete amounts of sample.²⁴

Laser-excited atomic fluorescence spectroscopy has been coupled with several different atomizers, each one with its peculiar characteristics, advantages and disadvantages. The main requirements for an atom cell in atomic fluorescence spectrometry are high density of analyte atoms, long residence time of the analyte atoms in the optical path, high volatilization efficiency, low quenching properties, low radiance or background, high reproducibility and simplicity of operation.²⁸ It is evident at first glance that all these requirements cannot be fulfilled simultaneously.²¹ Early studies^{35,36}

of LEAFS were performed in flames because of its simplicity, low price, and technical maturity.²¹ However, flames gradually lost favor to other atomization techniques because of low sensitivity obtained, relative to other atomizers, generally achieved due to dilution of the analyte in the analytical zone and susceptibility to matrix interferences caused by the components of the gas mixture.^{21,37} Inductively coupled plasmas torches from commercial ICP-OES instruments have been used with few alterations for LEAFS.³⁸ Limits of detection, principally with complicated matrices, so far reported (in the low ng ml⁻¹ range) although better than those obtained with ICP-OES, have been considered disappointing for LEAFS.¹⁵ The main reason for the relatively poor limits of detection is the high background levels in the plasma.³⁷ A definite advantage of the ICP-LEAFS, however, is the favorable properties of the ICP plasma to atomize refractory elements.⁸

Cathodic sputtering techniques in cells such as glow discharge (GD) and hollow cathode lamps (HCL) as a means of atomization for LEAFS have had a remarkable evolution in the last few years.¹⁵ In general, better sensitivity has been achieved using pulsed mode instead of dc mode, mainly because signal-to-noise ratio is improved when the atomic vapor is probed a few μ s after the pulse, as long as background emission is negligible.²¹ Because the atomization process is not thermal, cathodic sputtering techniques have enormous potential for analysis of refractory elements and for the analysis of layers of solid samples. Sputtering processes are reasonably free from chemical interferences although the atom density obtained in the discharge is orders of magnitude lower to those observed in thermal atomizers. In practice, conductive solid samples or liquid samples, previously dried on the surface of the cathode, have been analyzed by GD/HCL-LEAFS.^{8,15,21} The sample must be loaded in the chamber and then

kept at low pressure (a few Torr).¹⁵ Absolute limits of detection as low as 2, 1.2 and 0.08 fg for europium, yttrium and thulium, respectively, have been reported for 400 nL volumes of aqueous samples.³⁹

The idea of using laser energy as a means of atomizing samples is not new.⁴⁰ However, the use of the laser-induced plasma as a reservoir for LEAFS is relatively recent. The technique is attractive because of the spatial analysis capabilities of not only conducting but also non-conducting samples.^{15,21} In addition, as opposed to low pressures for glow discharges, analysis can be made under atmospheric pressure. Important applications involving the analysis of solid samples⁴¹ and aerosols⁴² have been developed with limits of detection in the ppb to ppm range. LA-LEAFS is still in its infancy and it has enormous potential for surface analysis and analysis of solid samples.⁸

The most successful atomization technique that has been coupled with LEAFS is undoubtedly electrothermal atomization. This technique is very mature due to the extensive atomic absorption spectrometry work using this type of atomizer.^{8,21} Electrothermal atomization has shown great versatility in the direct analysis of solid and liquid samples, enabling the achievement of very low limits of detection, as a result of the high atom density produced and the excellent reproducibility. Further advantages are the small sample volumes required for the analysis and simplicity of operation. In addition, ETA allows a degree of automation profiting from the autosamplers and furnaces developed for ETA-AAS.¹⁵ A variety of elements have been analyzed by ETA-LEAFS with excellent limits of detection.^{8,10,15,21} However for refractory elements atomized in graphite atomizers, sensitivity limitations arise due to the formation of refractory carbides

and oxides.^{8,43} In the next section, the fundamentals, advantages and disadvantages of electrothermal atomization are described in detail.

Electrothermal Atomization

The electrothermal atomizer is in essence a small furnace heated resistively. The furnace can be made of several materials such as metals or quartz, but by far the most popular and versatile is the graphite furnace.⁴³ Each end of the furnace is connected to a high current programmable power supply. The furnace is normally heated in stages in which the temperature is progressively elevated at different rates until the sample is atomized. One example of furnace heating cycle is shown in Figure 3.1. The temperature and duration of each stage of the heating cycle is adjustable so those conditions can be optimized for a given element, type of sample and sample size. The heating cycle is usually composed by one or two drying steps where the temperature is slowly increased to temperatures up to 200°C in order to evaporate the solvent without splatter, leaving only a dry solid residue. The ashing step is used to ash the sample, converting organic matter to H₂O and CO₂ and vaporizing volatile inorganic components of the matrix. In this step, the final temperature is in the range between 350 and 1200°C, and it is chosen according to the sample being analyzed in order to remove matrix components without loss of analyte. In the atomization step, the ashed sample is vaporized to produce the atomic vapor. The temperature is rapidly raised to a pre-selected temperature (1500 – 3000°C). The atomic vapor is produced rapidly and

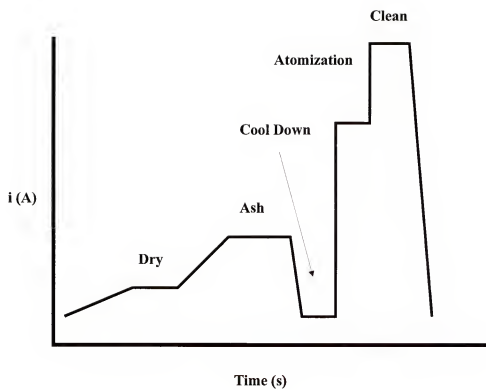


Figure 3.1. Example of a heating cycle.

diffuses out of the observation zone to produce a transient peak shaped response. The duration of the analyte signal, usually between 0.2 to 10 s is determined by the time taken to vaporize the sample and the residence time of the atoms in the gas phase.

Faster heating rates during atomization ($\approx 1000^{\circ}\text{C s}^{-1}$) cause the atomic population to build up rapidly before the atomic vapor diffuses out of the observation zone, thus creating a higher instantaneous atomic concentration and consequently larger signals. Finally, a high temperature cleaning step is used to leave the furnace clean for another cycle.^{24,43} Alternatively, a cool down step after the ashing step can be inserted in order to allow the dissipation of vapors out of the analytical zone prior to the atomization step.⁴⁴

There are three types of electrothermal atomizers that have been used for LEAFS experiments. The cup and the rod are open type atomizers while the tube is classified as a closed type electrothermal atomizer²¹ (see Figure 3.2). In open type atomizers, there is a strong temperature gradient within the analytical zone, which cause loss of analyte atoms due to molecule formation and condensation. Only a few volatile analytes can be efficiently atomized in an open atomizer. Comparative results from the literature have proven that generally the tube is by far superior to both the rod and the cup atomizers.²¹ The tube allows the achievement of better limits of detection because, in a closed atomizer, the number density of the analyte atoms is increased. In addition, the interferences from the atmosphere surrounding the atomizer are minimized. This increase in number density comes with a penalty: the concentration of other gaseous components from the sample matrix is correspondingly larger.^{21,24} During operation, the furnace tube is continually bathed in an inert gas such nitrogen and argon. The inert gas



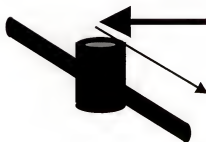
Graphite tube
Front illumination scheme



Graphite tube
Right angle detection



Graphite rod



Graphite cup



Figure 3.2. Electrothermal atomizers.

protects the atomizer surface from oxidation. The gas also transports the analyte atoms from the surface to the center of the atomizer and removes all gaseous substances produced during pre-atomization and cleaning steps.^{24,43}

Graphite

Many different materials such as high melting point metals have been used as the atomizer material, however, by far the most used material is graphite. Graphite is cheap, easy to machine and purify, has a low thermal conductivity, is electrically resistant and is a mechanically as well as chemically resistant material that can be heated to temperatures as high as 3000°C.^{43,45} Important furnace properties that govern the sensitivity in a graphite furnace based analytical techniques include permeability to gases, and reactivity with analyte elements such as reduction and formation of carbides and lamellar compounds.⁴⁶ L'vov in early works on ETA-AAS observed that ordinary graphite was very porous allowing the passage of hot gases even through thick walls. The porosity is also responsible for trapping analyte during the atomization process causing tailing of the analytical signal as well as memory effects.⁴⁰ The impregnation of the internal walls of the graphite tube with a pyrolytic graphite coating in order to decrease the degree of porosity of the ordinary graphite was recommended.⁴⁷ The coating is also responsible for increase of the tube lifetime and decrease of the reactivity with carbide forming elements. The coating of a pyrolytic carbon layer is achieved by allowing a gaseous hydrocarbon, typically methane, to diffuse through the porous graphite slowly depositing in the pores as a pyrolytically graphite at high temperatures (2300°C).⁴³ However, the performance of the pyrolytically coated graphite tube (PG tube) is not always superior to the non-pyrolytical graphite tube (NPG tube). The effect

varies greatly from element to element. PG tubes increase sensitivity for many refractory-oxide or carbide forming elements such as Ti, Mo and V, whereas significant improvements are not observed for elements which do not form stable carbide and oxides.⁴⁸ Matousek⁴⁹ suggested that the NPG surface enhances the sensitivity of Se, As, Te and Sb by retarding the release of dimers which are their atomizing species at low temperatures. Imai *et al.*⁵⁰ observed greater sensitivity for indium when the analyte was atomized in a NPG tube. The authors suggested that the active carbon surface play a role of a condensed phase reductant to reduce indium oxide species, responsible for analyte losses during atomization.

For the cases where the formation of carbides is a problem, the graphite also can be coated with noble metals like Pd and Ir^{51,52} or carbide forming elements such as Zr that makes the surface layer of the atomizer less reactive when the analyte is being atomized.⁵³ In both cases, relatively concentrated solutions of the coating element is deposited in the graphite furnace and heated to temperatures which the noble metals are reduced or the carbide layer is formed.

Atomization Mechanisms

The electrothermal atomizer, which originally was conceived to be a device sustaining a simple chemical environment for atomization of samples, has revealed itself to be a quite complex system. Although a significant amount of work has been dedicated to the understanding of the atomization process, the mechanism is still not well understood. The understanding of the types of processes involved has not been facilitated

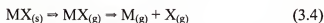
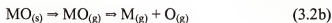
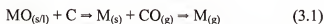
by the numerous experimental studies performed which often give widely different results.⁵⁴

Several approaches to the study of this problem have emerged, which are based on thermodynamics,⁵⁵ kinetics,⁵⁶ involve the identification of the reagents and final products by X-ray diffraction analysis,⁵⁷ molecular spectroscopy,⁵⁸ and mass spectrometry.⁵⁹ The dynamic version of the kinetic method, which involves measurement of the rate constants of a process under continuously increasing furnace temperature, presently enjoys the greatest popularity.^{60,61} Compared with the quasi-static version of the method, where temperature is kept constant, the dynamic version more closely approaches the realistic analytical conditions inside the tube atomizer. In the dynamic version, the experimental determination of the rate constant, k , for the atomization of an element over a fairly broad temperature interval is used to construct an Arrhenius plot ($\log k = f(T^{-1})$) in order to determine of the activation energy E_a of the process in question from the slope of the plot. The dynamic method has yielded a wealth of experimental information characterizing the atomization of several elements.⁶¹ Of course, many variables can affect the atomization process making it very complex. In a general way, interactions among the analyte, atomizer surface, protective gas and sample matrix components can have strong influence in the overall process. In addition, interactions in the vapor as well as in the condensed phase, and revolatilization can affect strongly the vaporization/atomization process.⁵⁴

From the atomization of simple analyte aqueous solutions, three potential routes to the atomic vapor in a graphite furnace have been proposed. First, elements such as Cu, Ag, Au, Pt, Ni, Pb, Sn and Ru, should be in the free atomic state at the appearance

temperature (the temperature at which atom formation is first observed) (Equation 3.1). The oxides of these elements decompose to free metals below the temperatures at which noticeable vaporization of these metals is occurring. Second, there are elements (In, Cd, Zn, Sr, Mn, Ca, Be, Al) where atomization occurs from the thermal dissociation of oxide species (Equation 3.2a and 3.2b). Third, the thermal decomposition of carbide species is the route common for Mo, V, Ti, Zr, Ta, Th and rare earth elements (Equation 3.3).

Alternatively, some elements which are initially present in the form of halides are formed by the thermal decomposition of the metal halide species (Equation 3.4).^{43,61}



Minimization of Interferences in Electrothermal Atomization

Originally, electrothermal atomization was a passive technique, i.e., after a sample had been deposited in the atomizer, the analyst had virtually no influence on the process of atomization, more recently, persistent attempts have been made to optimize this process in order to achieve predictable and controllable atomization.⁶² Numerous approaches have been proposed, and the most important are the use of optimal temperature programs of atomizer heating,⁶³ platform atomization^{64,65} and chemical

modification of the sample.⁵¹ Although described separately these techniques have been used jointly.

Optimal Temperature Program

The optimization of the temperature program is the simplest possible approach to eliminate potential interferences and maximize analyte signal. Here, the drying and ashing temperature and time are optimized in an attempt to eliminate the sample matrix while the atomization heating rate and final temperature is optimized in order to enable the achievement of an uniform and dense analyte atomic vapor cloud. This approach can be successful for samples in chemically simple and volatile matrices and for more stable analytes (less volatile and less reactive).⁶³

Stabilized Temperature Platform Furnace

The formulation of the stabilized temperature platform furnace (SPTF) concept was a qualitative jump in the development in the electrothermal atomization technique.⁶⁶ The platform is a thin pyrolytic graphite plate placed at the bottom of the furnace onto which the sample is deposited (Figure 3.3). Contrary to the technique where the sample is deposited in the wall of the tube, the platform is heated primarily by radiation from the walls; in this case, the atomization of the analyte is delayed occurring in a higher and more uniform temperature environment.^{24,64} Initially proposed by L'vov,⁶⁷ platform atomization minimizes losses of analyte commonly observed when there is strong temperature gradient between the wall and the analytical zone. The higher gas temperature at the time of volatilization favors molecular dissociation and reduces vapor

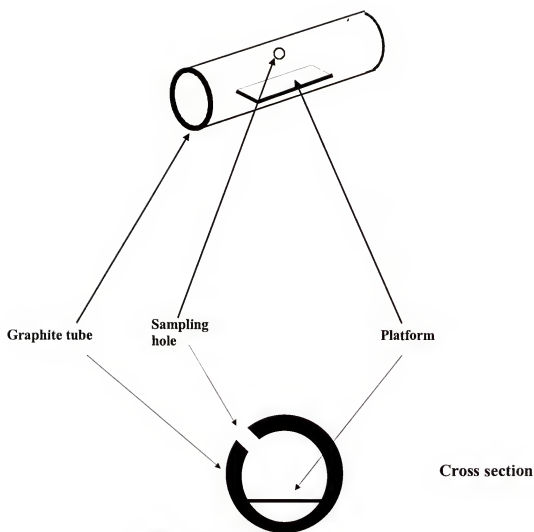


Figure 3.3. Graphite tube with platform

interferences especially for volatile and medium volatile elements. SPTF is nowadays a well established and largely used technique with the additional advantages of increasing the graphite tube life, and constraining the spreading of the sample.

Chemical Modification

The general aim of chemical modification is to improve the efficiency of the atomization through *in situ* changing the thermochemical behavior of both the analyte and the matrix components. Inevitably, the effect of any particular modifier is complex and diverse; thus to some extent, all four components of the analytical system are affected: the analyte, the matrix, the atomizer (the surface layer) and the gas phase.⁵¹ Chemical modifiers are generally used in large excess in comparison to the amount of analyte, and in terms of aggregate state, they can be gases, solids and liquids (solutions).^{51,66}

The most common effects of chemical modifiers on the analyte are thermal stabilization, allowing the analyte to atomize at higher temperatures where the matrix has been eliminated by ashing. Alternatively, chemical modification can increase the efficiency of atomization by increasing the volatility of the analyte. In addition, it can be responsible for the homogenization of various analyte species into only one species before atomization. The most common effects of chemical modifiers on the matrix are the increasing of volatility or thermal stabilization of interfering concomitants, making the temperature release of interferents different from that of the analyte. Modifiers can also be an aid for the ashing of organic matrices and used to facilitate the contact between the sample and the surface of the atomizer. Temporal variation of the composition of the

gas phase have been changed with chemical modifiers either improving in matrix combustion and/or acting as scavengers, to clean the furnace and react with potential interferents. Finally, chemical modifiers can alter the surface layer of the atomizer to decrease porosity and increase or decrease reactivity.⁵¹

The mechanisms of action of chemical modifiers are, in many cases, still not very clear.^{51,66} Of course, the mechanisms are different for each of the four components of the atomizer and will vary according to the chemical and physical type of the modifier being used. In terms of stabilization of the analyte, two mechanisms are proposed. First, it was proposed that the analyte and the modifier form chemical and thermal stable species with defined structure and properties.⁶⁸ More recently, the formation of analyte-modifier solid solution and/or isomorphous substitution of atoms (ions) in the modifier's crystal lattice by the analyte atoms (ions) was suggested.⁶⁹ In this case, thermal stabilization is explained by decreasing of the equilibrium partial vapor pressure for the analyte evaporation.

Chemical modification has become a commonly used technique in electrothermal atomization. Its effectiveness has been proved in many cases. However, there is a high demand for a more universal chemical modifier which will work for several situations as well as for high purity chemical modifiers that will not contaminate the furnace with the analyte of interest especially when ultratrace determinations are intended.^{51,66}

CHAPTER 4 EXPERIMENTAL

Instrumentation

The illustration of the experimental set up employed in this work is shown in Figure 4.1. The instrument is composed by three principal parts: the excitation source, the sample atomizer, and the detection-signal processing-acquisition system.

The instrumental arrangement employed was the front-surface illumination scheme. This scheme has been proven superior to other collecting ways, such as the right angle detection, where the fluorescence is collected at 90° to the laser beam.^{10,21} In the front-surface scheme, the fluorescence is collected at 180° angle to the illuminating laser. A mirror, in which a hole of about 3 mm diameter is drilled (pierced mirror), is placed in front of the furnace at 45° angle. The advantages of this scheme is that the reflector is achromatic (the focal length is the same for different wavelengths and the reflector also allow a more accurate imaging of the tube atomizer which can reduce blackbody radiation levels reaching the entrance slit of the monochromator. Pre and post filter effects are also eliminated because the atom cell is completely irradiated in the direction of the detector. The front illumination scheme is the most appropriate when graphite tubes are used while the right angle scheme is employed mostly for graphite cuvettes and modified graphite tubes.²¹

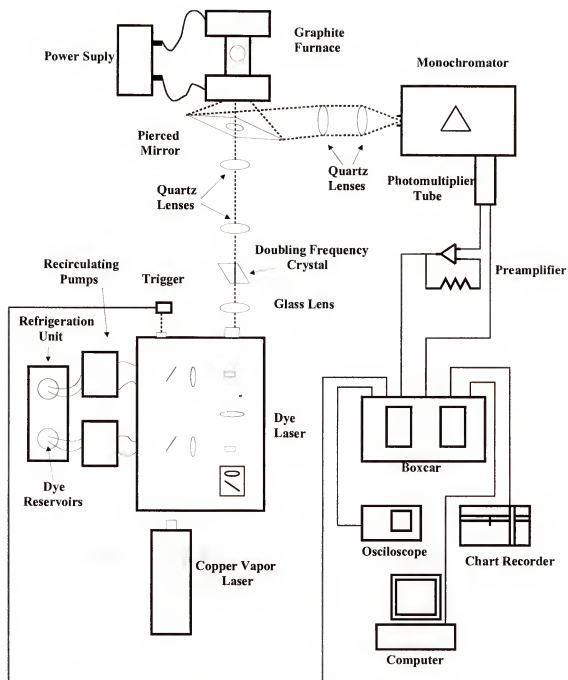


Figure 4.1. Experimental set up

The laser beam from the excitation source is passed through the pierced mirror and focused into the center of the graphite tube (analytical zone) by a 25.4 cm focal length quartz lens which was replaced later by a set of two 10 cm focal quartz lenses. The fluorescence radiation collected by the front pierced mirror is reflected at 90° and focused into the entrance slit of the monochromator by a set of two 20.4 cm focal length biconvex lenses. The fluorescence signal is then detected, processed and recorded. A detailed description of the main parts of the instrument is found in the sections below.

Excitation Source

The copper laser pumped dye laser used as the excitation source consists of three parts: the copper vapor laser (CVL) used as the pump laser, the dye laser and the nonlinear crystal for frequency conversion of the visible dye laser radiation into the ultra-violet region. The radiant power of the laser output generated both by the CVL and by the CVL pumped dye laser was monitored throughout the experiments with a thermocouple-digital voltmeter.

Copper vapor laser

The copper vapor laser (CU-15A, Oxford Lasers, Acton, MA) (Figure 4.2) used as the pump laser is classified as a metal vapor laser. It is an efficient cyclic self terminating laser emitting short (5-40 ns) pulses at very high repetition rates (7,000 to 12,000 Hz) on transitions in the green (510.6 nm) and yellow (578.2 nm) regions of the visible spectrum.⁷⁰ Metallic copper is placed inside an refractory ceramic tube and kept under neon atmosphere at 20 torr of pressure. High voltage is applied to the electrodes in

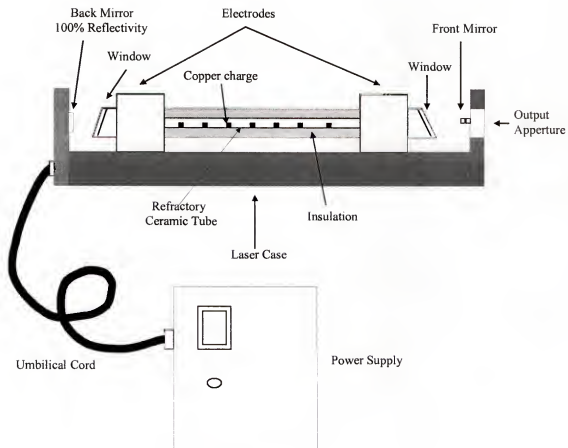


Figure 4.2. Copper vapor laser

order to heat the tube to about 1500°C and vaporize the copper. The vaporized copper acts as the active medium of the system. Copper atoms are excited according to the three level system illustrated in Figure 4.3. The neutral copper atoms are excited to the first resonance levels by electron impact. Although these levels are strongly coupled to the ground state, radiation trapping at number densities above 10^{12} cm^{-2} substantially increases the upper state lifetime. Laser action occurs through transitions to the metastable 2D levels. Due to a build up of atoms in the lower levels (both by stimulated emission and direct electron pumping), the inversion ceases. Following return of the metastable atoms to the ground state, the laser is pulsed again repeating the cycle.⁷¹

The laser optics has an unstable resonator design in order to improve the output beam divergence (0.4 mrad). Other typical operating characteristics are 1-2 hour warm up time, average power of 7 W, pulse energy in the millijoule range, and kW of peak power. This laser can be operated for more than 300 hours before there is a need to be for new copper load.⁷⁰

Dye laser

Tunability over UV and VIS spectral range, a high peak power, a great degree of spatial and temporal coherence leading to very high power densities and narrow bandwidths and reasonable lifetimes are some of the features that make the tunable dye laser an excellent radiation source for atomic fluorescence.^{32,72}

In a dye laser, the characteristic wavelength of the pump laser is absorbed by the dye molecules which fluoresce over a small band of wavelengths characteristic of the chosen dye. One of the mirrors in the oscillation cavity is a grating (wavelength selective

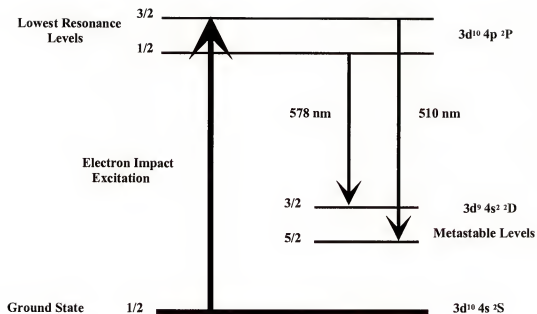


Figure 4.3. Copper vapor laser energy level diagram

device) that causes the dye, in the oscillator cell, to lase at a wavelength that is tunable by changing the angle of the grating. A second dye cell (amplifier cell) in the path of the oscillator output beam amplifies the laser output of the oscillator. One dye can only be tuned over a limited range of wavelengths (between 5 and 10 nm); consequently several different dyes or mixtures of dyes are used to cover different wavelength ranges of the spectrum.¹³

The CVL was used to pump a dye laser (model DL II Molelectron) in order to obtain wavelengths other than the CVL characteristic wavelengths. Because of the relatively low photon energy (compared with a N₂ or an excimer laser) and consequent slow dye degradation, the copper vapor lasers serves as an excellent pump source for dye lasers.⁷² Dye laser output at wavelengths between 550 to 890 nm with conversion efficiency up to 30 % can be generated. A great part of this range has enough energy to be frequency doubled using non-linear crystals.¹³ The laser dye is cooled in a refrigeration unit and pumped through both the oscillator and amplifier quartz cells of the system. A list of the dyes employed to generate the excitation wavelengths is shown in Table 4.1. Methanol (optima grade) from Fisher Scientific, Fair Lawn, NJ) was used as the solvent in the dye cells. The concentrations of the dyes in the solutions were optimized by monitoring the output energy power with a thermocouple digital voltmeter, while a concentrated dye solution was placed in the dye reservoirs. The concentrations were usually fixed when the difference between the laser and stimulated emission intensities were maximized. Stimulated emission intensity was measured by blocking the laser beam with a paper card between the grating and the oscillator cell to eliminate laser activity.

Table 4.1. Experimental characteristics of the output dye laser beam

Element	Doubled Frequency Output Wavelength (nm)	Energy per pulse (μ J)	Dye ^a	Non- linear Crystal
Ge	269.13	0.5	Rhodamine 560	KDP-A
Pt	270.24	3	Rhodamine 560	KDP-A
In	275.39	2	Rhodamine 575	KDP-B
Pb	283.30	2.5	Rhodamine 590	KDP- R6G
Tm	291.48	2	Rhodamine 590- Rhodamine 620 (90-10 %) mixture	BBO

^a Dissolved in methanol

Non-linear crystal

The useful regions of the spectrum between 190 to 320 nm, which cannot be directly obtained with a dye laser, can be reached by various optical frequency conversion techniques. In this work, this was achieved by using frequency doubling of the dye laser output. In the frequency doubling technique, the output of the dye laser is divided in half by using a doubling crystal. Second harmonic generation (SHG) consists in the absorption of two photons of same frequency ν_i by a material in its ground state, and only a single photon of frequency ν_{ii} results. A non-centrosymmetric crystal is commonly used as the frequency conversion material. The efficiency of SHG is usually between 1 to 20 % depending on the material used and wavelength and energy of the input radiation ref.

The laser beam from the dye laser was focused slightly before the surface of the crystal by means of a glass lens to avoid burning damage of the material. The various dye-crystal combinations can be seen in Table 4.1. Potassium dihydrogen phosphate (KDP) crystals from Inrad and a barium beta borate BBO (Lambda Physik) crystal were used. The crystal was fixed in a translation platform and the fine tuning was made by manual rotation of the crystal until the maximum output energy was reached. The rotation was made around a plane which is phase matched with the dye laser output in order to avoid destructive interference of the two laser beams. A filter (UG 5) placed after the KDP crystal was used to block the laser fundamental frequency that was not converted during the frequency-conversion process.

Sample Atomizer

A graphite furnace (Perkin Elmer, Model HGA-400, Norwalk, CT) was used as the sample atomizer. This transversally heated atomizer allowed the use of temperature programs with up to 7 steps. Very fast temperature ramp times (ms) as well as temperatures as high as 2800⁰C can be used. The furnace, which is originally designed for atomic absorption, had its windows modified in the laboratory in order to minimize scatter noise; scatter is not a crucial problem for atomic absorption experiments but does degrade the signal to noise (S/N) of the fluorescence signals.¹⁰ The modification consisted in replacing the original window housing with a fused silica window mounted at 45⁰ angle with the incident laser beam. While fused silica has low intrinsic fluorescence, the 45⁰ angle minimized stray excitation radiation that reaching the entrance slit.

Pyrolytic graphite tubes (Perkin Elmer), with or without platforms, laboratory made non-pyrolytic graphite tubes made with spectroscopic carbon (National Carbon Co. Inc, Cleveland, OH) were used. Modifications in the tube atomizers will be described in the experimental chapters

Detection-signal processing-acquisition system

A 0.34 m spectrometer (Model 340 E, Spex, Edison, NJ) was employed as the wavelength selector device. Table 4.2 shows the specifications of the spectrometer. The entrance slit of the spectrometer was modified to decrease the amount of blackbody radiation reaching the detector. The modification consisted in placing two fixed metallic

Table 4.2 Specifications of the Spex spectrometer

Focal length (mm)	340
Dispersion (nm mm ⁻¹)	2.5
Resolution (nm)	0.15
Aperture (f/n)	5.9
Range (nm)	200 – 1000
Accuracy (nm)	± 0.5
Precision (nm)	± 0.1
Focal plane (mm)	30
Grove density (groves mm ⁻¹)	1200

blades (0.2 mm apart from each other) perpendicularly to the original entrance slits in order to achieve a rectangular shaped aperture. The low level fluorescence radiation and background radiation were converted into an electrical signal by means of a photomultiplier tube (PMT) (R928 Hamamatsu Corp., Bridgewater, NJ). The photomultiplier tube operated with an anode-to-cathode voltage of - 900 V supplied by a high voltage power supply. Some of the advantages that the PMT offered were fast detection with high amplification and excellent noise properties. The output current from the PMT was then converted into voltage and amplified in a laboratory-constructed transimpedance amplifier which consisted of a OP-37 operational amplifier (Precision Monolithics, Inc., Santa Clara, CA) with a 10^4 k Ω feedback resistor in parallel with a 15 pF capacitor. This circuit was powered by two 9 V batteries. The voltage pulse was sent to a boxcar integrator (Stanford Research Corporation, Palo Alto, CA). The boxcar was externally triggered with the signal from a fast photodiode fed with the scatter radiation from the CVL. Gatewidth and delay time of 300 and 30 ns, respectively, were set for all experiments. The output of the boxcar integrator was sent to an analog-to-digital converter (ADC) that was interfaced with a computer for data acquisition, analysis and storage. Because of the inability of the ADC converter to digitize data at a rate faster than 1.2 kHz, it was necessary to divide the 10 kHz trigger signal from the boxcar by a multiple of 10. In this manner, the ADC working at a 1000 Hz rate, could transfer all data points taken. The interface contained a buffer memory which accumulated non-transferred data points. A chart recorder, directly connected to the signal output of the boxcar, was also used to optimize of the analytical measurement.

Wavelength Tuning

The wavelength of the laser was tuned exactly to the atomic transition in order to maximize the signal. Since the analyte signal in the furnace was transient, it was not suitable as a monitor for optimization of laser wavelength. Therefore, a hollow cathode lamp was placed behind and in-line with the graphite tube atomizer, was used as the source.

Cleaning of Glassware

All glassware (volumetric flasks, volumetric pipets, beakers) as well as the polytetrafluoroethylene (PTFE) bottles were washed, rinsed and soaked overnight in a bath filled with 20 % nitric acid solution. The soaked glassware was then rinsed thoroughly again with either Ultrapure deionized water (Millipore, resistivity of 18.2 M Ω) or Deionized ultrapure filtered water (DIUF water) (Fisher Scientific, Fair Lawn, NJ).

Procedures

Analyte Solutions

Analyte standard solutions of different concentrations (germanium, indium, platinum, lead and thulium) were prepared by sequential dilution of 1000 $\mu\text{g g}^{-1}$ atomic absorption solutions (High Purity Standards, Charleston, SC) using ultrapure deionized water or DIUF. In some cases, when specified, acid solutions were used to make the dilutions).

Other Solutions

All acid solutions, sodium hydroxide solutions, the solutions used in the experiments involving interference effects as well as matrix modifier solutions were prepared from analytical grade reagents without any further purification and ultrapure deionized water. Sodium hydroxide, sodium chloride, sulfuric acid, sodium nitrate, sodium chloride, sodium fluoride, sodium bromide, oxalic acid, ascorbic acid and ultratrace analysis grade nitric oxalic and hydrofluoric acids were obtained from Fisher Scientific (Fair Lawn, NJ). Lithium solutions used as matrix modifier were prepared by dilution of a 1000 ppm atomic absorption standard solution (High Purity Standards, Charleston, SC) in 0.01 M nitric acid solution. Pd and Pd /Mg nitrates modifiers were prepared from palladium nitrate (Alfa products, Dewar, MA) and magnesium nitrate (Fisher Scientific, Fair Lawn, NJ). $\text{NH}_4\text{H}_2\text{PO}_4$ solution was from a 10% atomic absorption commercial solution (Perkin-Elmer). The atomic absorption standard solution ($1000 \mu\text{g g}^{-1}$) of selenium was obtained from Alfa products, the arsenic from Fisher Scientific and the silicon from High Purity Standards.

Samples

Samples analyzed were divided into those into those which are already in liquid form (water, urine, blood) or in solid form (soils, sediments, automotive catalysts). The samples used to validate the analytical methods developed were either standard reference materials from NIST or laboratory-prepared samples.

Because the concentration of the analyte was low, there was always a concern about sample contamination which could be introduced either by addition of chemical

compounds with uncertain degree of purity (acids, chemical modifiers and water etc..) or by using a contaminated storage vessel. This was avoided by using pure and ultrapure reagents and meticulously clean glassware. Sample manipulation such as transfer, grinding, filtering and others, are another potential source of sample contamination. To avoid contamination, a big effort was made to keep the sample preparation to a minimum. Liquid samples were placed in the atomizer directly either without dilution or after a simple dilution procedure with water or acid solution. On the other hand, solid samples were submitted to fast microwave digestion procedures in closed vessels involving a minimum volume and number of reagents. Sampling into the furnace was made by means of a Eppendorf micropipete with disposable polypropylene tips. Volumes sampled were in general 10 μL .

Water samples. Tap water samples were collected directly from a laboratory faucet or prepared using GeO_2 99.99 %.

Blood samples Blood samples were either NIST 955a certified for lead or blood samples obtained from the University of Florida Infirmary and spiked with a specific amount of standard analyte solution. Blood samples were either diluted with water or nitric acid solution.

Urine samples. Urine samples (SRM 2657 toxic metals in urine) were certified for platinum. The sample was spiked with analyte solution in order to prepare samples for the other analytes of interest. Urine samples were sampled without dilution and with minimum dilution using water.

Automotive catalyst samples. These samples were certified for platinum (SRM 2556 recycled auto catalyst pellets) and were microwave digested with HF. The sample were then diluted to decrease concentration of acid and adjust concentration of analyte.

Soils and sediment samples. These samples were microwave digested with HF, HNO₃, or a mixture of those acids. Certified samples were SRM (coal fly ash), SRM 2711 (Montana soil), and SRM 1648 (urban dust). Laboratory prepared samples were prepared by spiking washed sand (Mallinckrodt, Paris, KY) with analyte solution. The sand was ground before mixed with an analyte solution. This mixture was allowed to dry overnight in an oven and then and then mixed in a shaker.

Preconditioning of the Graphite

Graphite tubes, platforms and filters were pre-conditioned before the introduction of samples. The pre-conditioning procedure consists of submitting the graphite to the heating cycle suggested by Perkim-Elmer.⁷³

Microwave Digestion

A big effort in this work has been made to simplify sample preparation procedures since it is usually the most time consuming and laborious step of an analytical method. Microwave digestion techniques have reduced sample decomposition time and consequently the overall sample preparation time when compared to conventional hot plate wet digestion methods. This is especially true when solid samples such as soils are involved. Abu-Samra and collaborators,⁷⁴ using an open vessel, were the firsts to use microwave heating for organic matter decomposition. One major improvement made in

1980s^{75,76} was the introduction of pressurized closed-vessel digestion. High-pressure closed-vessel systems offer several advantages over open vessels for microwave digestion procedures. In closed systems, higher temperatures are achieved, which leads to faster reaction times and the decomposition of difficult samples. Sample decomposition is facilitated in this case because the oxidation potential of acid reagents is increased when temperatures extend above their normal boiling points. Also, intermediate reactive products may form at high temperatures causing some reactions that would never occur in normal pressure conditions. Other advantages include the elimination of both the risk of contamination from the atmosphere and loss of volatile species, resulting in more accurate and precise analyte determinations. In addition, reagent volumes to be employed are greatly reduced, decreasing both the blank signal levels due to possible contaminants present in the reagents and the amount of decomposition products produced. Finally, domestic microwave units with no or little modifications can be safely used for these procedures.

Theory

The differences in the physical mechanisms involved can explain the difference in heating times between conventional and microwave digestions. In conventional systems, a sample vessel is conductively heated by a hot plate. The sample vessel, usually a poor heat conductor, first absorbs the energy from the hot plate transfer it to the sample. When vaporization of the liquid surface starts, convection currents are formed in the solution, producing a temperature gradient as vaporization starts at the liquid surface. Therefore, only a small portion of the solution is at the same temperature of the applied heat,

resulting in non-uniform heating and increased heating times.⁷⁷ In microwave heating, the microwaves travel through the transparent vessel and directly couple the solvent. Therefore, the entire sample is heated simultaneously enabling the boiling point of the solvent to be reached under one minute.

The heating of a sample by microwave energy depends upon absorptive polarization, which is due to the molecular dipole rotation and intermolecular friction that occurs in molecules possessing significant dipole moment, and upon the ionic conductance of the medium. The principles of the heating are governed by the dielectric loss theory. According to this theory, as microwaves penetrate a sample, there is loss of energy from the electromagnetic field to the sample at a rate dependent upon the sample's dissipation factor. The dissipation factor is a ratio of the sample's dielectric loss factor to its dielectric constant and it is expressed as:

$$\tan \delta = \frac{\epsilon''}{\epsilon'} \quad (4.1)$$

where $\tan \delta$ is the dissipation factor, ϵ' is the dielectric constant, and ϵ'' is the loss factor.^{77,78}

The dielectric loss factor measures the sample's ability to dissipate microwave energy as heat to the sample, and it depends on frequency and temperature. The dielectric constant, on the other hand, measures the sample's ability to block microwave energy as it tries to penetrate. The larger the dissipation factor, the greater the sample's ability to convert electromagnetic energy into heat energy at a given frequency and temperature. Samples that possess sizeable dipole moments and are free to rotate are

likely to have larger dissipation factors. Teflon which is commonly used as the sample vessel material has a $\tan\delta = 0.00015$, making it virtually transparent to microwave heating.

Ionic conductance is the second parameter influencing the efficiency of microwave heating. In an applied electromagnetic field, a conductive migration of dissolved ions occurs. This migration produces a current flow that results in IR losses, or heat transfer, due to resistance to ion flow. The magnitude of current produced by ions depends on their relative concentration and mobility in the system. Therefore, ion migration losses depend on the size, charge and conductivity of the ions, as well as their interaction with solvent molecules. As the ion concentration increases, there is greater ion mobility, which causes an increase in current and heat transfer.

While both ionic conductance and dipole rotation influence the efficiency of microwave heating, the temperature determines which process dominates. Initially, dipole rotation controls the dielectric loss to the sample. As the temperature increases, ionic conductance dominates the conversion of microwave energy into heat. The fraction of contribution from each process depends on ionic mobility and concentration. If these two parameters are small, then the dielectric loss is mainly the result of dipole rotation.^{77,78}

Instrumentation

Microwave oven unit

An unmodified domestic microwave unit (General Electric, Model #JES65T) was employed for the sample digestions during this work. The device is operated at $2430 \pm$

13 MHz with output energies of 600 – 700 W. A scheme of the microwave unit is shown in Figure 4.4. Microwave energy is generated by the magnetron. The waves travel through the waveguide to the microwave cavity. The waveguide is made of a reflective material for high transport efficiency. At the exit of the waveguide is the mode stirrer, a fan shaped blade that distributes the energy in many directions throughout the microwave cavity. In the cavity, microwaves are reflected back and forth between the walls until all the energy has been absorbed by the sample. The part of the energy that travels back towards the waveguide are directed by a dummy load by the circulator in order to be dissipated as heat preventing damage of the magnetron.⁷⁹

Microwave acid digestion vessel

A schematic diagram of the high-pressure acid digestion vessel (Parr Instrument Company, Moline, IL) used for sample decomposition is shown in Figure 4.5. The complete vessel consisted of a 45 mL Teflon sample cup encased in the hard polymeric outer case of the digestion bomb (Model 4782). Teflon is the material of choice to construct the sample cup because it is chemically inert and is practically microwave transparent allowing energy to flow directly to the sample while also serving as an insulator, restricting heat flow from the reaction zone. Although Teflon has melting point at approximately 306 °C, it must not be heated above 150 °C in order to avoid deformation of the material and consequently breaking of the seal of the system.⁸⁰

The outer case of the bomb assembly is constructed of a microwave transparent polymer resin. It has a compressible pressure relief disc that served as a safety release. If

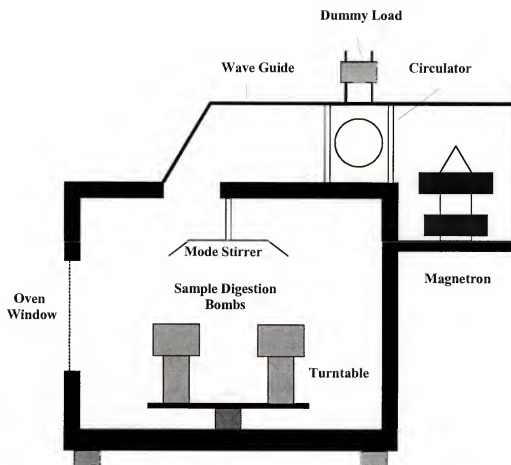


Figure 4.4. Diagram of the microwave oven unit

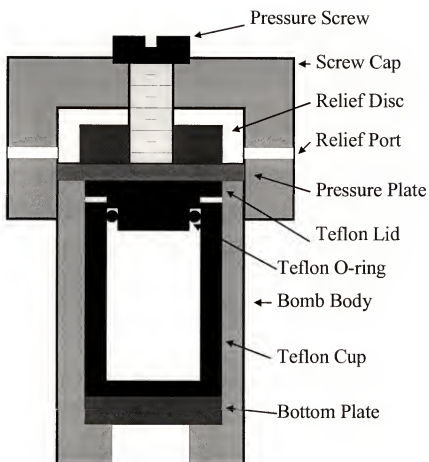


Figure 4.5. High pressure acid digestion vessel (digestion bomb and Teflon cup)

the pressure inside the vessel exceeded the maximum allowable value, the O-ring seal, located between the inner top rim of the sample cup and its cap, became distorted. This process allowed the excess gases to escape compressing the relief disk, venting through the pressure ports located on the side of the outer cast cap which prevented destruction of the bomb. The pressure that built up inside the bomb was estimated by the position of the retaining screw (which holds the relief disc within the screw cap). For each 500 psi pressure increase, the screw head was pushed out 1/32 inch. This rough estimation allowed the analyst to verify if the system was being subjected to excess of power, digestion times that were too long or excess of mass sample load.⁸⁰

Procedures

Microwave Oven Calibration

The microwave oven was calibrated in order to determine the power absorbed by the sample at a given power level setting of the unit. Equation 4.2, used for power measurement are derived from the elementary heat capacity theory of a given mass at constant pressure.⁷⁸

$$P = \frac{C_p K \Delta T m}{t} \quad (4.2)$$

where P is the power (W) absorbed, K is the factor converting calories to Joule (4.184 J cal⁻¹), C_p is the heat capacity (cal g⁻¹ °C⁻¹), m is the mass of sample (g), ΔT is the difference between the temperatures after and before microwave heating and t = time (s).

Assuming that the majority of the power delivered by the magnetron to the oven cavity is absorbed by the sample, the power measurement can be indirectly accomplished by measuring the change in temperature of a given quantity of water. The temperature of ten grams of water, placed in the digestion vessel inside the microwave oven, was measured before and after it was submitted to two minutes of microwave radiation. This procedure was repeated for each of the power levels of the unit. Figure 4.6 shows the calibrated power curve of the microwave oven used for the experiments in this work. By a simple mathematical transformation of Equation 4.2 and knowing the heat capacity of the acid used to digest the sample, the final temperature reached by the sample as well as the time of exposure necessary to reach that final temperature can be predicted.

Sample digestion procedure

Soil, sediment and auto catalyst samples were placed inside a dessicator 24 hours before its use in order to remove humidity. For all digestion procedures, a mass of 0.1 g of sample was used. The composition of the acid mixture used was dependent on the sample to be digested. Maximum volumes of acid were fixed at 6 mL and only concentrated trace analysis grade acids were employed. Two digestion bombs were used at a time in the microwave cavity. The first one contained the sample and the acid mixture (in general nitric acid or a nitric acid/ hydrofluoric acid mixture), while in the second, only the acid mixture was placed as a blank. These amounts of sample and acids were below the loading limits advised by the manufacturer in order to avoid excessive build up of gases in the bomb. The power levels were chosen to allow

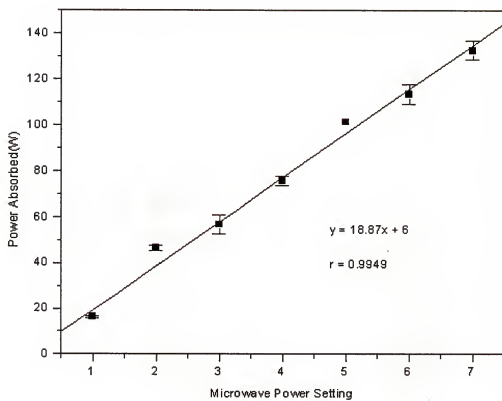


Figure 4.6. Calibrated power curve of the microwave unit.

Temperatures around 170°C and pressure below 1200 psi. Both the digested sample and blank were allowed to cool down before transferring the content to volumetric flasks of appropriate volume. The sample was then diluted with deionized water to decrease the concentration of the remaining acid to a level compatible to the analysis in the atomizer and to adjust the concentration of the analyte.

CHAPTER 5

LASER-EXCITED ATOMIC FLUORESCENCE OF Ge, In and Pt IN A GRAPHITE FURNACE

Brief overview of the importance and current methods to determine ultratrace concentrations of Ge, In and Pt

The need for ultrasensitive methods for the determination of germanium, indium and platinum, especially in the electronic and biomedical fields, has become apparent in recent years. The electrical characteristics of electronic and semiconductor materials are highly dependent on trace amounts of elements including In and Ge. These elements can be present as undesirable impurities or playing a role as dopant elements. Silicon solar cells are an example of how such impurities can have a strong effect in altering the bulk properties of silicon which reduce the minority-carrier diffusion between active centers and also induce contact interface degradation and shunt-resistance effects.⁸¹ The concentration of these impurities in the silicon melt ranges from 10^{12} atoms cm^{-3} to values as high as 10^{17} atoms cm^{-3} corresponding to required detection limits from 0.02 to 2000 part per billion.

In the medical field, important biological and metabolic activities have been recently related to the presence of germanium. Organic compounds of germanium have an important function in adjusting immunity, anti-decrepition and inhibiting the growth of cancer cells. On the other hand, kidney failure has been related to long time exposure to this element.^{82,83} In the case of indium, no important metabolic activity is known to be

related to this element; however, indium compounds are highly toxic, teratogenic and related to damages in the heart, kidney and liver.⁸⁴

Industrial and biomedical applications of platinum, as well as human exposure to this metal, have increased substantially during the last two decades based upon the levels of platinum detected in the environment and in human fluids and tissues.⁸⁵ Most directly affected are workers who are involved in the catalyst recycling industry and patients who takes anti-cancer platinum-based drugs or have platinum implants to join bones. Humans are also exposed to platinum particulate emissions from catalytic converters either near roads or in urban areas.^{85,86}

Small concentration changes of platinum in the environment and human body must be closely monitored since its environmental and biological impacts are still unclear and so has been the object of several studies.^{85,87} Therefore, ultrasensitive analytical methods are very desirable, since normal concentrations of the metal in biological samples are below the limit of detection of most analytical techniques.

Several spectrophotometric methods for germanium, indium and platinum determination in different types of samples have been developed.⁸⁸⁻⁹³ Complexing agents were usually used in order to obtain an analyte derivative with a high molar absorptivity coefficient. The best limits of detection (LOD) reported was in the sub $\mu\text{g mL}^{-1}$ range reflecting the relatively poor sensitivity of these methods. In addition, in order to overcome the poor selectivity, the extraction of the metal from the sample with cation exchange resin or by complex formation has to be carried out, making the experimental procedure laborious.

Sensitive results have been obtained by using electrochemical methods such as direct pulse polarography (DPP) and adsorptive stripping voltammetry (ASV), for the determination of total platinum germanium and indium in simple matrices.⁹⁴⁻⁹⁹ These methods have resulted in limits of detection in the low ng L⁻¹. In those techniques, the analyte must be absorbed on the hanging mercury drop electrode. Particularly in ASV, the analyte is accumulated during a fixed interval of time on the surface of the mercury drop before detection to improve the sensitivity of the method.^{96,97} However, when these methods were used for complex samples, matrix interference problems can arise.⁹⁸ Surface active compounds can adsorb competitively and partially block the electrode surface. Another possibility is the adsorption of other metal complexes with or without electroactive effects, and finally organic complexing materials can bind with the analyte making it non-labile for electrode detection.⁹⁵ Some metals, in particular selenium, were found to interfere seriously in the determination of germanium.⁹⁹ Usually, a previous extraction of the analyte of interest is needed. Detection limits as low as 0.1 ng mL⁻¹ have been reported. Sample pre-treatment procedures, such as digestion in hot acid and ultraviolet irradiation, have been suggested to minimize interferences.⁹⁹

Radiochemical neutron activation analysis with or without coupling with liquid extraction and pre-concentration allows excellent detection power in the ppb range.^{100,102} In addition, no time consuming sample pre-treatment is necessary. However, its low throughput and the specialized nature of the technique limit its use as a routine method.

Flame atomic absorption and atomic emission spectrometry are not sufficiently sensitive techniques for ultratrace analysis.¹⁰³⁻¹¹⁶ Graphite furnace atomic absorption spectrometry has usually been the technique of choice for germanium, indium and

platinum determinations, and therefore, several methods of analysis have been reported with good results obtained in several types of samples despite limitation in linear dynamic range and matrix interferences. Direct sample analysis using atomic absorption spectrometry has been applied for Ge, In and Pt in graphite furnaces with and without pre-coating of the graphite tube.¹¹⁷⁻¹³⁴ Usually a pre-digestion of the biological samples used to minimize absorption of the incident radiation by molecular species or to avoid attenuation of the incident light by fumes released during the furnace programming steps. A careful optimization of time and temperature of the drying and ashing steps in order to eliminate matrix interferences prior to sample atomization and avoid sample pre-treatment have resulted in detection limits in the pg range for Pt and Ge.^{121,130-133} Problems related to correlation between analyte concentration in aqueous standard solution with those in complex samples were unavoidable, making impossible, in many cases, the use of the calibration curve method. For Ge and In, the hydride generation technique has been used to separate the analyte from the matrix and to pre-concentrate it.¹³⁴⁻¹⁴³ Hydride generation was highly dependent upon pH and concentration of the hydride reactant (sodium borohydride) as well as prone to interferences from transition metals which easily decompose the analyte hydride.¹⁴⁴ Indium hydride was very unstable.¹⁴³ The improvements obtained with hydride generation were not significant enough to overcome the labor demands of the procedure.

ICP-MS based methods lead, in general, to excellent detection limits (ng L^{-1}).^{145,149} However, this technique requires digestion or a strong dilution when complex matrices are involved which decrease the analytical power of these methods. The dilution is necessary in order to decrease the content of organic matter that clogs the inlet

of the mass spectrometer as well as contaminates the instrument. Dilution is also important to decrease the concentration of salts which usually causes suppression of the analyte signal.^{150,151}

While there is no LEAFS based method for the determination of germanium in the literature, laser-enhanced atomic fluorescence was first attempted for ultratrace measurement of platinum by Goforth and Winefordner.¹⁵² Electrothermal atomization (ETA) was performed in a graphite cup, leading to an absolute limit of detection of 1 pg for aqueous samples. The graphite cup, which was not an ideal atom reservoir, used by these authors was a factor that could have limited the sensitivity achieved. Even though these authors reported the lowest detection limit at that time, they suggested that a more efficient probing of the atoms generated in the furnace by means of a high repetition rate copper vapor laser could have improved the results. In a recent study,¹⁵² the use of a pyrolytic graphite tube as the atomization reservoir resulted in limits of detection of 70 fg for Pt. However, a low repetition rate laser was employed. In both papers mentioned above, ETA LEAFS was not employed for determination of platinum in complex samples.

The potential of laser-excited atomic spectrometry as a practical method of analysis of indium was first pointed out by Dittrich *et al.*¹⁵⁴ In that work, the authors studied various atomizers, concluding that carbon tube atomizers were the most satisfactory. A laser operating at relatively low repetition rate was employed and a limit of detection of 0.14 pg for In in aqueous standards was achieved. Chekalin *et al.*^{155, 156} achieved limits of detection of 10^{-6} $\mu\text{g g}^{-1}$ using laser-enhanced ionization in a rod-flame system. In a later study, Dougherty *et al.*¹⁵⁷ were able to obtain an 80 fg limit of

absolute detection using a commercial graphite furnace using the right detection scheme and a 80 Hz repetition rate XeCl excimer laser pumped dye laser. Using the same analytical scheme used by Dougherty (410.1/451.1nm) but with a pierced mirror 180° geometry, Vera *et al*¹⁵⁸ were able to achieve an impressive 10 fg absolute limit of detection for In with a Nd:YAG pumped dye laser operating at 30 Hz. Even though a very low limit of detection was reached, improvements could have been made by using a high repetition rate laser source and by choosing an analytical scheme more suitable for the pierced mirror arrangement employed. A better limit of detection (1 fg) has been obtained by using laser-enhanced ionization with previous vaporization in a graphite tube and detection in an acetylene miniflame.¹⁵⁹ The system used dual Nd:YAG pumped dye lasers and a two-step excitation scheme, with the sample being transferred from the graphite tube to the flame by an argon flow.

Results and Discussion

Choice of the Laser Repetition Rate

The pulse repetition rate of the copper vapor laser can be varied over a range of values between 8 and 14 kHz. A change in pulse repetition frequency has a direct result on the laser current. Consequently, any change in the pulse repetition frequency will usually cause the power supply unit to automatically adjust the laser voltage in order to maintain the level of electrical input power and therefore cause changes in the laser pulse energy. A pulse repetition rate versus the laser power plot was made and it is shown in Figure 5.1. A 10 kHz repetition rate value was chosen as the optimum laser setting because it combined the highest repetition rate with high laser power output.

Optical Saturation Conditions

Optical saturation of the excitation transitions of the three elements was not achieved. This was verified by the fact that the fluorescence signal of the analytes was still increasing when the spectral irradiance of the source was increased to maximum. The analytical signal dependence upon the laser irradiance is characteristic of systems not under saturation conditions. In order to verify how far the systems were from the saturation region, approximate values of the spectral irradiance calculated using experimental parameters were compared to the theoretical values estimated using a modified spectral irradiance equation.

The spectral irradiance ($\text{W cm}^{-2} \text{ nm}$) necessary to saturate the excitation transition lines can be approximately estimated by equation 5.1.²⁵ Since the wavelengths used to excite indium, germanium and platinum were higher than 260 nm, the modified saturation spectral irradiance equation for 300 nm wavelength was employed and is given by:

$$E_r = \frac{6 \times 10^4}{Y} \quad (5.1)$$

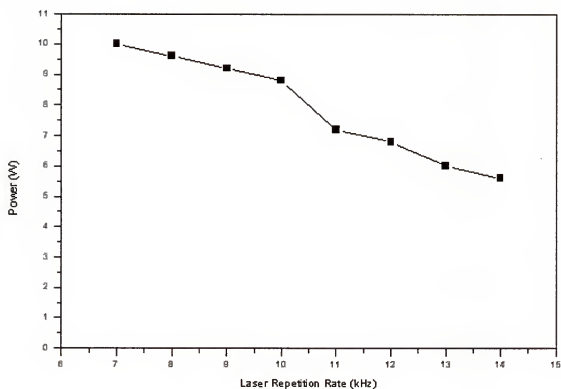


Figure 5.1. Copper vapor laser output power in function of the laser repetition rate.

where E_T is the theoretical spectral irradiance at 300 nm and Y is the quantum efficiency of the fluorescence transition (5.2). For equation 5.1, it is assumed that the atom has 2 energy levels. The quantum efficiency is defined by:

$$Y = \frac{A_{3,2}}{A_{3,2} + A_{3,1}} \quad (5.2)$$

where $A_{i,j}$ are the radiative transition probabilities of the $3 \Rightarrow 2$ and $3 \Rightarrow 1$ transitions. The experimental laser spectral irradiance can be calculated by equation 5.3.

$$E_{EXP} = \frac{P}{\Delta t S \Delta \lambda} \quad (5.3)$$

where P is the laser power (J), S is the cross-sectional area of the rectangular shape laser beam (0.01 cm^2), and Δt and $\Delta \lambda$ are the FWHM pulse length ($40 \times 10^{-9} \text{ s}$) and $\Delta \lambda$ spectral band width (0.01 nm) respectively. Table 5.1 shows the approximate theoretical and experimental calculated spectral irradiances.

Although experimental results have shown that saturation was not achieved, under furnace conditions in all cases, both the calculated theoretical and experimental spectral irradiance values are approximate, indicating that saturation conditions are very close to being achieved. Uneven energy distribution, within the laser beam and collisional deactivations in the furnace could be factors that did not permit saturation of the atomic system.

Imaging Considerations

The imaging of the fluorescence at the monochromator entrance slit was found to be critical. The image of the tube consisted of a bright ring (black body emission) surrounding a dark circle (image of the center of the tube). As described in Chapter 4, the entrance slit was of rectangular shape and kept within the dark circle of the image. The slit was blinded with fixed blades in the horizontal direction while in the vertical direction, adjustments could be made (Figure 5.2). The slitwidth vertical aperture (in mm) was optimized by studying the fluorescence signal to background ratio of lead atomized at 2000⁰C (Figure 5.3). The analytical scheme used for lead is the same described in Chapter 6. According to the plot, the optimum slitwidth was 0.5 mm. While smaller slitwidths the imaging of the fluorescence in the aperture is blocked or difficult to optimize, with larger slitwidths the contribution of the blackbody emission degrades S/B ratio. This value was fixed and used for all the studies in this dissertation.

For every detection wavelength, it was also necessary to carefully optimize the position of the pair of focusing lenses in order to spatially resolve the blackbody emission from the atomic fluorescence signal. In addition, the position of the laser beam passing through the graphite tube was optimized. Studies of the atomization event in the graphite tube, performed by Gilmudinov *et al.*^{60,162} using shadow spectral filming technique, have shown that the dynamics of the formation of atomic vapor varies spatially as a function of time in a different fashion depending upon the element. Therefore, it is important to probe the area of the analytical zone where the atomic population is denser during the

Table 5.1. Comparison between the calculated values of the experimental ($E_{\lambda\text{EXP}}$) and theoretical ($E_{\lambda\text{T}}$) spectral irradiances.

Element	$E_{\lambda\text{EXP}}$ ($\text{W cm}^{-2} \text{ nm}$)	$E_{\lambda\text{T}}$ ($\text{W cm}^{-2} \text{ nm}$)
In	5×10^5	1.2×10^5
Ge	1.25×10^5	3.6×10^5
Pt	7.5×10^5	4.8×10^5

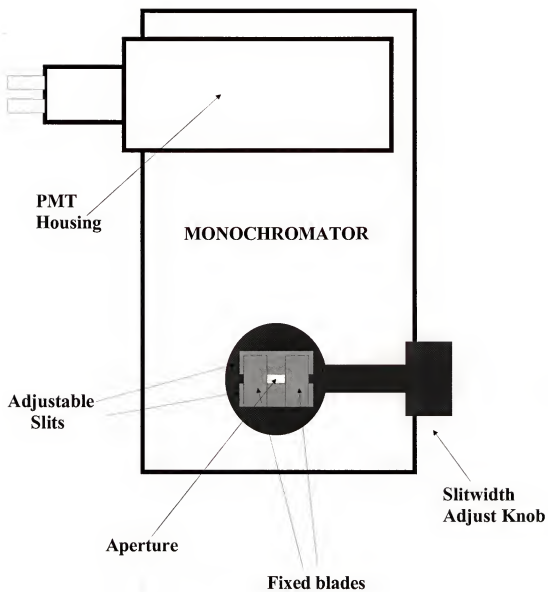


Figure 5.2. Modified slitwidth.

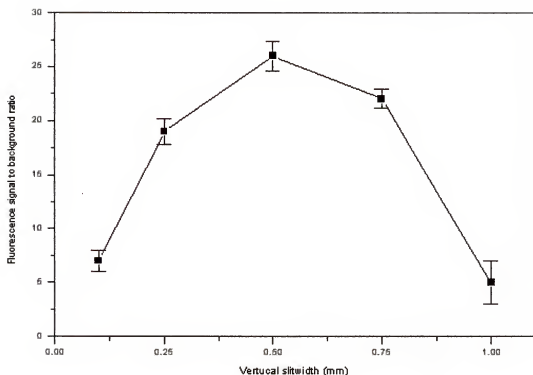


Figure 5.3. Signal to background ratio in function of the monochromator's slitwidth. Results based on the fluorescence signal of 10 pg of lead atomized at 2000°C.

time interval limited by the initial build up and the diffusion of the atomic vapor. Since the area of the center of the tube that can be imaged into the slit is small, a simple comparison of the signal to noise ratio obtained with the laser beam passing through three or four different areas of the analytical zone was made. The position which gave the best S/B was chosen.

Choice of the Fluorescence Analytical Schemes

A careful choice of the fluorescence analytical scheme, specially for methods involving atomization in tube atomizers, is necessary to maximize the analyte signal and minimize the level of blackbody radiation reaching the entrance slit and therefore maximizing signal to background ratio.

First, the analytical schemes must originate from a low energy level or from the ground state in order to ensure high atomic population. The excitation wavelength was tuned exactly to the atomic transition, using a hollow cathode lamp as the atom source (see Chapter 4) in order to maximize the signal. Second, the detection wavelengths were below 350 nm, minimizing blackbody radiation, and the difference between the excitation and detection wavelengths were chosen to be as large as possible to reduce stray light contribution to the background signal. Finally, the wavelengths of the excitation transitions were chosen to be in the optimum range of the Cu-laser pumped dye source, ensuring a reasonable energy output. For germanium and platinum different analytical schemes were evaluated (Table 5.2). The Stokes direct line fluorescence scheme was found to be a better choice over the Stokes stepwise-line fluorescence

schemes. For germanium, the main scheme was the one with detection at 326.95 nm. This direct line Stokes scheme had a fluorescence intensity stronger than the direct line Anti-Stokes with detection at 265.16 nm and equivalent to the direct line Stokes with detection at 275.45 nm. However at 275.45 nm, the background level is higher than at 326.95 nm due to stray light contribution. Figures 5.4, 5.5 and 5.6 show the principal fluorescence analytical schemes chosen for indium, germanium and platinum respectively.

Atomization Techniques and Furnace Parameters.

In the electrothermal atomization technique, furnace parameters and the quality of the material of the atomizer are intimately related with the atomization efficiency.⁴⁸ Therefore, these parameters have crucial influence on the intensity and shape of analytical signals and must be studied and compared. Minimization of matrix interferences is highly desirable in order to avoid analyte loss during the atomization step, and minimize both molecular background and attenuation of both the incoming laser radiation and the fluorescence by the fumes released by the matrix. A special effort was made in the optimization of the pre-atomization cycle as well as in the choice of the best atomization technique to eliminate as much as possible pre-digestion and pre-separation procedures. With wall atomization, the sample was deposited directly on the wall of the tube to be atomized. On the other hand, when platforms were employed, the sample was kept away from the wall in order to achieve a delay in the sample vaporization - atomization and consequently, analyte atomization under more isothermal conditions.

Table 5.2. Evaluation of possible excitation-detection schemes of Ge and Pt.

Element	Fluorescence analytical scheme ($\lambda_{\text{exc}}/\lambda_{\text{fl}}$) ^c	Signal to background ratio (S/B)
Pt ^a	270.24 nm/277.10 nm ^d	4.4
Pt ^a	270.24 nm/289.80 nm ^d	3.8
Pt ^a	270.24 nm/320.40 nm ^e	28.8
Ge ^b	269.13 nm/265.16 nm ^f	5.6
Ge ^b	269.13 nm/275.45 nm ^e	10.4
Ge ^b	269.13 nm/326.95 nm ^e	19.1

^aAtomization at 2200^oC of the 10 ng g⁻¹ aqueous solution of the analyte.

^bAtomization at 2300^oC of the 10 ng g⁻¹ aqueous solution of the analyte.

^cExcitation (λ_{exc}) and fluorescence (λ_{fl}) wavelengths.

^dStokes stepwise-line fluorescence scheme.

^eStokes direct-line fluorescence scheme.

^fAnti-Stokes direct-line fluorescence scheme.

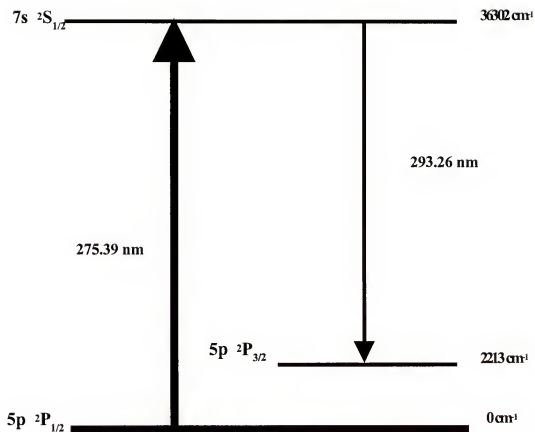


Figure 5.4. Energy level diagram for the fluorescence determination of indium.

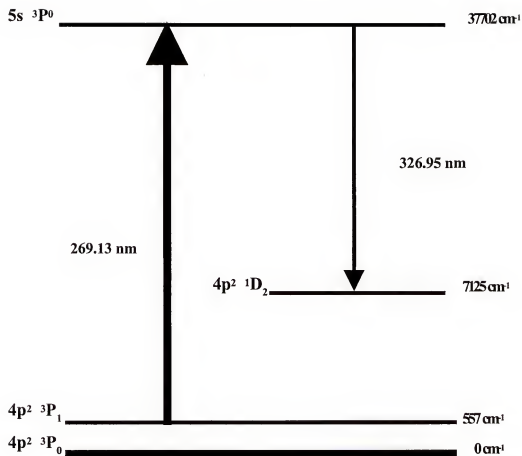


Figure 5.5. Energy level diagram for the fluorescence determination of germanium.

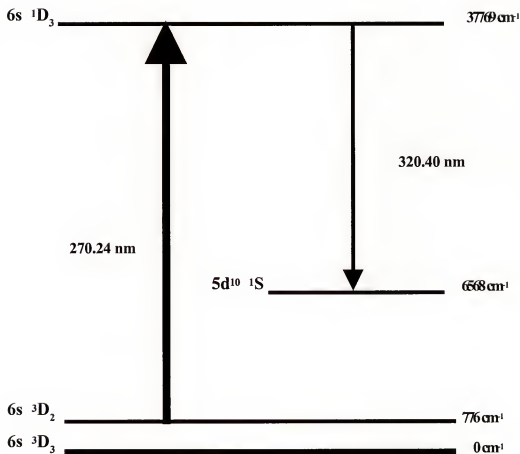


Figure 5.6. Energy level diagram for the fluorescence determination of platinum.

The platform minimized the probability of the analyte atoms to form molecular compounds after atomization.^{24,43} However the use of platform technique does not always guarantee best atomization performance. It is dependent on the element being analyzed⁷³ and therefore comparative studies between the techniques must be done.

During the temperature optimization studies, aqueous solutions of analyte were employed. The sample was dried using a two step drying step and no ashing was employed. The choice of atomization temperature was made as a function of signal to background ratio. In general, a temperature high enough to achieve an efficient atomization but low enough to minimize the contribution of the blackbody radiation were desirable.

Indium.

Indium is relatively reactive element making it strongly affected by matrix interferences and very sensitive to the atomization parameters. From GF-AAS literature,⁴⁸ it is well known that the quality of the carbon surface of the atomizer governs the signal sensitivity. In the particular case of indium, more sensitive results have been obtained using non-pyrolytic graphite tubes instead of coated ones.^{50,55,58} The signal increase is attributed to the active role of carbon in the reduction of indium oxides to atomic indium. Aware of that fact, a comparative study of the fluorescence signals of indium obtained using pyrolytic and non-pyrolytic graphite tubes was performed. Considering only atomization from the walls, a better result was obtained with a non-pyrolytic than with a pyrolytic graphite tube. For 10 pg of indium deposited, an increase in peak area was around 30%. For both types of graphite, atomization temperature curves, in terms of signal to background ratio, had practically the same profile (curves B

and C of Figure 5.7), and similar single fluorescence peaks were observed. With the more isothermal conditions obtained with the platform atomization technique, indium S/B values were around six times higher than those obtained with wall atomization (Curve A of Figure 5.7). McAllister¹⁶¹ has pointed out that losses of indium in oxide form (In_2O) during pre-atomization steps, could be minimized by using platforms. Based on those results, platform atomization and an atomization temperature fixed at 1600°C were used throughout the work. Maximum ashing temperatures were observed to be around 800°C for platform atomization as it can be seen in Figure 5.8.

Germanium.

Low sensitivities for germanium when using the graphite tube as the atomization cell have been attributed to losses of this element as volatile GeO .^{117,134} Since GeO is formed by the reduction of GeO_2 in the presence of hot carbon in the furnace, the ashing temperature has an important influence on the final atom density of the probed volume and consequently on the analyte fluorescence magnitude.

In addition to control of the ashing temperature, we chose platform atomization and pyrocoated graphite tubes to minimize germanium losses and maximize germanium atomization. Dittrich *et al*,¹¹⁷ using GF AAS, observed a more efficient atomization of germanium using the platform technique rather than wall atomization. By using the platform, evaporation and sublimation of GeO are minimized during the ashing step, and so more GeO molecules will be more likely to dissociate in the hot gas in the graphite tube. Pyrocoated graphite tubes reduces the contact surface of the graphite, minimizing

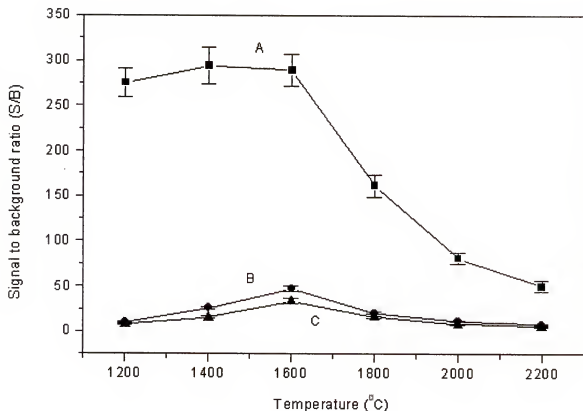


Figure 5.7. Atomization temperature curves for 10 pg of indium. (A) Atomization curve with platform technique, (B) Atomization curve with wall atomization in non-pyrolytic graphite tube, (C) Atomization curve with wall atomization in pyrolytic graphite tube.

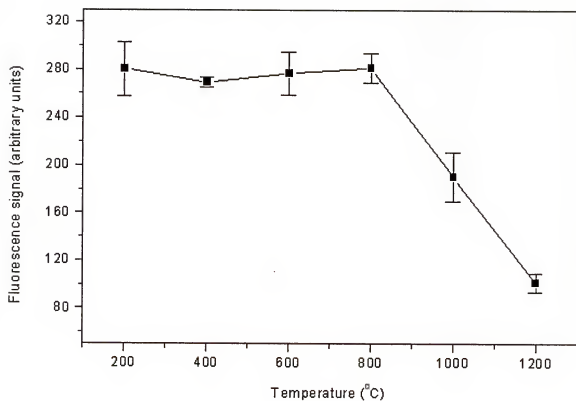


Figure 5.8 Ashing temperature curve for indium. Fluorescence signal of 10 pg of indium atomized at 1600°C using platform atomization.

both, the premature reduction of GeO_2 to GeO^{121} and minimizing the trapping and retarded release of analyte due to adsorption of analyte into the porous surface of the non-pyrolytic graphite.⁴³ Figure 5.9 shows comparative atomization temperature profiles that confirms the relative inefficiency of wall atomization (about 45 % less sensitive than platform atomization) as well as the advantage of the coated over the non-coated graphite tube. Considering these results, platform atomization and a temperature of 2400°C were chosen and used for germanium throughout the work. The result of the ashing studies using the optimized parameters for atomization is shown in Figure 5.10. Maximum ashing temperature was observed to be 400°C .

Platinum.

Figure 5.11 shows the atomization curves of platinum for two different atomization techniques. With wall atomization more intense fluorescence signals were observed. The best signal to background ratio was observed with temperature of 2000°C (curve A). A similar temperature profile (curve B) with similar peak shape was observed when the platform technique was used. However, the intensity of the fluorescence was lower (about 44% of the peak area observed for wall atomization).

Figure 5.12 shows clearly that ashing at temperatures as high as 1400°C can be used without loss of analyte. Further experiments confirmed that ashing times up to 30 s could be used for temperatures above 1000°C without analyte loss. Those ashing parameters are more than enough to eliminate organic matrix components responsible for the molecular background prior to the atomization step.

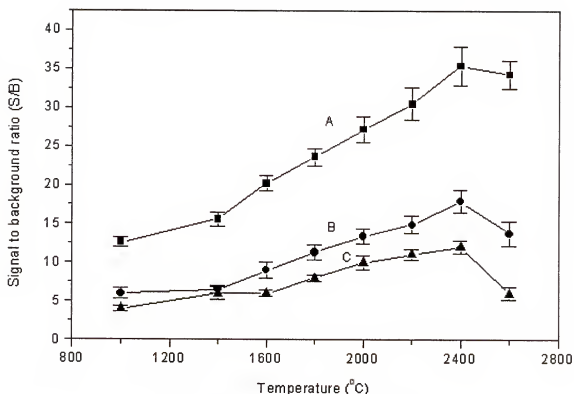


Figure 5.9. Atomization temperature curves for 5 pg of germanium. (A) Atomization curve with platform technique, (B) Atomization curve with wall atomization in pyrolytic graphite tube, (C) Atomization curve with wall atomization in non-pyrolytic graphite tube.

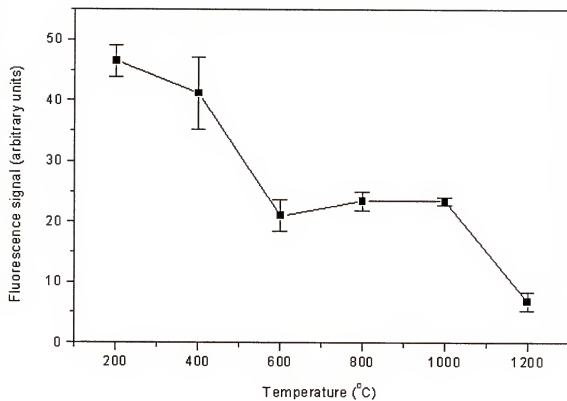


Figure 5.10. Ashing temperature curve for germanium. Fluorescence signal of 5 pg of indium atomized at 2400°C using platform atomization.

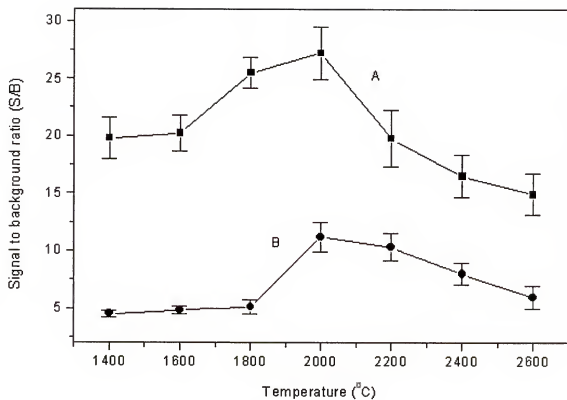


Figure 5.11. Atomization temperature curves for 2 pg of platinum. (A) Atomization curve with platform technique, (B) Atomization curve with wall atomization in pyrolytic graphite tube.

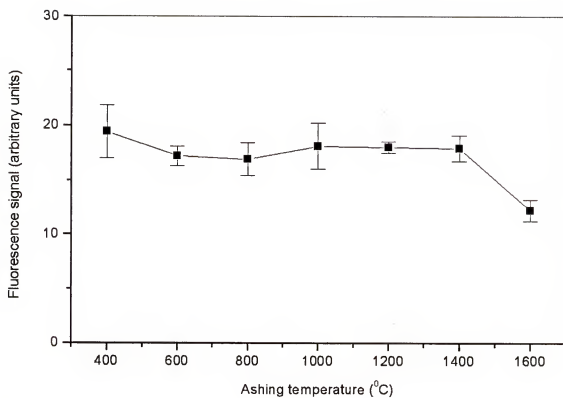


Figure 5.12 Ashing temperature curve for platinum. Fluorescence signal of 2 pg of platinum atomized at 2000°C using platform atomization.

The heating programs chosen to be used for the aqueous standards of Pt, Ge and In are listed in Table 5.3. These heating programs were used throughout this work excluding when variations were included to analyze real samples or for studies with chemical modifiers, acids and bases and potential inorganic interferents.

Limiting Noises

Representation of the noises associated with the fluorescence measurement of indium, platinum and germanium are shown in Figures 5.13. These profiles were obtained using optimized atomization conditions. Results show that for In, stray light is the dominant noise, while for both, Ge and Pt, blackbody radiation emission is the dominant noise. Further experiments using blood as biological matrix indicated that after the proper ashing treatment, the levels of scattered light from matrix particulates in the gas phase is not relevant.

Influence of Acids and Bases

The influence of acids and NaOH on the analyte signals was studied. The objective was to evaluate the effect of such compounds on the overall behavior of the analyte during the pre-atomization and atomization cycles, ensuring a safe choice of acid or base to be used for sample dissolution as well as for the digestion of complex samples. Ashing steps with temperatures of 800⁰C for In, 400⁰C for Pt and 1000⁰C for Ge were included in the heating program displayed in Table 5.3.

Table 5.3. Heating programs for water samples analysis.

Step ^a	Temperature (°C)/Ramp time (s)/Hold time (s)		
	In	Ge	Pt
Dry 1	100/20/15	100/5/20	120/10/10
Dry 2	300/20/20	150/5/10	250/10/20
Ash	-	-	-
Atomization ^{b,c}	1600/0/15	2400/0/15	2000/0/15
Cleaning	2500/1/6	2700/1/6	2600/1/6
Cool down	20/10/10	20/10/10	20/10/10

^a300 mL min⁻¹ argon flow, except for argon flow, except for the atomization step.

^bNo argon flow.

^cSignal record.

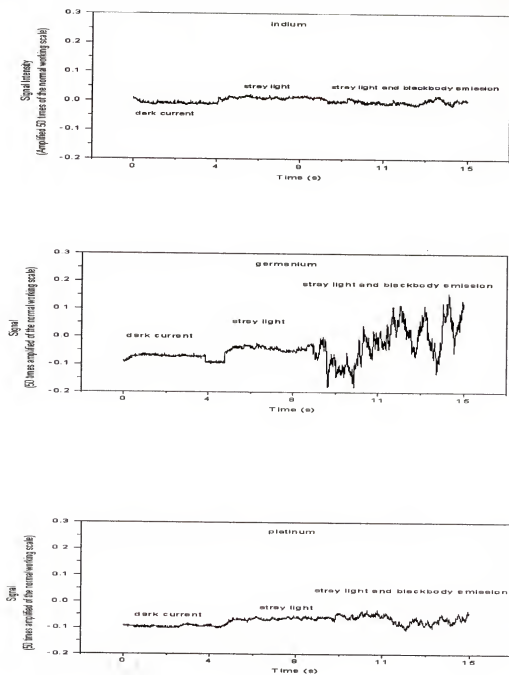


Figure 5.13. Representations of the noises associated with the measurement of In, Ge and Pt.

Indium.

While a decrease in the signal was observed with HCl (especially at higher concentrations of acid), probably due to the formation of volatile InCl_3 , the presence of hydrofluoric acid did not seem to affect the analyte signal. A decrease in fluorescence intensity was also observed with sodium hydroxide at all concentrations tested. An increase in the background with increasing concentration of sulfuric acid was also observed decreasing signal to background ratio. However, the most important observation was the six-fold increase in signal obtained in the presence of nitric acid 0.01, 0.1 and 1 M. Therefore, HNO_3 may be acting as a chemical modifier, stabilizing indium during the heating process inside the graphite furnace.

Germanium.

Some authors have reported enhancements of germanium atomic absorption signals in non-pyrolytic graphite tubes in the presence of nitric acid and sodium hydroxide.^{117,119-121} These results are related to an increase in the Ge atomic population during atomization and were attributed to formation of thermally stable compounds, minimizing analyte losses due to reduction reactions from direct contact with carbon of the tube. In our studies, the presence of HNO_3 and NaOH at final concentrations from 0.01 to 0.1 M had little influence on the fluorescence intensity of the analyte. The same was observed for sulfuric acid; however, in this case, the blanks containing relatively a high concentration of H_2SO_4 showed increased background levels. Since loss of analyte in the form of GeCl_2 is expected, hydrochloric acid would not be a good choice for pre-treatment of samples.

Platinum.

The fluorescence signals of 10 ng g^{-1} of Pt prepared in water and in 0.01, 0.1 and 1.0 M of acid or base were measured. For H_2SO_4 at 0.1 and 1.0 M, the Pt fluorescence signal was smaller than the aqueous standard solution with almost total depression of the signal at 1.0 M. Also, a background signal, which increased proportionately with the concentration of the acid, was observed. In the nitric acid case, the signal decreased approximately 50 and 80 % for 0.1 and 1.0 M, respectively. Pt solutions with 0.01 M HNO_3 had analytical responses statistically similar to the aqueous standards. No signal difference from the aqueous standard was noticed in solutions containing 0.01 and 0.1 M of NaOH. However, all Pt solutions containing the base at 1.0 M resulted in reduced fluorescence. Analytical signals of aqueous Pt standards were statistically similar with those solutions containing HCl at 0.1 and 0.01 M. Reductions of approximately 20% were obtained for solutions with 1.0 M HCl. No interferences were obtained for HF at all concentrations tested.

It is clear by the evaluation of the results above that H_2SO_4 and HNO_3 cause problems if used to digest any platinum containing samples. HCl and NaOH can be employed for the treatment of samples, but the final concentration must be kept at levels of 0.1 M or below in order not to affect the fluorescence response. Hydrofluoric acid can be readily employed in concentrations up to 1.0 M.

Chemical Modification Studies

Chemical modification studies were performed in order to find an appropriate chemical modifier capable of stabilizing indium and germanium during the pre-

atomization cycle, achieving increased analyte fluorescence signals and improved ashing temperature limits. Ultimately, the objective was to minimize the influence of the matrix on the sensitivity of the calibration curves, achieving improved limits of detection with easier calibration procedures for the analysis of real samples. Chemical modifiers were not evaluated for platinum because ashing temperature studies demonstrated that temperature as high as 1400°C can be used without losses of analyte. This behavior can be explained by the relatively less reactive properties of platinum (noble element). Therefore, it does not form volatile species with carbon or oxygen during the pre-atomization cycle.

Chemical modifiers were tested in two ways. First, the aqueous analyte solution was mixed with the chemical modifier solution and submitted to a normal furnace run. The chemical modifier concentration excess was varied. Fluorescence signals of the chemical modifier solutions were measured as blanks. In a second approach, called one drop coating method, volumes of 100 µL of a 1000 µg g⁻¹ solution of the chemical modifier was sampled in the furnace and dried before the 10 µl of analyte aqueous solution or water (blank) was inserted into the furnace. Organic matrix modifiers were dried at 800°C while metallic modifiers were dried at 1000°C. For the coating, a 100 s ramp time was employed.

Indium.

Based on the observations obtained with nitric acid in the previous section, the behavior of the indium fluorescence signal was studied as a function of the concentration

of the acid in the analyte solution. The experimental results showed that for a fixed 10 ng mL⁻¹ final concentration of indium, the maximum increase in the fluorescence intensity was observed with 0.02 M of HNO₃ and remained constant up to 1 M concentration of the acid (curve A of Figure 5.14). In order to investigate the role of nitrate in stabilization, the experiment was repeated using sodium nitrate instead of nitric acid in the analyte solution (curve B of Figure 5.14). Surprisingly, in this case, the maximum signal increase was only 30% of that observed with HNO₃. In addition, above 0.05 M, the signal intensity dropped until the fluorescence was totally quenched at 0.2 M salt concentration.

Several chemical modifiers, known from the graphite furnace atomic absorption literature, were evaluated and compared with the results achieved with nitric acid.

Organic matrix modifiers like ascorbic and oxalic acids form both active and thermally stable carbon species at different temperature ranges during the furnace heating process.

Those carbon species are responsible for the reduction of indium oxides (In₂O, In₂O₃) to atomic indium, minimizing losses of the analyte as molecular vapors.⁵⁰ On the other

hand, metallic matrix modifiers were believed to stabilize indium either by formation of M/In metallic systems, where M is the metallic modifier,^{162,163} or stabilizing the analyte

by decreasing its vapor pressure and thus increasing its thermal stability by formation of a solid solution of the analyte in the excess chemical modifier.¹⁶⁴

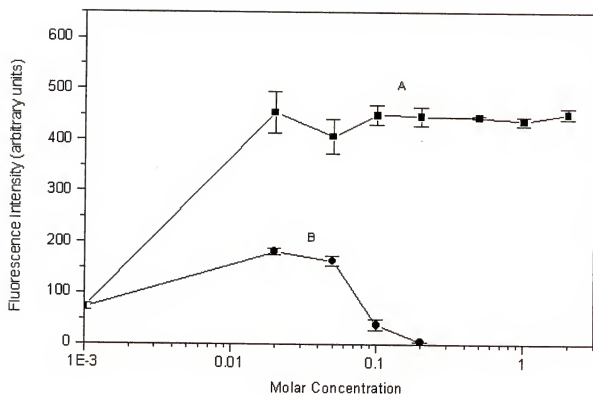


Figure 5.14. Effect of increasing concentrations of (A) nitric acid and (B) sodium nitrate in the fluorescence intensities of 10 ng mL^{-1} of indium solution.

When the chemical modifier was mixed with the analyte in the solution, the amount of indium (10 pg) was fixed, while the amount of the chemical modifiers was varied from 0.1 ng to 0.1 μg (from 10^2 to 10^5 times excess). The analyte peak area was monitored at a fixed atomization temperature of 1600°C . The results are displayed in Table 5.4. All results were compared with the fluorescence signals of both aqueous solutions of indium and indium solutions prepared in nitric acid. Effects on the ashing temperatures are also shown in Table 5.4. Improvements of signal comparable to those obtained with nitric acid were also observed for ascorbic acid, oxalic acid, palladium and lanthanum. For Pd and La, increases in the maximum ashing temperature were observed. Similar ashing temperature improvements were obtained with tungsten and tantalum. However, fluorescence signals were, respectively, about 80 and 60% of those observed with HNO_3 . Corrosive effects on the graphite caused by lanthanum were observed, as expected. These effects are well described in the literature and they are claimed to be caused by formation of carbides.¹⁶⁵

Studies with pre-coating of the graphite furnace were also performed. For all metallic chemical modifiers, the pre-coating procedure did not result in an increase of the analyte fluorescence intensity. On the contrary, the signals were lower than those observed with an aqueous solution of indium. Since graphite plays an important role in the stabilization of indium, those observations could be explained by the metal coating preventing contact of the analyte with the walls of the tube. On the other hand, the results obtained in pre-coated tubes with organic chemical modifiers were better than for the non-coated graphite tube, probably because of the layer of carbon deposited during

Table 5.4. Effects of different matrix modifiers on the fluorescence signal of indium.^{a,b}

Matrix modifier (MM)	Concentration of chemical modifier in the analyte solution used to achieve maximum Signal/Blank ratio	Signal/Blank for chemical modifier-analyte mixture in solution ^{c,d}	Maximum ashing temperature (°C) ^e	Signal/Blank for MM pre-coating procedure ^{f,g}
No MM	-	1.00	800	1.00
HNO ₃	0.02 molar	5.75	1000	—
Ascorbic acid	10 µg mL ⁻¹	5.54	1000	1.73
Oxalic acid	10 µg mL ⁻¹	5.22	1000	1.52
Palladium	1 µg mL ⁻¹	5.53	1200	0.50
Tungsten	10 µg mL ⁻¹	4.58	1200	0.36
Tantalum	10 µg mL ⁻¹	3.47	1200	0.35
Lanthanum	10 µg mL ⁻¹	5.60	1200	0.9

^a Analyte concentration fixed at 10 ng mL⁻¹^b Results obtained in platform atomization in a pyrocoated tube.^c Matrix modifier previously mixed with the analyte in solution.^d Signal/Blank is the ratio between the fluorescence signal of the analyte solution for a specific experimental condition and the fluorescence signal of the respective blank solution.^e Maximum ashing temperature where no significant loss of analyte is observed when chemical modifier is mixed in the analyte solution.^f Results obtained in platform atomization in a pyrocoated tube coated with matrix modifier.^g Signal/Blank is the ratio between the fluorescence signal of the aqueous analyte solution and the fluorescence signal of water used as the blank.

The pre-coating process. However, the improvements observed were still inferior to those obtained with chemical modifiers mixed with the analyte in solution.

Although the blank signal of the chemical modifiers used in these experiments were the same as with deionized water, there is always concern with contamination of the sample when chemical modifiers were used, especially when ultratrace analysis was intended. The contamination risk is high because usually a large excess of the chemical modifier is employed, and consequently, the reagents used should be of high purity. Since no improvements better than these obtained with nitric acid were achieved, trace analysis grade HNO_3 was employed as the chemical modifier.

Germanium.

Dittrich *et al.*,¹¹⁷ working with non-pyrolytic tubes and wall atomization, observed an increase in atomic absorbance of Ge when an excess of metallic nitrate was present. We evaluated three different concentrations of several metal nitrates reported in Dittrich's work and tested their effect using our experimental conditions. From Table 5.5, we can conclude that in the presence of all metal nitrates mixed with the analyte solution at $1 \mu\text{g g}^{-1}$ level, no significant, change in the germanium fluorescence signal is seen. At $100 \mu\text{g g}^{-1}$ chemical modifier concentration, a decrease of signal was observed for LiNO_3 while no changes occurred for Pd, Mg and Mg/Pd nitrates. Concentrations higher than $500 \mu\text{g g}^{-1}$ resulted in a decrease in fluorescence. Similar results were observed for oxalic acid. The apparent disagreement with Dittrich's results is explainable by the use, in our case, of a pyrocoated tube and a platform atomization which minimized the Ge losses with no need of use of chemical modifiers. The reduced

Table 5.5. Matrix modifier effect on the fluorescence peak area of germanium^{a,b}

Matrix modifier	Signal-Blank ratio for chemical modifier-analyte mixture in solution ^{a,c}	
	Concentration	
	1 $\mu\text{g g}^{-1}$	100 $\mu\text{g g}^{-1}$
-	1.0	1.0
H ₂ C ₂ O ₄	0.95	0.98
Pd(NO ₃) ₂	1.02	0.96
LiNO ₃	0.93	0.46
MgNO ₃	0.98	0.93
Pd/MgNO ₃	0.96	0.95

^a Germanium standard solution 2 ppb prepared in water solution

^b Results obtained in platform atomization in a pyrocoated tube.

^c Signal/Blank is the ratio between the fluorescence signal of the analyte solution for a specific experimental condition and the fluorescence signal of the respective blank solution.

fluorescence observed may be either a result of collisional deactivation of analyte atoms in the excited state, due the presence of excess of atomic and molecular species from the salts in the plasma formed during atomization. Pre-coating the tube with PdNO_3 did not affect the magnitude of the analyte signal.

In terms of improvements in ashing temperatures, Pd/Mg gave the best result. Palladium- magnesium is a well-known matrix modifier used to thermally stabilize some elements, among them germanium, allowing the use of higher ashing temperatures with minimal analyte losses. This approach becomes essential when the analyte must be determined in matrices with large amounts of organic matter such as blood. Most of the time, no matrix modifier seems to be necessary in simple matrices and in those cases, ashing temperatures up to 400°C can be used. On the other hand, the presence of Pd-Mg allows the use of ashing steps up to 1000°C without significant losses of analyte. Figure 5.15 shows a comparison between the ashing temperature curves obtained with and without the Pd-Mg chemical modifier.

Influence of Salts and Potential Interferents

The influence of several compounds on the fluorescence signals of the analytes was investigated. It was not the intention to do a thoroughly study involving all possible potential interferents. The concomitant species were chosen either because they are naturally found in real samples such as biological and semiconductors or because they are known interferents in graphite furnace or hydride generation atomic absorption techniques. The range of the concentration of the concomitant species was varied from 1 to 1000 times the concentrations of the analyte were.

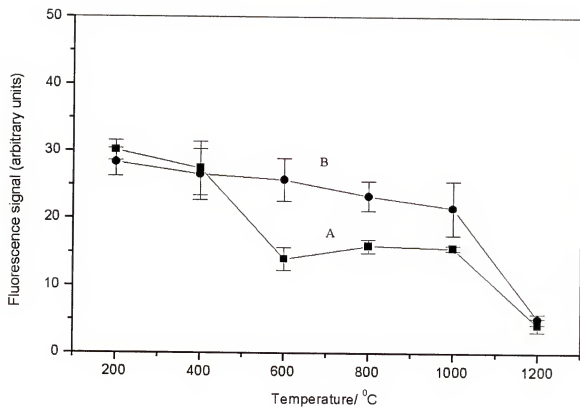


Figure 5.15 Ashing temperature profile of germanium: (A) No chemical modifier
(B) Pd/MgNO₃ chemical modifier.

The presence of silicon at any of the concentration tested had no effect in the fluorescence signals of both germanium and indium. Similar observation were observed for arsenic and selenium which are strong interferents in hydride generation methods for germanium and indium.¹⁴⁴

In the presence of chloride, the germanium fluorescence signal shows a decrease of around 50% when the excess of concomitant is above 100 times. For indium, the decrease in signal was 15 % and 60 % for 100 and 1000 fold excess of NaCl, respectively. For platinum samples, NaCl levels up to 1000 fold higher than the analyte can be directly analyzed without any problems related to decreased sensitivity, which is well suited for some biological samples where the salt concentration levels are below such values. Significant decrease of signal is observed for synthetic samples containing 0.1 M of the salt. Results obtained with NaCl can be explained by collisional deactivation of analyte atoms in the excited state, due to the presence of excess of atomic and molecular species from the salts in the analytical zone formed during atomization. For indium and germanium, the formation of volatile chlorides during the heating process in the furnace can also account for losses of indium and germanium.

Analytical Figures of Merit

Calibration curves were obtained using the conditions optimized for each of the elements. Peak areas of the time profiles were employed to measure the intensities of fluorescence. Peak area measurements turned out to give better reproducibility than peak height measurements. In addition, by using peak area, there was easier correlation of analyte fluorescence signals from aqueous standards with those obtained from complex

samples. Neutral density filters were used to maintain the linearity of the detector within the range studied. Calibration curves of indium, germanium and platinum are shown in Figures 5.16, 5.17 and 5.18. The volume of sample was fixed at 10 μL and each point in the curve was the average of at least 4 measurements. The representative value of the background was obtained by the average of 16 blank measurements. Since the objective was ultratrace determinations, the maximum amount of analyte tested was fixed at 1 ng (10 μL of 1 $\mu\text{g g}^{-1}$ analyte solution). This was done in order to avoid overloading the furnace with excessive amounts of analyte relative to the amount that is intended to be determined. In Table 5.6, analytical figures of merit are shown. All three curves (Figures 5-16-5.18) showed linear behavior over the range of amounts of analyte studied. Absolute limits of detection were calculated based on the $\text{ALOD} = 3s_b/m$, where s_b is the standard deviation of 16 blank measurements and m is the sensitivity of the calibration curve. All limits of detection were in the femtogram range. Precision studies were made with samples with 10 ng g^{-1} of analyte. These precision studies were performed with aqueous as well as with blood samples in order to verify the effect of a complex matrix on the precision of the measurements. The confidence level was 99.9 % with 10 sample measurements. Precision was around 2 times worse for blood samples than for aqueous samples.

Fluorescence temporal profiles of germanium, indium and platinum in aqueous solutions are shown in Figure 5.19, 5.20 and 5.21. These profiles were achieved using the optimized experimental conditions for maximum sensitivity.

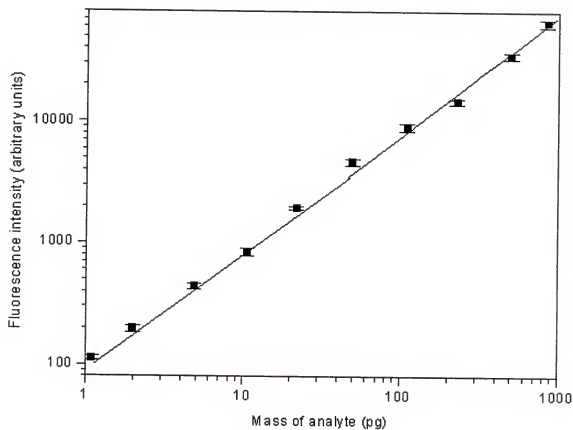


Figure 5.16. Calibration curve for indium.

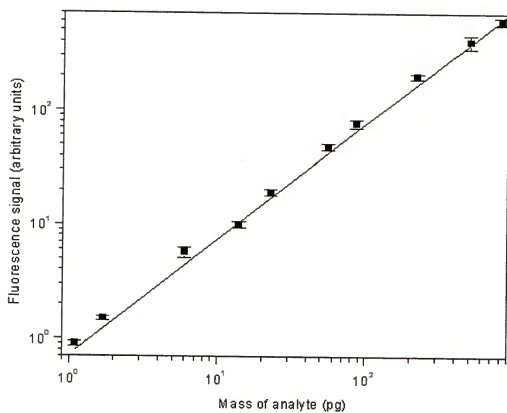


Figure 5.17. Calibration curve for germanium.

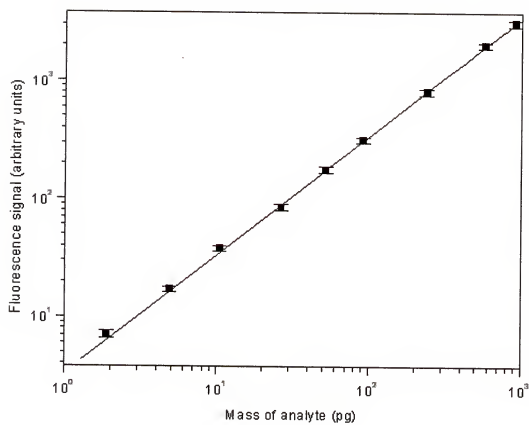


Figure 5.18. Calibration curve for platinum.

Table 5.6. Analytical figures of merit of the ETA-LEAFS methods developed for In, Ge and Pt.^{a,b}

Element	Absolute limit of Detection (ALOD) ^c (fg)	Linear Dynamic Range (LDR) ^d	Coefficient Correlation ^e of the Curve	Precision ^f water samples (blood samples) (%)
In	1	4	0.9980	3.5 (8.0)
Ge	670	3	0.9981	4.1 (9.1)
Pt	55	4	0.9991	4.5 (8.0)

^aResults obtained with the optimized conditions to achieve best S/B ratio.

^bResults obtained with aqueous solutions of the analyte except for the precision studies, where blood samples with analyte were also used.

^cAbsolute limit of detection estimated using the equation $ALOD = 3s_b/m$, where s_b is the standard deviation of 16 blank determinations, and m is the inclination of the calibration curve

^dValue of the linear dynamic range obtained over the range of concentrations studied.

^eCoefficient of correlation is the percent relative to standard deviation.

^fResults of the precision studies obtained at 10 ng g⁻¹ level of analyte.

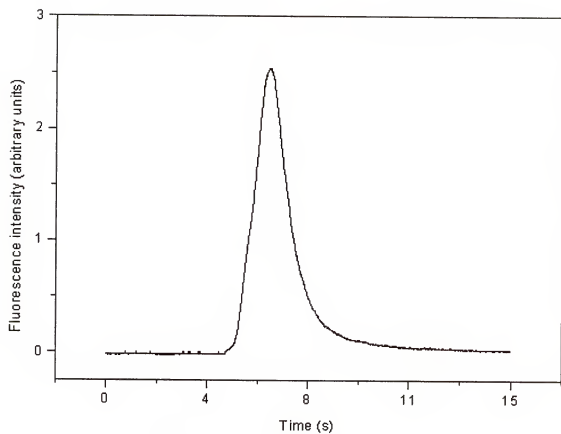


Figure 5.19 Fluorescence time profile of 5 pg of indium prepared in a aqueous solution of nitric acid (0.05 M).

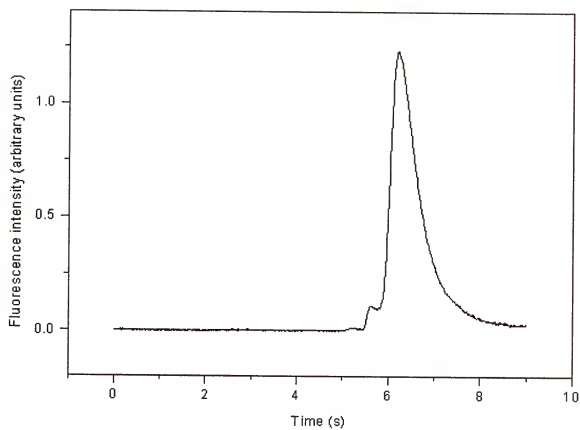


Figure 5.20. Fluorescence time profile of 5 pg of germanium prepared in water.

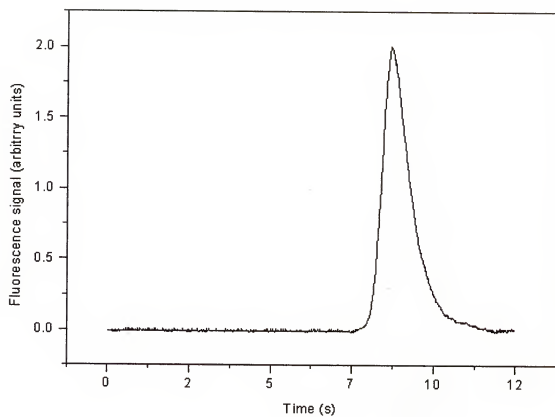


Figure 5.21. Fluorescence time profile of 8 pg of platinum prepared in water.

Sample Analysis

Several types of real samples were analyzed in order to evaluate the electrothermal atomization laser atomic fluorescence methods developed. The optimized heating programs for each type of sample are displayed in the previous tables describing the determination of Ge, In and Pt in the complex samples.

The two types of samples analyzed are described in terms of the analyte content. First, laboratory prepared samples were those where the matrix originally did not contain the analyte of interest. Those matrices were spiked with a microvolume of the analyte solution of known concentration. In these cases, the original sample without the analyte spiking was measured as blanks. In order to be sure that the original sample did not contained detectable quantities of analyte, a comparison between the signal obtained with the laser tuned and detuned by 0.05 nm from the fluorescence transition were made. If no significant differences were found between the two runs, the sample was considered analyte free. The experimental analyte recovery calculated based on the expected analyte amount of the laboratory prepared sample. There were some cases where the concentration of analyte in the laboratory prepared sample were determined by ICP-MS in order to be compared with the ETA-LEAFS method. Second, standard materials with either certified or non-certified values of the analyte were evaluated. The experimental values were directly compared with the certified or non-certified values. In some cases, the non-certified value of the analyte was determined by ICP-MS in order to be compared with the experimental values obtained by ETA-LEAFS.

The percent of recovery was given by:

$$\% \text{Recovery} = (\text{Analyte experimental value} / \text{Analyte reference value}) \times 100$$

The analyte reference value is the certified value of the reference, expected value of the laboratory prepared sample or the value obtained by ICP-MS of the non-certified reference material or lab prepared sample.

Primarily the intent was to use the calibration curve method for the determination of the analyte concentration in the sample. Simple interpolation in a calibration curve made with aqueous standards enables a simple and fast procedure. However in order to obtain successful correlation between the sample and the aqueous standards, matrix interferences (in general non-spectral interferences) that affect the analyte signal must be eliminated. For the cases where experimental procedures to eliminate the matrix interferences failed, standard addition method was used to obtain the experimental value of the analyte concentration. Standard addition method generally is a successful method to account for the effects of the matrix on the analyte signal. Blank measurements were achieved by detuning the laser by 0.05 nm from the atomic transition. The general shortcomings of this method are the necessity to prepare a large number of solutions with different standard additions, which is a laborious procedure, and to find a blank that matches the components of the matrix of the sample being analyzed.¹⁶⁶ The alternative procedure of removing the analyte from the matrix with a previous separation step in order to allow the use of the calibration curve method was not employed because of the amount of labor and time consumption added to the analytical procedure.

The results obtained with the ETA-LEAFS methods developed to determine indium, germanium and platinum in several different samples are shown in tables and described in the subsections below. The experimental results obtained by the calibration curve method or/ and the standard addition method are compared with the expected analyte concentration value. The experimental results are based on at least 3 different analysis made in different days. A summary of the results is given.

Indium

Table 5.7 and 5.8 show the heating programs employed for the different samples and the sample analysis results, respectively.

Urine samples: Urine samples spiked with indium were prepared by 1/1 w/w and 1/5 w/w dilution with nitric acid solution 0.05 M. Non-spiked urine samples diluted in the same manner were used as blanks. The signal levels of the urine measured as blanks and aqueous nitric acid solution were the same. For the less diluted sample (1/1, w/w), it was observed that the fluorescence signal of analyte in urine was around 12 % less intense than the signal of an aqueous standard of equivalent indium concentration. Furthermore, increases in ashing time were found not to alleviate the problem. Since it seems improbable that any organic matter remained after the pre-atomization cycle, the decrease of signal was attributed to quenching of the analyte fluorescence signal by inorganic species of the matrix. A further dilution of the sample (1/5 w/w) was attempted and equivalent analyte signals from both urine and aqueous samples were obtained. The 1/5 w/w diluted urine sample was then analyzed using the standard addition and the calibration curve methods. The indium recoveries achieved with both methods were statistically similar (confidence interval at 99 %, n = 6 measurements).

Table 5.7. Heating program for indium determination in complex samples.

step ^a	Temperature (°C) /Ramp time (s) /Hold time (s)		
	Sample		
	Urine	Montana soil and urban dust	Blood
dry 1	100/20/15	100/20/15	100/20/15
dry 2	300/20/20	300/20/20	300/20/20
Ashing	1000/20/20	800/15/20	1000/20/20
Atomization ^b	1600/0/15	1600/0/15	1600/0/15
,c			
Cleaning	2500/1/6	2500/1/6	2500/1/6
Cooling	20/10/10	20/10/10	20/10/10

^a 300 mL min⁻¹ argon flow, except for atomization step.^b No argon flow.^c Signal record.

Table 5.8. Sample analysis results for indium.

Sample ^g	Expected concentration value ^a	Experimental value using standard addition method ^f (recovery)	Experimental value using calibration curve method ^f (recovery)
Blood ^b	20 ng g ⁻¹	20.93 ± 0.13 ng g ⁻¹ (104.5 %)	—
Urine ^b	20 ng g ⁻¹	21.08 ± 0.17 ng g ⁻¹ (105.4 %)	20.60 ± 0.13 ng g ⁻¹ (103.0 %)
Urban dust (SRM 1648) ^{b,c}	1.09 ± 0.11 µg g ⁻¹ ^{d,f}	1.17 ± 0.07 µg g ⁻¹ (107.3 %)	1.19 ± 0.06 µg g ⁻¹ (109.2%)
Montana soil (SRM 2711) ^{b,c}	1.21 ± 0.10 µg g ⁻¹ ^{d,f}	1.24 ± 0.09 µg g ⁻¹ (102.5 %)	1.20 ± 0.1 µg g ⁻¹ (99.2 %)

^a The expected concentration value is either the concentration of indium expected in a laboratory prepared standard or the concentration of indium determined by ICP-MS in a standard material with non-certified value of the analyte.

^b Laboratory prepared standard.

^c Microwave digested samples.

^d Value obtained using ICP-MS.

^f The experimental values are average of 4 different analysis performed in four different days.

^g All samples prepared in HNO₃ 0.05 M (final concentration) to enhance Indium signal.

Blood samples: Blood samples were diluted (1/25 w/w) with 0.05 M nitric acid solution to facilitate sample introduction into the furnace and to decrease the organic matter content. Only the standard addition method was employed in this case since it was observed that fluorescence signals of indium in blood standards were around 31 % less than those obtained with aqueous standards, probably due to matrix related problems. This difference decreased to 25 % when nitric acid was replaced by palladium as the chemical modifier to allow higher ashing temperatures (1200⁰C) to be employed. Since the use of palladium did not solve the matrix related problem, nitric acid was used during the analysis of blood.

Montana soil and urban dust samples: Soil and urban dust samples were microwave digested prior to the analysis. Microwave acid digestion enabled a rapid digestion of these samples. In the first Teflon cup, 0.1 g of sample, 5 mL of concentrated nitric acid and 1 mL of concentrated hydrofluoric acid were placed. The second one, which was used as the blank, contained only the acid mixture. Both cups were placed inside digestion bombs and microwave digested for 5 minutes at 113 W. After the digestion, the samples were allowed to cool down to room temperature and then transferred to 25 mL volumetric flasks where the volumes were completed with deionized water in order to adjust the concentration of the analyte to the range of the calibration curve. The samples were analyzed using both the calibration curve method and the standard addition method. The concentration of indium in the samples was also determined by ICP - MS using the standard addition procedure for comparison. For both Montana soil and urban dust samples, the experimental results obtained using both calibration curve method and

standard addition methods are statistically similar (confidence interval at 99 %, n = 6 measurements) to the results achieved by ICP-MS.

Calibration curves made with laboratory made aqueous, urine (1/5, w/w dilution) and standard addition curve for the determination of indium in blood are shown in Figure 5.22 in order to illustrate the results obtained above.

Germanium

The heating programs employed for the determination of germanium in the different samples are shown in Table 5.9 and the sample analysis results are displayed in Table 5.10.

Water samples. Because of the lack of germanium reference materials, a 2 ppb standard solution of that element was prepared using GeO_2 99.99% in ultrapure water. A calibration curve interpolation method was employed successfully due to the simplicity of the matrix. Tap water samples from the faucet of the laboratory were also analyzed by our method (see Table 5.10). Excellent recovery results were obtained.

Blood samples. The method was also tested with blood samples. Blood, which had demonstrated no presence of detectable germanium in previous studies, was employed. The blood was spiked with a known amount of germanium. The calibration curve method failed to give the correct results using an ashing step at 400°C or using the Pd/Mg NO_3 modifier to allow ashing at 1000°C . The standard addition method was then used to compensate for matrix interferences using ashing at 1000°C to minimize more efficiently the blood matrix. The calibration procedure allowed excellent recovery. The lack of correlation between the calibration curves made with aqueous standards and the blood sample with the Pd/Mg NO_3 modifier is shown in Figure 5.23.

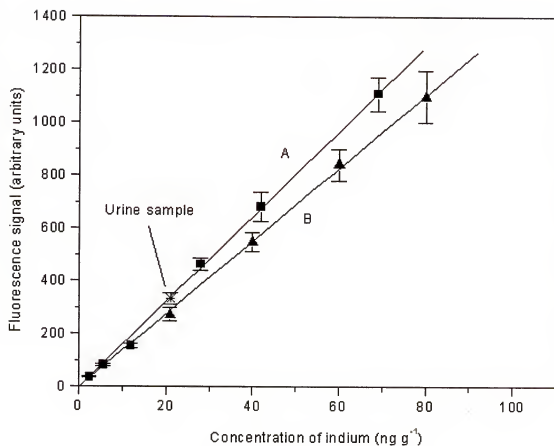


Figure 5.22. Determination of indium in urine and blood. (A) calibration curve made of aqueous standards (B) standard addition in blood. Each point in the curve is an average of 6 measurements.

Table 5.9. Heating program for germanium determination in different samples.

Step	Temperature ($^{\circ}\text{C}$) / Ramp time (s) / Hold time (s)	
	Sample	
	Water	Blood
dry 1	100/5/20	100/5/20
dry 2	150/5/10	250/15/20
Ashing	-	1000/0/15
Atomization ^{b,c}	1600/0/15	2400/0/15
Cleaning	2500/1/6	2700/1/6
Cooling	20/10/10	20/10/10

^a 300 mL min⁻¹ argon flow, except for atomization step.^b No argon flow.^c Signal record.

Table 5.10. Sample analysis results for germanium.

Sample	Expected concentration value ^a	Experimental value using standard addition method ^d (recovery %)	Experimental value using calibration curve method ^d (recovery %)
Water (tap)	$1.63 \pm 0.06 \text{ ng g}^{-1}$ ^{c,d}	-	$1.60 \pm 0.09 \text{ ng g}^{-1}$ (98.2)
Water ^b (laboratory-made standard)	2.00	-	$1.99 \pm 0.09 \text{ ng g}^{-1}$ (99.4)
Blood ^{b,c}	18	$17.46 \pm 0.54 \text{ ng g}^{-1}$ (97.0)	-

^a The expected concentration value is either the concentration of germanium expected in a laboratory prepared standard or the concentration of germanium determined by ICP-MS.

^b Laboratory prepared sample.

^c Value obtained using ICP-MS.

^d The experimental values are average of 4 different analysis performed in four different days.

^e Pd/MgNO₃ used as chemical modifier to improve ashing conditions.

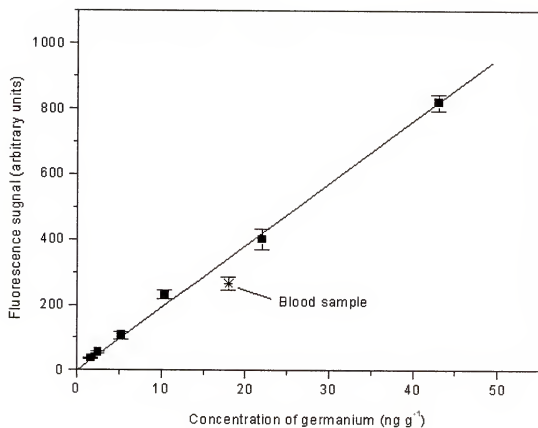


Figure 5.23. Non correlation between the signal of germanium in blood sample and the germanium calibration curve made with aqueous standards. Each point in the curve is an average of 6 measurements.

Platinum

For the determination of platinum in complex samples, the heating programs employed are shown in Table 5.11. Results of the sample analysis are displayed in Table 5.12 and commented below.

Urine samples. Urine samples certified for platinum was employed. For urine samples with no dilution, the fluorescence intensity of platinum is significantly affected by the concomitants of the matrix. Even when high temperatures ashing steps were employed, fluorescence signals about 40 % lower than the respective Pt water standard were observed. However, when the urine sample was diluted with 5 parts of water, it was observed that the analyte fluorescence signals measured from the diluted urine samples and in pure water were equivalent. This fact can be verified by the sensitivities of the calibration curves constructed with water standards and with 1:5 diluted urine (Figure 5.24). The dilution of the sample minimized the interference problems, allowing the determination of the analyte by using the calibration curve procedure.

Automobile catalyst samples and Pt spiked sand samples. These samples were successfully analyzed by employing the calibration curve method after the samples were microwave digested. For the digestion 5 mL of hydrofluoric acid was employed for 0.1 g of sample. Digestion time was fixed to 5 minutes, and the power was set at 113 W.

Blood samples. For blood, a 1:25 dilution with pure water was used to minimize matrix interferences, but even with this magnitude of dilution, the analyte fluorescence signal was significantly lower than the equivalent platinum water standard. Therefore, only the standard addition method was used to determine platinum in blood samples. It is clear

Table 5.11. Heating programs for determination of platinum.

step ^a	Sample			
	(temperature(°C)/ramp time(s)/hold time(s))			
	Blood	Urine	Pt spiked washed sand	Automotive catalyst
dry 1	130/10/10	130/10/10	180/10/10	120/10/10
dry 2	250/10/10	250/10/10	350/10/10	350/10/10
Ashing	1200/10/20	1200/10/20	-	1000/10/10
Atomization ^{b,c}	2000/0/5	2000/0/5	2000/0/5	2000/0/5
Cleaning	2600/1/6	2600/1/6	2600/1/6	2600/1/6
Cooling	20/10/10	20/10/10	20/10/10	20/10/10

^a 30 mL min⁻¹ argon flow, except for atomization step.

^b No argon flow.

^c Signal record.

Table 5.12 . Sample analysis results for platinum.

Sample	Expected value	Experimental value using standard addition method ^e (recovery)	Experimental value using calibration curve method ^e (recovery)
Auto catalyst (SRM 2556) ^d	0.637 $\mu\text{g g}^{-1}$	0.682 \pm 0.02 $\mu\text{g g}^{-1}$ (107 %)	0.671 \pm 0.1 $\mu\text{g g}^{-1}$ (105.3 %)
Toxic metals in urine ^g (elevated levels) (SRM 2657)	120 ng g^{-1} ^b	120.7 \pm 3.9 ng g^{-1} (100.6 %)	122.3 \pm 1.2 ng g^{-1} (101.9 %)
Blood ^c	126.87 ng g^{-1}	137.0 \pm 2.8 ng g^{-1} (108 %)	—
Soil (Pt spiked washed sand) ^{c,d,}	44.20 \pm 1.11 $\mu\text{g g}^{-1}$ ^f	45.2 \pm 1.9 $\mu\text{g g}^{-1}$ (102.2 %)	45.9 \pm 2 $\mu\text{g g}^{-1}$ (103.1 %)

^aThe expected value is either the certified or a non-certified value of a standard reference material or the value expected for a laboratory prepared sample.

^b Non-certified value.

^c Laboratory-made standard samples.

^d Microwave digested samples.

^e Average of 4 different analysis.

^f Concentration measured using ICP-MS.

^g For calibration curve method the urine sample was diluted 1:5 with purified water.

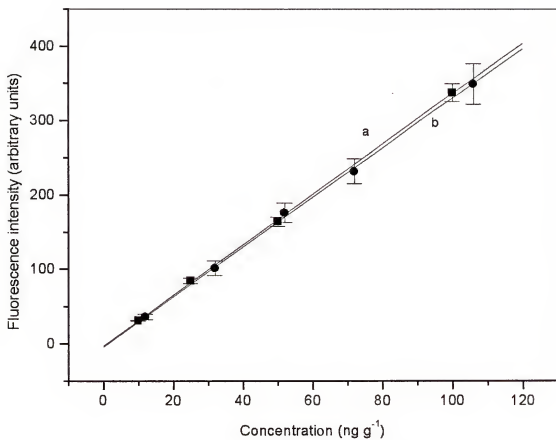


Figure 5.24 Calibration curves constructed with platinum water standards (a) and with 1:5 water diluted urine containing platinum (b). Each point of the curves is an average of 6 measurements.

here that just as in ETA-AAS, high concentrations of organic matter affect the magnitude of the analyte signal, making difficult the comparison with water standards and therefore the use of the calibration curve method. The experimental results indicate that collisional quenching of the excited atomic population is probable the main mechanism of signal reduction taking place; quenching could be minimized with further dilution of the sample with the consequence of decreasing the sensitivity of the method.

Conclusion

Ultrasensitive methods for the determination of indium, germanium and platinum were developed. The high sensitivity achieved is a result of the use of a powerful excitation source with high repetition rate to ensure better probing of the atomic population generated in the atomizer, optimization of the experimental parameters and instrumental design. Fluorescence analytical schemes were chosen taking in consideration the maximization of the signal to background ratio. Atomization techniques as well as the influence of the quality of the graphite were compared in order to obtain the best atomization efficiency. For indium and germanium, platform atomization was chosen, while wall atomization was found to be the best for platinum. Tubes or platforms made of pyrolytic graphite were chosen. Furnace parameters were optimized to maximize the atomization efficiency, ensure low levels of background reaching the detector and to eliminate as much as possible matrix components of the sample. Chemical modification studies were made. For indium, nitric acid was found to stabilize the analyte, improving the fluorescence signal by a factor of six. In the case of germanium, ashing temperatures as high as 1000⁰C could be employed by using

Pd/MgNO₃ chemical modifier. A study of the influence of acids and NaOH was made in order to ensure a safe choice of reagents for the digestion of soils and sediments. A brief study of potential interferents was made. High concentration of salts was found to cause little differences in fluorescence signals when compared to analyte aqueous standards. Special concern was taken to keep the sample preparation to a minimum. The methods were successfully tested in complex biological and environmental samples. The use of the calibration curve method could be used for soils and sediments after a rapid microwave digestion procedure and for urine after a simple (up to 5 fold) dilution. Blood samples were analyzed by the standard addition method because of matrix interferences could not be eliminated completely. Absolute limits of detection in the femtogram range, good linear dynamic range and excellent precision were achieved.

CHAPTER 6
FILTER FURNACE LASER-EXCITED ATOMIC FLUORESCENCE
SPECTROMETRY FOR THE DETERMINATION OF LEAD IN WHOLE BLOOD

Introduction

The detection of trace levels of lead in the environment and in human biological fluids has been of crucial importance in public health. Psychological, neurological, and intelligence-deficit damage have been correlated to the presence of lead in the organism.¹⁶⁷ The magnitude of lead contamination in the environment is high, which increases the human exposure to this heavy metal.⁸⁴ Although, to date, toxic responses have primarily been based upon individuals who have levels of lead above 100 ppb, it would be advantageous to develop analytical methods capable of detecting levels of lead in biological fluids at concentrations well below the established levels of concern (100 ppb). This monitoring capability, ultimately, would prevent the build up of lead in the organism before it reached a critical level.¹⁶⁸

There are several analytical methods capable of determining lead at levels of concern (100 ppb) set by the CDC (Center of Disease Control) and EPA (Environmental Protection Agency).¹⁶⁹ Some of the most popular methods include electrochemical techniques, such as anodic stripping voltammetry¹⁷⁰ and coulometric stripping potentiometry,¹⁷¹ and graphite furnace AAS.^{48,172} Graphite furnace AAS is perhaps the most accepted technique because it is very sensitive (limits of detection of 5 pg), and it is

suitable for the analysis of small amounts of biological fluids. Techniques capable of lower detection limits include isotope dilution inductively coupled plasma mass spectrometry which has achieved a limit of detection of 16 fg when coupled with electrothermal sample introduction,¹⁷³ and laser induced fluorescence.^{39,157,174-177} A few groups have developed methods for the determination of lead by ETA-LEAFS with limits of detection in the low femtograms.^{157,174,175} A limit of detection one order of magnitude lower (0.1 fg) was developed by Wagner *et al* using the same copper vapor pumped dye laser LEAFS system used in this dissertation.¹⁷⁷

The intent of this chapter is to describe the use of filter furnace atomization for the direct analysis of lead in blood by laser-excited atomic fluorescence spectrometry. The filter furnace technique is employed as the atomization technique to achieve correlation of the lead fluorescence intensity between aqueous and blood standards and simplifying the determination procedure by allowing the use of calibration curves constructed with aqueous standards to determine the amount of lead in blood samples.

Although electrothermal atomization is considered one of the most efficient means to atomize samples, this technique is far from perfect. Problems arise due to interactions that can take place between the analyte, the carbon of the graphite atomizer and principally the components from the matrix containing the analyte of interest.⁵⁴ Analytical matrices containing high amounts of organic matter often present problems related to the decrease of analyte sensitivity. The two main causes are losses of analyte during the heating cycle because of formation of volatile molecular species containing the analyte of interest and/or increase of molecular background. The problem is usually addressed and, in many cases, minimized by the optimization of the temperature program

together with the stabilized temperature platform furnace (SPTF) technique^{43,178} and by chemical modification.⁵¹

Although the choice of proper ashing temperatures and heating rates is very effective for elements with high thermal and chemical stability, this approach is not always effective for elements which form volatile molecular species like lead.¹⁷⁷ A platform, which delays the atomization of the analyte until a steady state temperature is reached between the walls and the center of the tube, in many cases is a useful approach to minimize problems related with the formation of compounds after the vaporization of volatile species. Chemical modifiers can chemically transform the analyte of interest making it less volatile, and so higher ashing and/or atomization temperatures can be applied. Chemical modifiers also can be employed to interact with interfering species in order to achieve a time-resolved release of products during the heating cycle achieving a separation of the analyte from the matrix components. A disadvantage of using chemical modifiers is that they are usually employed in concentrations of the order of thousands fold higher than the analyte concentration present in the sample. This procedure can introduce impurities into the sample and cause false analytical results, principally if detection of ultratrace amounts of a common element like lead is intended. In addition, finding an appropriate chemical modifier is not always guaranteed.^{51,66}

Filter Furnace Atomization

The graphite filter furnace (FF) is a new concept of electrothermal atomization, recently introduced by D.A. Katskov¹⁷⁹ and it has been applied successfully in atomic absorption spectroscopy.¹⁸⁰ The possibility of the introduction of larger volumes of

sample, decreased pre-atomization time and temperatures, and elimination of spectral background as well as chemical interferences without the use of chemical modifiers are improvements that the FF technique have to offer over the commonly used platform atomization technique. The filter is inserted inside a pyrolytic graphite tube where the sample is deposited in the gap between the wall of the tube and the filter, outside the analytical zone (Figure 6.1). The concept of FF is to physically separate the matrix vapor from the analyte atomic vapor by partition in the porous graphite. In other words, the porous graphite delays the diffusion of the molecular matrix vapor resulting in a temporal resolution between the atomic (analyte) and molecular (background) signals.¹⁷⁹

The most important criterion for the choice of graphite was its permeability. Graphite from National Carbon (Cleveland, OH) was found to have large porosity allowing a fast release of atomic vapors of relatively volatile elements such as lead. A piece of carbon rod was machined with the dimensions shown in Figure 6.1. The most critical one was the thickness of the wall that separates the sample cavity and the analytical zone. A thickness of 0.6 mm was chosen to allow excellent diffusion of atomic vapor and still be strong enough to permit the manipulation of the filter without breaking.

Results and Discussion

Lead is an element with relatively high volatility, which complicates the use of pre-atomization steps without loss of analyte in complex matrices.¹⁷⁷ Molecular background, even though it is much less a problem for atomic fluorescence than for atomic absorption, can degrade limits of detection in the analysis of samples with high content of organic matter. The interference caused by matrix components can decrease

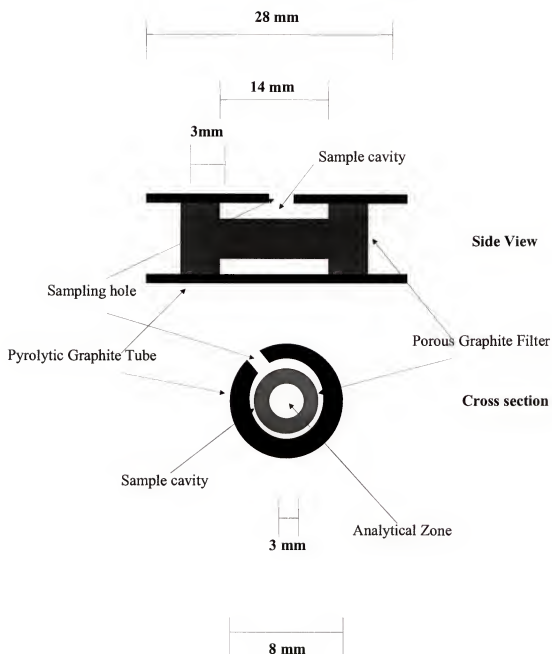


Figure 6.1. Filter furnace.

the analytical signal of the analyte compared to aqueous analyte standards of the same concentrations. Ideally, a method to analyze complex samples should allow the correlation of complex standards to aqueous standards simplifying the calibration curve procedure by eliminating the need for standards of the complex sample. In previous work by Wagner *et. al.*,¹⁷⁷ correlation was successfully accomplished for lead by using a photodiode placed behind the furnace in line with the laser beam. The two channel system corrected the decrease of laser intensity caused by matrix of the complex sample relative to the aqueous standard. Potentially, the Katskov filter is a cheaper and simpler alternative to achieve such correlation of standards. In addition, it is easily adapted to use in commercial graphite furnaces.

Unlike absorption-based methods, the selective nature of the fluorescence minimizes interferences due to other atomic species and most potential molecular interferences are greatly reduced. At the same time, although the graphite tube is considered to be the best atomizer because of the increased concentration of the analyte vapor in the probed zone, there is an increase in interferences due to the concentrated gas components in the small volume when complex matrices are measured. The potential of the filter furnace (FF) technique to minimize this type of matrix interference was demonstrated by Katskov¹⁸⁰ when absorption signals of lead and cadmium in diluted whole blood, obtained with the FF technique were similar to those obtained with SPTF coupled with Zeeman background correction.

Permeability of the Filter and Fluorescence Time Profile

It is found in the literature¹⁸¹ that the permeability of atomic vapor through graphite is highly dependent on the volatility of the element being atomized and on its physico-chemical interactions with the porous graphite. The elements were divided in three major groups. First, high volatility elements, such as Pb, Cd and Bi, do not interact with graphite, and their vapors are rapidly released through the porous graphite at atomization temperatures in the 1000 – 1600°C range. Second, medium volatility elements, such as Cu, Pt, In and Sn, have a more pronounced time delay in the release of atoms are accompanied by a tailing in the signal observed by using atomic absorption spectrometry. These elements also had to be atomized at higher temperatures than normal in order to provide faster release of vapors. Finally, the third group is composed of carbide forming or graphite soluble elements, such as Co, Fe and Al, which are atomized at 2400°C, which is close to the tolerance limit of the FF.

Lead is an ideal element to be used in FF atomization because it is in the first group described before. A comparison of the fluorescence time profiles for FF and SPTF atomization techniques for lead and platinum are shown in Figures 6.2 top and bottom, respectively. During the work with platinum, the FF atomization technique was also evaluated. As is seen by Figure 6.2 bottom, the signals (in terms of peak area) of the fluorescence time profiles obtained with both FF and wall atomization were statistically similar. However, the broadening made the reproducibility much poorer (19 %) in contrast to the 6 % obtained with wall atomization. It was also observed that for the FF higher temperatures (2400°C) than for wall atomization had to be used to obtain reasonable results; the high temperatures consequently degraded the signal to noise due

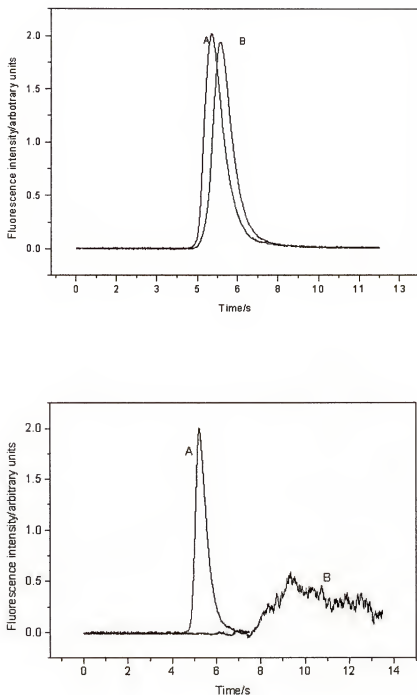


Figure 6.2. Comparison between fluorescence time profiles using an open pyrolytic tube (A) and through a porous graphite filter inserted into the pyrolytic tube (B). Top plot represent the results for lead and bottom plot represent the results for platinum.

higher blackbody radiation. Opposite to that scenario, the lead fluorescence profiles were similar not only in peak intensity but also in shape for the same atomization temperature. Only a short delay in time was observed. Based on these results, a good analytical performance can be expected for lead.

Comparison of Atomization Techniques for Blood Analysis

In order to illustrate the usefulness of the method, the filter furnace technique was compared with the stabilized temperature platform furnace (STPF) technique for the determination of lead in whole blood by laser atomic fluorescence spectrometry. The fluorescence analytical scheme chosen for the determination lead is shown in Figure 6.3. SRM 955a1 blood samples were 1/20 w/w diluted with a 0.01M nitric acid solution prepared with nitric acid ultratrace grade and deionized ultrafiltered filtered water. This dilution was found to be important primarily to improve reproducibility during sampling; however, later the dilution was found important to reduce the amount of organic mass inserted in the furnace. Atomization parameters for STPF and FF are shown in Table 6.1. A slow two part drying step was employed to avoid splattering of the sample in both cases. For SPTF, two different ashing steps were evaluated. First, a 900°C temperature was used to completely ash the blood matrix prior to atomization. In this case, the Pb signal intensity (peak area) of a 6.8 ng g⁻¹ blood standard was approximately 20% smaller than the Pb signal intensity of 6.8 ng g⁻¹ aqueous standard (Figure 6.4). This difference can be accounted by losses of lead by vaporization and/or by the formation of lead organic compounds at relatively moderate temperatures (above 400°C).⁵¹ To overcome those problems, a lower ashing temperature (300°C) was used. However, in this case, the

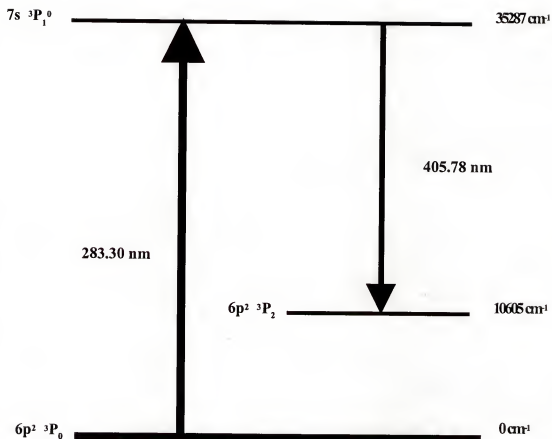


Figure 6.3. Energy level diagram for the fluorescence determination of lead.

Table 6.1. Furnace programs employed for the determination of blood by Filter Furnace (FF) and Stabilized Temperature Platform Furnace (STPF).

Step ^a	Temperature (°C)/Ramp time (s)/Hold time (s)	
	STPF	FF
Dry	80/20/30	80/20/30
Dry	180/20/20	180/20/20
Ash	(300 or 900)/10/35	300/10/40
cool down ^b	-	20/10/30
Atomization ^c	1900/0/14	1900/0/14
Clean	2500/1/10	2500/1/10
Cool down	20/10/10	20/10/10

^a Argon flow except during the atomization step (stop flow).

^b Modified internal argon flow.

^c Signal record.

lead signal intensity for 6.8 ng g^{-1} Pb aqueous standards were 27 % higher than for 6.8 ng g^{-1} Pb blood standard (Figure 6.4). The difference in intensities in this case can be attributed mainly to the attenuation of the excitation laser radiation as well as the emitted fluorescence by the smoke released and to fluorescence quenching of excited species by the high concentration of molecular species in the analytical zone during atomization.¹⁷⁷

The use of the filter furnace was preceded by a preconditioning step consisted of four firings using the thermal program employed for the SPTF technique. Several heating programs were evaluated for the FF technique to be employed. The best program, shown in Table 1 included a pre-atomization cycle with two drying steps and a low temperature ashing step (300°C), to avoid the problems related to the use of the high temperature pre-atomization discussed above. A cool down/cleaning step, immediately before atomization of the sample, was used in order to allow dissipation of smoke from the analytical zone resulting from imperfections of the fitting of the filter in the graphite tube. In order to increase the rate of dissipation of smoke, a modification of the internal argon flow of the HGA 400 furnace during the cool down was made. Details of the operation of the graphite furnace can be found elsewhere.⁷³ This modification consisted of a solenoid valve, inserted in the tubing on one side of the internal argon flow (Figure 6.5). The solenoid valve was manually turned on at the beginning of the cool down step closing one side of the internal argon flow in order to flush the analytical zone. The solenoid valve was turned off to restore the normal flow prior to the atomization of the sample. This modification of the internal flow improved the reproducibility of the results obtained with the same filter as well as those obtained with different filters.

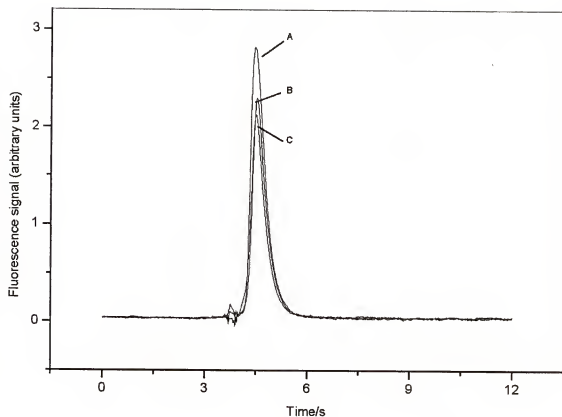


Fig 6.4. Fluorescence temporal profiles of lead using stabilized platform temperature furnace (SPTF) technique. (A) 6.8 ng g^{-1} lead aqueous standard (B) 6.8 ng g^{-1} lead blood standard using 900°C temperature ashing step (C) 6.8 ng g^{-1} lead blood standard using 300°C temperature ashing step.

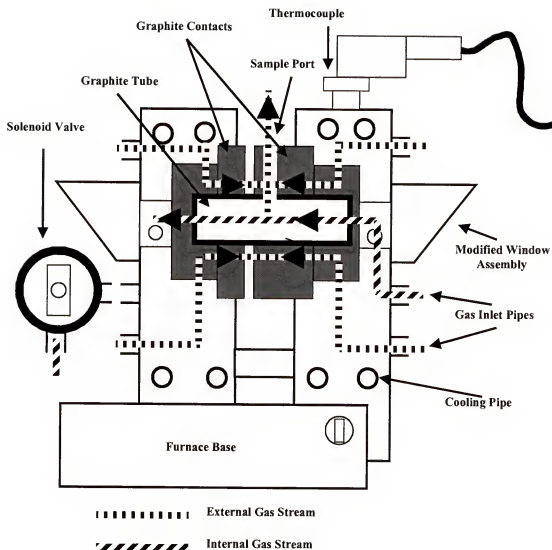


Figure 6.5. Electrothermal atomizer (model HGA-400) with modified argon flow.

Influence of the Amount of Blood in the Recovery and Reproducibility

Laser-excited atomic fluorescence using a copper vapor laser has proven to be a very sensitive method for the determination of lead where a limit of detection of 0.1 fg has been reported in a previous study, made in our laboratory using this same system,¹⁷⁷ in contrast to 5 pg that has been achieved by graphite furnace atomic absorption spectrometry.⁴³ Taking advantage of this high sensitivity, the amount of blood deposited in the filter furnace was reduced to 1 μL to minimize the amount of organic matter and the amount of fumes released. The reduction of the volume of the blood sampled improved the recovery of lead when compared to higher volumes of sample. A comparison of the recoveries is shown in Table 6.2. Volumes of sample above 10 μL were not evaluated because in this case, part of the blood sample was expelled from the filter cavity during the heating program. The reproducibility of the results was also improved with the reduced sample volume as can also be seen in Table 6.2. For comparison, a reproducibility around 6.0 % was found for 1, 2 and 5 μL when experiments with 6 ng g^{-1} lead aqueous standards were performed. In addition, an increase in the lifetime of the graphite filter was also observed when working with the smaller amount of organic sample. The graphite filter was replaced by a new one after the sensitivity decreased more than 10 %. The lifetime of the filter furnace in these optimized conditions was found to be around 40 firings.

Fluorescence time profiles of lead in both aqueous and the blood standard of the same concentration can be seen in Figure 6.6. The figure shows that signals from both

Table 6.2. Effect of the volume of blood samples deposited in the filter furnace on the recovery and reproducibility of lead fluorescence signal.

Volume of Sample ^a	1 μ L	2 μ L	5 μ L
Recovery (%) ^b	98.3	94.1	88.5
Relative Standard Deviation (%) ^b	6.8	11.3	13.8

^aLead in blood (NIST 955a-1) prepared using a 1/20 w/w sample/0.01 M nitric acid solution.

^bEach result is based on 10 replicates.

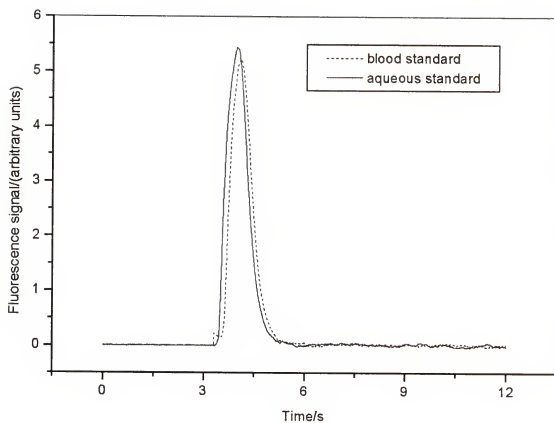


Fig 6.6. Fluorescence temporal profiles of lead using filter furnace (FF) technique using 15.3 ng g^{-1} lead aqueous standard (—) and 15.3 ng g^{-1} lead blood standard (---).

standards are similar, indicating that interferences of the blood matrix in the analyte signal were successfully remedied.

Calibration Curves and Blood Analysis

Calibration curves constructed using blood standards and water standards are compared in Figure 6.7 and found to correlate, indicating excellent correlation between them. This correlation means that our method enables a precise determination of lead in blood samples using a calibration curve made with aqueous standards. A calibration curve made using SPTF technique is also shown in Figure 6.7 for comparison.

The validity of the method was evaluated by analyzing blood samples with a certified concentration of lead (SRM 955a). Results displayed in Table 6.3 show that very good recoveries of lead were obtained by using the proposed method.

Conclusion

In conclusion, the Filter furnace technique allowed the use of calibration curves made with aqueous standards to determine lead in blood samples. The laboratory-made Katskov type graphite filter is cheap, easy to make and can be easily employed in commercial graphite tube furnaces. This sensitive filter furnace laser atomic fluorescence spectrometry method has the potential to simplify the ultratrace determination of lead present in complex matrices.

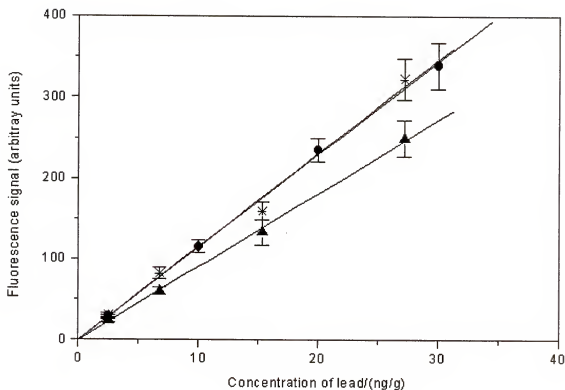


Fig 6.7. Calibration curves of lead. (●) Aqueous standards using filter furnace technique (*) Blood standards using filter furnace technique (▲) Blood standards using stabilized temperature platform furnace technique. Blood calibration curves were made using NIST blood standard samples diluted 1/20 w/w with water.

Table 6.3. Determination of lead in reference materials^a by FF-LEAFS.

NIST sample	Nominal concentration of lead (ng g ⁻¹)	Experimental result by calibration curve method ^b (recovery %)
955a-1	50.1 ± 0.9	54.3 ± 4.5 (108.4)
955a-2	135.3 ± 1.3	129.8 ± 8.7 (95.9)
955a-3	306.3 ± 3.2	296.2 ± 19.3 (96.7)
955a-4	544.3 ± 3.8	537.5 ± 39.5 (98.8)

^a 1 µL of sample introduced in the furnace.^b Each experimental result is based on 10 repetitions.

CHAPTER 7

DETERMINATION OF THULIUM BY LEAFS IN A RHENIUM LINED TUBE ATOMIZER

Ultratrace Determination of Thulium

There is an increasing demand for high purity materials based on rare earth elements (REE). For example, ultrapure europium and lanthanum oxide are used as a gain media in a solid state laser and opto-magnetic materials. Trace quantities of REE impurities, including thulium play important roles in optical, electrical and magnetic properties of such materials; therefore, selective and sensitive methods are required for quality control, product certification and evaluation of material performance.¹⁸² Rare earth contamination of natural drinking water supplies has also gained relevance recently.¹⁸³ The use natural phosphates as fertilizers in agriculture has spread rare earth elements, present in natural phosphate ores, in the environment. Part of that material can end up as run-off to rivers and lakes and part also can contaminate ground water.¹⁸⁴ Although sharing similar chemical and physical behavior, it was recently determined that toxicological effects of Gd and Tm are more severe than those observed for Pr, Nd, Sm and other rare earths.¹⁸³ Studies on rats indicated that intoxication by Tm caused perinuclear vacuolization of the liver parenchyma.¹⁸⁵ By extrapolation of the results obtained for rats to human beings, the admissible drinking water concentration calculated for thulium was 10 ppb. The determination of even lower concentrations of Tm in

biological fluids has been used to monitor the build up of thulium in the human organism.¹⁸³

The complex spectra emitted by REE in the inductively coupled plasma (ICP) impose enormous difficulties for the determination and identification of these elements by ICP emission spectroscopy.¹⁸⁶ Mutual spectral interferences and limits of detection in around 10 ppb makes the technique not applicable for many of the biological and environmental samples. Time consuming pre-concentration in cation-exchange resins can improve sensitivity. However, due to similar chemical and physical properties of REE, separation steps are laborious, expensive and sometimes not efficient.^{187,188} Shinotsuka and Ebihara¹⁸⁹ working with chondritic meteorites, have demonstrated that inductively coupled plasma mass spectrometry (ICP-MS) have detection limits similar to those obtained with neutron activation analysis (NAA) (sub ppb) with the advantage of a simpler and experimental procedure. In the case of thulium, even though ICP-MS is a sensitive technique, EuO^+ was found to interfere with the determination of Tm^+ .⁺ Since Tm is a monoisotope the use of another isotope to avoid such interferences is not possible.¹⁸² Sample aerosol desolvation can minimize but not completely avoid the formation of oxides.¹⁹⁰ An alternative way is the use of either TmO^+ or Tm^{+2} but unfortunately limits of detection obtained by using these alternative ion species were rather poor compared to the limit of detection obtained with Tm^+ .⁺¹⁸⁹ The isotope dilution ICP-MS technique, to improve accuracy and precision, also cannot be applied for thulium.¹⁸⁹ Limits of detection reported for hydrogeochemical surveys,^{183,192} analysis of wines¹⁹² and high purity europium¹⁸² were in the sub ppb range.

Electrothermal atomic absorption spectrometry of REE in graphite furnaces is plagued by the formation of refractory carbide compounds which reduces sensitivity and imposes memory effect problems.^{43,193,194} Pre-concentration in cation-exchange resin or treatment of the graphite tube with calcium enabled limits of detection in the pg range.^{195,196} Gupta,¹⁹³ using direct determination without pre-concentration, achieved limits of detection using a graphite tube lined with tantalum foil one order of magnitude better (4 pg) than with a pyrolytic graphite tubes. These results reflected the usefulness of metal surfaces to atomize REE elements. Finally, an impressive 0.08 fg was obtained using laser atomic fluorescence in a miniature glow discharge.³⁹ Although no real samples were determined, the authors showed the high selectivity and sensitivity of laser atomic fluorescence for the determination of thulium. The design of the miniature cell allowed a single sample to be measured in 5 minutes.

Metallic atomizers

Introduction

In the last twenty years, considerable developments in electrothermal atomization techniques have been made to the eliminate of the negative properties of common graphite atomizers. First, because of it's porosity, part of the analyte can penetrate the atomizer, causing delayed atomization.^{43,64} Second, a relatively lower rate of atomization is observed which is responsible for non-isothermality of the atomization process.^{43,64} Third, because of reactions between the analyte and the graphite, the formation of thermally stable carbides as well as intercalation metal-graphite can occur for several

elements (almost all rare earth elements, B, Sc, Y, Si, Ti, V, U, Zr).^{43,197} Finally, higher background emission from the carbon surface is observed.¹⁹⁸

The introduction of pyrolytic graphite and platform atomization techniques have minimized the problems related to the porosity of the graphite and non-isothermality, respectively. However, those technical advances could not impede the formation of refractory carbides and the subsequent consequences. The formation of refractory carbides makes necessary the use of higher temperatures to improve the atomization efficiency of the analyte increasing background levels which degrades limits of detection especially for atomic fluorescence methods. Since refractory carbides are not efficiently, atomized at temperatures commonly used in electrothermal atomizers ($< 3000^{\circ}\text{C}$), sensitivity is usually poor and memory effects arise.^{194,197}

A possible way to eliminate these problems is to use alternative materials such as metals for the atomizer. Those metals chosen must have high thermal conductivity, elevated melting points and be relatively inert chemically under the operational conditions. Platinum, molybdenum, tungsten and tantalum are the metals commonly used, with the two later ones being the most popular.^{199,200} L'vov and Pelieva¹⁹⁷ improved the sensitivity 3 to 100 fold with minimization of memory effects and achieved a reduction of $200\text{--}900^{\circ}\text{C}$ in the atomization temperature by lining the graphite furnace with a metal film. These results were compared to the ones obtained using a non-pyrolytic tube. Similar results were achieved by Wall,²⁰¹ using a tungsten foil inserted in the graphite tube. Others developed atomizer tubes and coils completely made of metal.^{198,200,202,203} Compared to tungsten and tantalum, platinum and molybdenum have lower melting points which limit the use to elements with low atomization temperatures.

Tungsten and tantalum have been the metals of choice due their higher melting points. However, because of the ease in formation of low melting point oxides, an inert protective atmosphere must be used to bathe the atomizer during atomization at high temperatures, otherwise the metal surface will be destroyed after only a couple of runs. Although protective atmosphere improves the lifetime of these atomizers, it is still relatively short (100 runs).²⁰⁴ In addition, a decreased reproducibility of the analyte signal has occurred due to the degradation of the metallic surface.²⁰⁵ Another drawback is that atomization under the gas flow regime both dilutes the atomic vapor and removes part of the analyte atoms from the analytical zone potentially decreasing the sensitivity of measurements.⁷³

Atomization Mechanisms

In early studies involving metallic atomizers, researchers believed that the generation mechanism of free atoms were principally by thermal dissociation of the oxides of the particular analyte; however possible reactions of the analyte oxide with the surface of the metallic atomizer were not taken into account.^{206,207} At the beginning of the 1990's, researchers demonstrated that in many cases, the material of the atomizer (in specific case of tungsten) participate in atomization reactions and even after several atomization runs, the surface maintains its metallic characteristics.²⁰⁸ These results observed for tungsten can be extrapolated to other metallic surfaces.

Suzuki *et al*²⁰⁹ proposed that the protective atmosphere also plays a major role in the atomization mechanisms. In fact, it was found that the presence of hydrogen improved the atomization efficiency for many elements. It was also found that the

generation of free atoms depended on the type of inert atmosphere and based on signal appearance temperatures and activation energies, atomization mechanisms of elements in pure argon atmosphere differed from those in argon-hydrogen atmosphere.

Taking into account the atmosphere and the metallic surface, the atomization mechanisms to generate free atoms from the analyte oxides was not only due to thermal dissociation, but also reduction by hydrogen and reduction by the metallic surface.²⁰⁸

Intent of the Chapter

The intent of the work in this chapter is to develop a sensitive laser-induced atomic fluorescence method for the determination of thulium in urine and coal fly ash using a metal lined atomizer. Because of better resistance to oxidation and better fitting characteristics, higher sensitivity and better reproducibility was intended to be achieved by using a rhenium-lined graphite tube atomizer when compared to pyrolytic graphite and tungsten and tantalum-lined graphite tubes.

Results and Discussion

Analytical Scheme and Laser Repetition Rate

A Stokes direct line non-resonance fluorescence scheme shown in Figure 7.1 was chosen. Based on the requirements mentioned in chapter 5, this scheme has potential for excellent signal to noise for our experimental conditions. High fluorescence intensity is guaranteed by excitation from the ground state using a wavelength in the optimum energy range of the copper vapor pumped dye laser, while low background is ensured by acquisition at a wavelength below 400 nm and well apart from the excitation one.

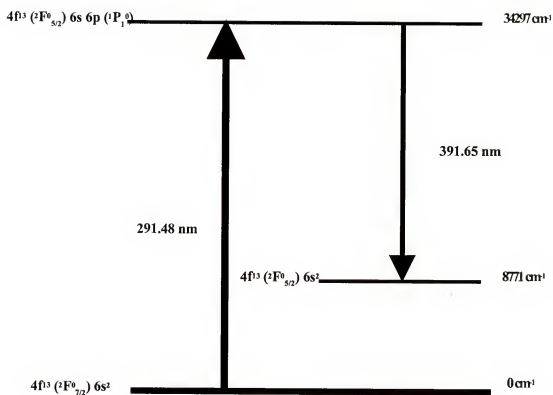


Figure 7.1. Energy level diagram for the fluorescence determination of thulium.

The laser repetition rate was set in the optimum value of 10 kHz, and the output energy (2 μ J) was insufficient to saturate the transition.

Atomization and Furnace Parameters: A Comparative Study Between Different Tube

Atomizers

Atomizers employed

A comparative study between tube atomizers was made with the objective to improve analytical performance in terms of signal intensity, reproducibility and long term stability.

Sample was directly atomized from a graphite surface using commercial pyrolytic graphite tubes. The samples were atomized from the wall as well from a platform inserted in the tube. Graphite tubes without platforms were also treated with solutions of metals such as Pd and Ir prior to the atomization of the analyte. In a second approach, the noble metal was mixed with the analyte in solution.

For the metal lined tubes, the internal cavity of the graphite tube was lined with different metal foils. Rectangular pieces (2.5 cm x 2,5 cm) were cut from metal foil [tungsten (0.05 mm thick), tantalum (0,127 mm thick) and rhenium (0.1 mm thick)]. A hole (2 mm in diameter) was pierced in each metal piece in a place to coincide with the position of the sampling hole of the graphite tube after the metal was inserted to fit its internal cavity. After the foil was carefully inserted, a thermal conditioning process was carried out in order to remove the initial stress of the material and allow the metal to expand and fit the walls of the furnace closely. The thermal conditioning process consisted of four or five heating cycles where the temperature was raised up to 2200°C

using a ramp 100 s time and kept at that temperature for 15 s. The furnace was then cooled down to room temperature using a 10 s ramp.

Atomization from graphite atomizers

Pyrolytic graphite. A comparison between fluorescence signals of thulium obtained by wall and platform techniques was made. The heating program employed to atomize the aqueous analyte samples can be found in Table 7.1. Based on experimental results, it was concluded that wall atomization technique is advantageous over platform technique for thulium. A comparison between the temperature profiles between the two techniques is shown in Figure 7.2. Based on the net fluorescence signal, the temperature of 2500°C allowed the best results. Fluorescence time profiles of thulium (10 ng g⁻¹) using both techniques are shown in Figure 7.3. Figure 7.4 show fluorescence time profiles of thulium and two subsequent runs taken to evaluate memory effects of Tm in the pyrolytic graphite. Results show that memory effects are not very critical if two 2800°C cleaning runs are employed. At such high temperatures, however, the pyrolytic coating of the tube is rapidly degraded.

One drop coating method. Noble metal solutions (100 µL of concentration 100 ng g⁻¹) as well as solutions of W, Ta and Re were deposited in the graphite tube and heated to 1000°C before the sample was inserted and atomized. Alternatively, the metal solutions (chemical modifiers) were mixed with the analyte in solution. The ratio analyte/modifier was fixed at 10⁻³. The heating programs used in both approaches are shown in Table 7.1. Based on the results in Table 7.2, the coating with noble metals (Pd, Ir and Ru) and Re did not improve significantly the results when compared with pyrolytic graphite. On the other hand, the formation and release in the analytical zone of volatile oxides from Ta

Table 7.1 Heating programs for aqueous solutions of thulium.

	Pyrolytic graphite atomizer	One drop coating technique	Metal lined atomizer ^a
Step	Time (s)/ Ramp time (s)/hold time (s)		
Dry 1 ^b	120/15/15	120/20/20	100/30/15
Dry 2	180/10/10	-	180/15/10
Ash	-	-	-
Chemical modifier pyrolysis ^c	-	1000/1/6	-
Cool down ^d	-	20/10/30	-
Dry ^e	-		-
Sample atomization ^f	variable/0/12	variable/0/12	Variable/0/12
Cleaning	2800/1/6	2800/1/6	2500/1/6
Cool down	20/10/10	20/10/10	20/10/40

^aGraphite tube lined with rhenium, tungsten or tantalum.

^bDrying of the chemical modifier in the one drop method.

^cUsed to impregnate the chemical modifier in the graphite tube.

^dCool down of the atomizer to allow the introduction of analyte sample in the one drop method.

^eDrying of the analyte in the one drop method.

^fSample atomization temperature to be optimized.

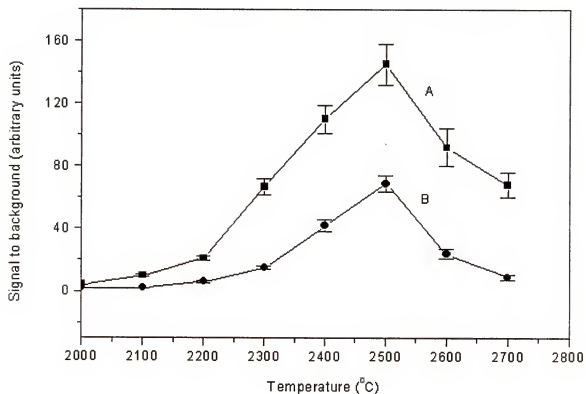


Figure 7.2. Atomization temperature curves for 10 pg of thulium. (A) Wall atomization in a pyrolytic graphite tube. (B) Platform atomization.

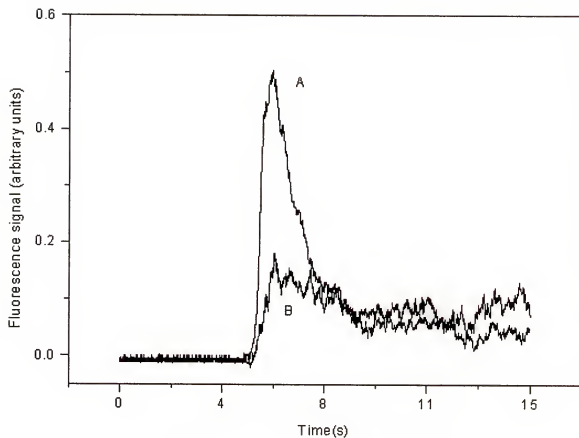


Figure 7.3. Fluorescence temporal profile of thulium (10 pg) using (A) wall atomization and (B) platform atomization. Sample atomized at 2500°C.

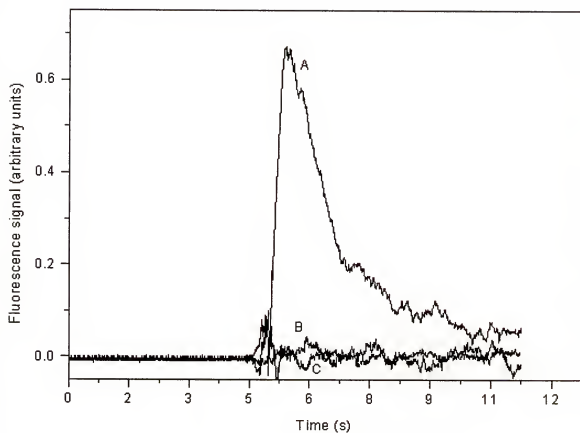


Figure 7.4. Fluorescence temporal profiles of (A) 10 pg of Tm, (B) first subsequent run without sample (first memory run), and (C) second consecutive run without sample (second memory run).

Table 7.2. Comparative results using two chemical modifier procedures.^{a,b}

	One drop method (pre-coating procedure)	Chemical modifier mixed in solution
No chemical modifier	1	1
Pd	1.3	0.75
Ir	1.08	0.68
Ru	1.27	0.71
Re	1.03	0.63
W	0.59	0.60
Ta	0.66	0.53

^aResults displayed compares the S/B value observed with chemical modifiers with the one observed without chemical modifier, taking in consideration the later as a unity.

^bAnalyte concentration fixed at 10 ng g^{-1}

^cPre-coating the graphite tube with $100 \mu\text{L}$ of a 100 ng g^{-1} chemical modifier solution.

^dAnalyte/chemical modifier ratio fixed at 10^{-3}

and W, deposited in the furnace from the coating solutions, could have caused quenching of the analyte fluorescence signal as indicated by the experimental values.

When the chemical modifiers were mixed in solution, the magnitude of the fluorescence signals were lower than the observed without chemical modifiers in all cases.

Atomization from metal atomizers

The lining of the internal cavity of the graphite tube with the metal foil is a critical procedure. With improper lining, the precision, and sensitivity of the analytical are greatly deteriorated.^{197,205} A proper lining requires that the metal foil must be in close contact with the walls of the graphite tube. It has been reported in the literature that tungsten and tantalum suffer from deformation; both become fragile and crack, which makes further determinations impossible to do.²⁰⁵ During the experiments in this chapter, the deformation of the foil was observed, specially for tantalum, under argon flow. The deformation caused the foil to bend and pull away from the graphite tube walls and caused the foil to crack. These observations had direct impact on the sensitivity and lifetime of the analyte signals as will be seen later. Trying to overcome deformation problems, Yizai *et al*²⁰⁵, developed a graphite tube lined with a tungsten spiral and a tantalum foil. In their design, the tantalum foil was held in place with two tungsten spirals, one at each end of the graphite tube, pressing the tantalum foil against the graphite tube. This design, although avoiding deformation, is not straightforward to built. For both, tantalum and tungsten lined atomizers, it is mandatory to use an inert atmosphere during the entire heating cycle. The inert atmosphere prevents tungsten and tantalum from forming relatively volatile oxides that destroy the metal lining. A direct

consequence of the use of gas flow during atomization is the loss of analyte signal sensitivity because of the dilution of the atomic vapor in the analytical zone. Modern furnace systems use a reduced flow of inert gas during atomization commonly called atomization under miniflow regime, in order to allow a flux of protective argon while still minimizing dilution of atoms in the analytical zone.⁷³ However sensitivity is still affected.

Rhenium foil was found to be resistant to oxidation under the atomization conditions used for thulium. Comparative results of the thulium fluorescence between the rhenium foil atomizer under stop flow regime and tungsten and tantalum lined atomizers under argon miniflow regime can be seen in Figure 7.5. Complementary, the influence of the several miniflow conditions on the signal sensitivity of the analyte using the rhenium lined atomizer is shown in Figure 7.6.

Significant irreproducibility of the analyte signal was found for all metal lined furnaces (Rh, W and Ta) when the same heating program employed for graphite atomizers were used. Modifications in the heating program were made (see Table 7.1) to solve this problem. By using a longer drying step ramp time as well as employing a longer cool down time, reproducibility equivalent to those obtained with the graphite surface was achieved. This heating program was found to work for all three metal linings.

In terms of the metal lining itself, rhenium foil showed advantages over Ta and W. First, rhenium is more flexible and easier to place inside the graphite tube; in addition, the foil stayed in close contact with the walls of the tube throughout all firings.

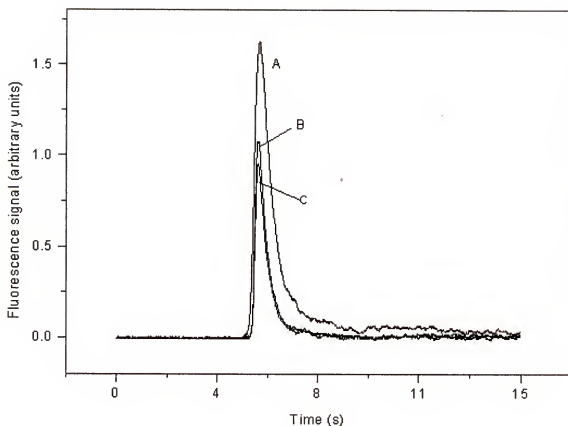


Figure 7.5. Fluorescence temporal profile of thulium (10 pg) in (A) rhenium lined atomizer under stop flow regime of atomization, (B) tungsten lined atomizer under miniflow (50 mL/min) atomization regime and (C) tantalum lined atomizer under miniflow (50 mL/min) atomization regime. Sample atomized at 2300°C.

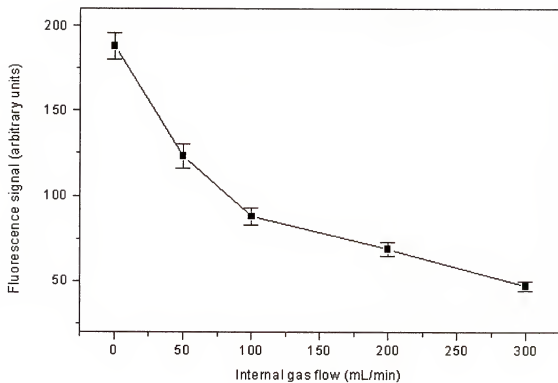


Figure 7.6. Influence of the different argon flows during atomization of 10 pg of thulium in a rhenium lined atomizer.

For tungsten, there was a great difficulty in fitting the foil inside the tube. The procedure of rolling the foil and inserting inside the tube many times caused breakage of the W foil. In addition, the fitting was usually not very good because parts would not stay in complete contact with the graphite tube walls. Tantalum is a very flexible metal foil, which is easy to place inside the tube and easy to fit in close contact with the tube walls. However, tantalum foil showed an extensive degree of deformation after a certain number of firings. Parts of the tantalum foil started to separate from the walls of the tube, and since the tantalum foil lost its flexibility after a few firings, it no longer made a close fit to the walls.

Improvements in the lifetime of both tungsten and tantalum atomizers have been reported by the use of argon mixed with a small percent of hydrogen gas.^{200,204} The presence of H_2 makes the environment inside the atomizer more reductive, minimizing the oxidation of W and Ta. For some analytes, the signal intensity and the maximum temperature of atomization are also affected because of changes in the atomization mechanism. For example, improvements in signal have been reported for V and Ba^{206} while decreasing sensitivity has been observed for Ti.²¹⁰ On the other, hand no changes have been reported for Eu when argon and argon/ H_2 were compared.²⁰⁴ In general, there is an optimum percent of H_2 in the inert gas mixture.²¹⁰ In our experiments, argon containing 1 % hydrogen was employed in order to compare the results obtained only with argon in the W and Ta lined atomizers and with results obtained in the stop flow regime in the case of the rhenium lined atomizer. In Figure 7.7, a comparison of sensitivity of the thulium fluorescence signal as well as the study of the lifetime of the atomizers can be seen. According to our results, the signal intensity obtained with

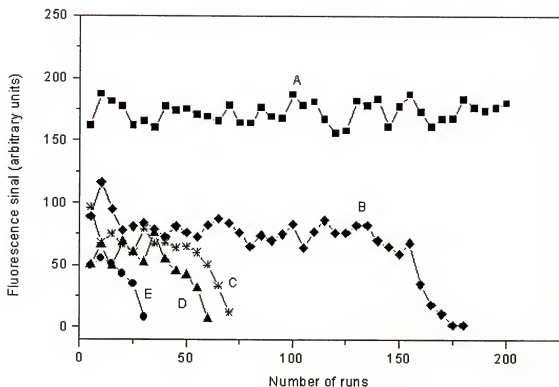


Figure 7.7. Comparative lifetimes of the metal lined atomizers. (A) Rhenium lined atomizer under stop flow regime (B) Tungsten lined atomizer under Ar:H₂ 99:1 miniflow regime (C) Tungsten lined atomizer under Ar miniflow regime (D) Tantalum lined atomizer under Ar miniflow regime and (E) Tantalum lined atomizer under Ar:H₂ 99:1 miniflow regime. 10 pg of thulium atomized at 2300°C. Only runs that are multiple of 5 are displayed in the plot.

foils were limited to a certain number of runs. In our experimental conditions, the worst results were obtained with tantalum in an atmosphere containing H_2 and in pure argon, where a substantial decrease of sensitivity were observed after around 20 and 35 runs, respectively. For tantalum, the presence of H_2 in the protective gas flow caused a more severe deformation of the metal foil. For tungsten, the presence of H_2 increased the lifetime of the atomizer from around 60 runs (only Ar) to around 150 runs. In terms of sensitivity, slightly better results were observed for W lined atomizers in the presence of H_2 than with only argon in the protective gas flow.

Comparative results between the rhenium lined and the pyrolytic graphite atomizers

In another comparison, the signal observed with the rhenium lined atomizer (in terms of peak area) was around 2 times more intense than those observed with pyrolytic graphite (see Figure 7.8). Another advantage was that for the metal lined atomizers, the maximum fluorescence signal-background ratio was obtained at $2300^{\circ}C$ (see Figure 7.9) which is at least $200^{\circ}C$ lower than the one observed for pyrolytic graphite. This decrease in atomization temperature resulted in less blackbody radiation levels reaching the detector (see noise profiles in Figure 7.10) and therefore improvements in limits of detection. Taking in consideration peak area, absolute limits of detection calculated for thulium ($3s_0/m$) for 10 μL of sample were 950 fg using pyrolytically coated graphite atomizer and 200 fg using the rhenium lined atomizer. In terms of reproducibility, rhenium lined atomizers was at least 2.5 times higher than the other metal lined atomizers. This difference could be attributed to the elimination of the flow during

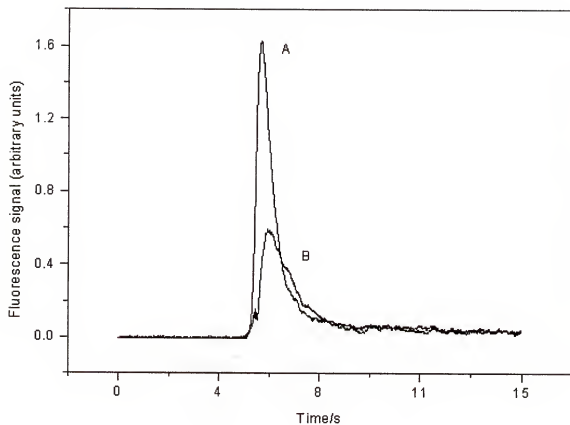


Figure 7.8. Fluorescence temporal profiles of 10 pg of thulium atomized in (A) pyrolytic graphite atomizer at 2500°C and (B) rhenium lined atomizer at 2300°C.

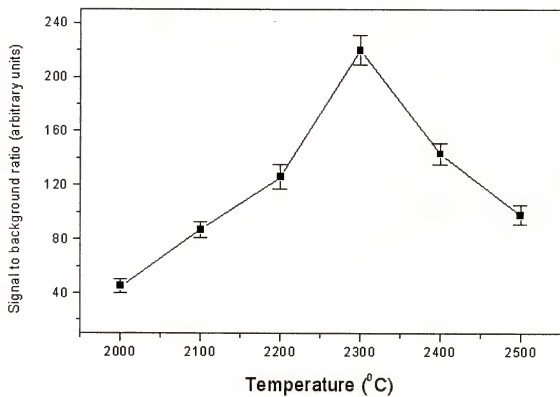


Figure 7.9. Atomization temperature curve for 10 pg of thulium in a rhenium lined atomizer.

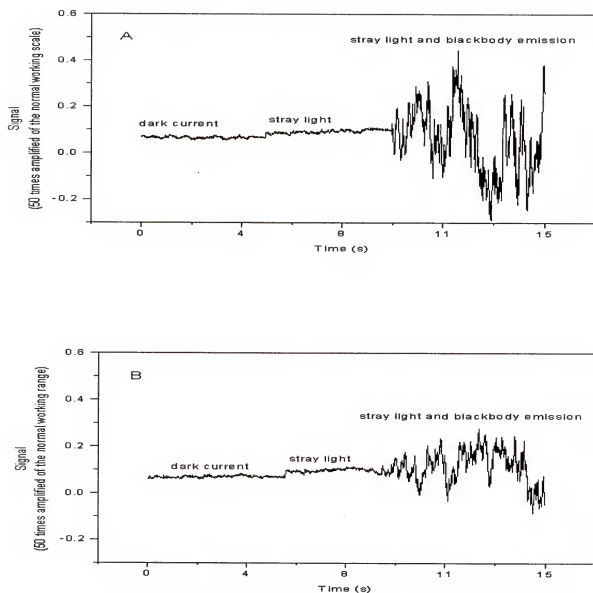


Figure 7.10. Representations of the noises associated with the measurement of T_m . (A) background emission at 2500°C and (B) background emission at 2300°C

atomization. While rhenium could be used throughout the 200 runs without substantial decrease in signal sensitivity, the lifetime of the other metal fluorescence signal of thulium obtained with rhenium lined atomizers was better than those obtained with pyrolytic carbon tubes (see Table 7.3). Rhenium lined atomizers gave better reproducibility using either peak area or peak height as the signal parameter. The fluorescence signal was linear (0.9992) over the studied range of concentrations (from 0.1 ng g^{-1} to $1 \text{ } \mu\text{g g}^{-1}$) (see Figure 7.10).

Sample Analysis

Thulium was determined by LEAFS using the rhenium lined atomizer in order to verify if the atomizer would perform properly for the analysis of real samples such as urine and coal fly ash.

Ashing temperature limits

A study was performed in order to determine the maximum temperature allowed for the ashing step without significant loss of analyte. The study was performed using the rhenium lined atomizer and 10 ng g^{-1} thulium aqueous standard solution. Results showed that temperatures up to 1000°C can be employed.

Sample preparation

Urine samples: Urine samples were spiked with a known amount of thulium and 1/1 w/w diluted with water in order to allow the use of the calibration curve method. Non-spiked urine samples diluted in the same manner were used as blanks.

Trace elements in coal fly ash (NBS 1633): This sample was digested in a microwave oven using a pressurized closed vessel prior to the analysis. The amount of 0.05 g of

Table 7.3. Comparative relative standard deviation of the fluorescence signal of thulium^{a,b} obtained with the pyrolytic graphite tube and the rhenium lined graphite tube.

Pyrolytic graphite atomizer		Rhenium lined atomizer	
Peak area	Peak height	Peak area	Peak height
11.4 %	13.5 %	6.2 %	8.8 %

^aResults based on ten repetitions.

^b10 ng g⁻¹ thulium aqueous standard solution.

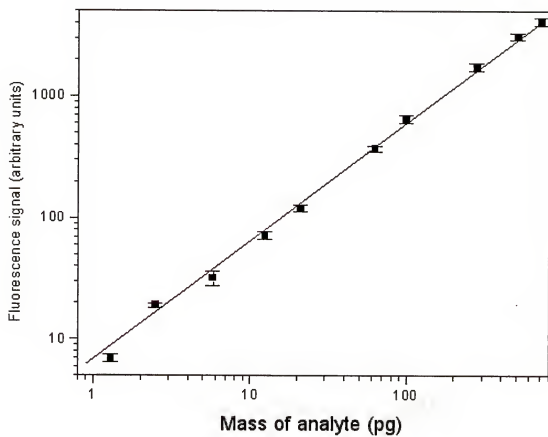


Figure 7.10. Calibration curve for thulium.

sample was placed in the Teflon cup together with 1 mL of concentrated hydrofluoric acid. The volume of acid was minimized to the minimum amount necessary to dissolve the sample in order to minimize acid corrosion of the metal foil. The sample was digested for 5 minutes at 113 W of power. After digested, the sample was diluted with water in a 100 mL volumetric flask.

Sample analysis results

Table 7.4 show the results of the determination of thulium in urine and coal fly ash samples. Only the calibration curve method was used and the result displayed is an average of three different analysis performed in three different days. The temperature program employed in these analyses was the same one described in Table 7.1 for metal lined atomizers with atomization temperature fixed at 2300°C and ashing temperatures fixed at 450°C and 1000°C for coal fly ash and urine samples respectively. Ramp and hold times of the ashing step were 20 and 25 s respectively.

Conclusion

A method for the determination of thulium by electrothermal atomization laser atomic fluorescence spectrometry was successfully developed. Problems related with the inefficient atomization of thulium in a graphite atomizer were avoided by using a metal lined tube atomizer. In this work, a rhenium foil was employed as the atomizer surface. Rhenium was shown to have superior performance over tantalum and tungsten in terms of fluorescence signal intensity and lifetime. When compared with the pyrolytic graphite tube, the rhenium lined atomizer enabled the achievement of limits of detection 4 times better. This improvement in terms of limit of detection was a result of improvement in

Table 7.4. Sample analysis results for thulium.

Sample	Expected concentration value ^a	Experimental value using calibration curve method ^b (recovery)
Urine	60 ng g ⁻¹	57.1 ± 4.8 ng g ⁻¹ (95.2 %)
Coal fly ash (NBS 1633)	2.1 µg g ⁻¹	1.95 ± 0.2 µg g ⁻¹ (93 %)

^aThe expected concentration value is the concentration of thulium expected in the laboratory prepared urine sample and the non-certified value reported in the coal fly ash reference material standard.

^bthe experimental values are average of 3 different analysis performed on three different days.

fluorescence intensity due to a more efficient atomization and a decrease of blackbody emission levels because the metal atomizer allowed atomization at lower temperatures.

The rhenium lined atomizer also enabled better reproducibility than the pyrolytic atomizer. Analysis of urine and coal fly ash samples was performed to evaluate the method with the rhenium atomizer. Very good recoveries of thulium in both samples were achieved.

CHAPTER 8

FINAL COMMENTS

Laser-excited atomic fluorescence spectrometry has been proven to be a formidable analytical tool. High sensitivity is guaranteed by using a laser source with high radiant energy while the selective nature of the fluorescence minimizes spectral interferences from molecular and atomic species other than the analyte of interest. Although the technique has been and successfully used at the laboratory stage, it is still rarely employed for industrial, medical and environmental monitoring. In addition, no commercial LEAFS instrument has been developed. This apparent lack of interest is due mainly to the relatively complex procedures involved and to its single element capability. It is clear that technological advances in laser and acquisition systems will facilitate operation and maintenance as well as will allow the determination of more than one element even if it is in a sequential manner. On the other hand, work still needs to be done in expanding the number of elements currently being determined by the technique as well as optimizing methods to analyze complex samples such as ones of biological, environmental interest.

In the work described in this dissertation, we developed methods based on ETA-LEAFS for the determination of indium, germanium, platinum, lead and thulium. A high repetition rate tunable copper vapor pumped dye laser was used. This excitation source enabled a more efficient probing of the transient atomic population generated in the tube atomizer. The acquisition design of the collection optics was chosen to eliminate post

and pre-filter effects and allow high discrimination between analyte and background signals. Electrothermal atomization technique was employed because it is an ideal technique to generate concentrated atomic vapors which is appropriate for analysis of samples with complex matrices.

Absolute limits of detection achieved were in the femtogram range in all cases due to careful choice of atomizer material (graphite, pyrolytic graphite and rhenium foil), and of atomization either from the wall or from a platform. Also important was the optimization of the furnace parameters and use of chemical modifiers to minimize loss of analyte and/or stabilize the analyte, increasing its tolerance to higher temperatures during the ashing step. Analytes were analyzed successfully in several complex samples. Simple calibration curve procedures could be employed for urine, soil, sediments and automotive catalyst samples. Minimum sample preparation was necessary. For urine, only a simple dilution was used, while fast and efficient microwave digestion procedures were developed for soil sediments and automotive catalysts samples. For the digestion procedures, a study of appropriate acids for the digestion procedure was performed. Because of interferences from the matrix, the determination of analytes in blood samples required the standard addition method. However for lead, a method using a porous graphite filter was employed to allow the use of the calibration curve method for the analysis of blood.

In terms of improvements in instrumentation, the use of a more compact and more powerful new generation of copper vapor laser together with a more versatile dye laser certainly could increase the wavelength range covered and consequently open up options to detect other elements. For some elements like germanium and platinum, which can

decay radiatively to different energy levels when excited with the excitation lines employed in this work, potential improvements in limits of detection could be obtained by the use of an intensified coupled charged detector that would detect the fluorescence at more than one wavelength.

Improvements in filter furnace fluorescence would be achieved by using inert refractory material rather than graphite opening up the possibility of using the filter technique for carbide forming elements.

It could be also very interesting to expand the use of the rhenium lined atomizer to other elements such as V, Eu, and Sc which would certainly profit from the elimination of contact with graphite.

APPENDIX
ACRONYMS USED IN TEXT

AAS	Atomic Absorption Spectrometry
ALOD	Absolute Limit of Detection
ASV	Adsorptive Stripping Voltametry
CVL	Copper Vapor Laser
DIUF	Deionized Ultrafiltered
DPP	Direct Pulse Polarography
ETA	Electrothermal Atomization
FF	Filter Furnace
FWHM	Full Width at Half Maximum
GD	Glow Discharge
GF	Graphite Furnace
HCL	Hollow Cathode Lamp
ICP	Inductively Coupled Plasma
LA	Laser Ablation
LEAFS	Laser-excited Atomic Fluorescence Spectrometry
LOD	Limit of Detection
MS	Mass Spectrometry
NAA	Neutral Activation Analysis

NBS	National Bureau of Standards
Nd:YAG	Solid state laser based on Yttrium, Aluminum and Granite doped with Nd
NPG	Non-pyrolytic Graphite
OES	Optical Emission Spectrometry
PG	Pyrolytic Graphite
PMT	Photomultiplier Tube
PTFE	Polytetrafluoretilene
S/B	Signal to Background ratio
S/N	Signal to Noise Ratio
SHG	Second Harmonic Generation
SRM	Standard Reference Material
STPF	Stabilized Temperature Platform Furnace

REFERENCES

1. D.C. Paschal, *Spectrochim. Acta* **44B**, 1229 (1989).
2. G. Tolg, *Anal. Chim. Acta* **283**, 3 (1993).
3. R.E. Sturgeon, *Spectrochim. Acta* **52B**, 1451 (1997).
4. N. Omenetto, B.W. Smith and J.D. Winefordner, *Spectrochim. Acta* **43B**, 1111 (1988).
5. G. Tolg, *Fresenius Z. Anal. Chem.* **329**, 735 (1988).
6. R. Cornelis, F. Borguet and J. De Kimpe, *Anal. Chim. Acta* **283**, 183 (1993).
7. R.E. Sturgeon, *J. At. Anal. Spectrom.* **13**, 351 (1998).
8. S. Sjöström and P. Mauchien, *Spectrochim. Acta Rev.* **15**, 153 (1993).
9. N. Omenetto, *J. Anal. At. Spectrom.* **13**, 385 (1998).
10. S Sjöström, *Spectrochim. Acta Rev.* **13**, 407 (1990).
11. N. Omenetto, *Spectrochim. Acta* **44B**, 131 (1989).
12. M.A. Bolshov, A.V. Zybin, V.G. Koloshnikov and M.V. Vasnetsov, *Spectrochim. Acta* **36B**, 345 (1981).
13. M. Broyer and J. Chevraleyre, *Appl. Phys. B.* **35**, 31 (1984).
14. J.A. Vera, M.B. Leong, N. Omenetto, B.W. Smith, B. Womack and J.D. Winefordner, *Spectrochim. Acta* **44B**, 939 (1989).
15. X. Hou, P. Stchur, K. Yang, R.G. Michel, *Trends Anal. Chem.* **17**, 532 (1998).
16. J. Enger, A. Marunkov, N. Chekalin and O. Axner, *J. At. Anal. Spectrom.* **13**, 351 (1998).

17. R. Lonardo, A.I. Yuzefovsky, K.X. Yang, R.G. Michel, E.S. Frame and J. Barren, *J. At. Anal. Spectrom.* **11**, 279 (1996).
18. K. Dittrich and H. Stark, *Anal Chim. Acta* **200**, 581 (1987).
19. J. Anwar, J.M. Anzano, G. Petrucci, and J.D. Winefordner, *Microchem. J.* **43**, 77 (1991).
20. J. Anwar, J.M. Anzano, and J.D. Winefordner, *Talanta* **38**, 1071 (1991).
21. D.J. Butcher, J.P. Dougherty, F.R. Preli, A.P. Walton, G.Wei, R.L. Irwin and G. Michel, *J. At. Anal. Spectrom.* **3**, 1059 (1988).
22. J.X. Zhou, X.Hou, K.X. Yang, and R.G. Michel, *J. At. Anal. Spectrom.* **13**, 41 (1998).
23. W. Slavin, *Spectroscopy* **6** 1621 (1991).
24. J. Ingle, Jr., and S. Crouch, Spectrochemical Analysis, Prentice-Hall, Englewood Cliffs (1988).
25. N. Omenetto and J.D. Winefordner, *Prog. Analyt. Spectrosc.* **2**, 1 (1979).
26. M.A. Bolshov, A.V. Zybin, V.G. Koloshnikov, and K.N. Koshelev, *Spectrochim. Acta* **32B**, 279 (1977).
27. Gornushkin, I.B Laser Excited Atomic Fluorescence Spectrometry as a Powerful Tool for Analytical Applications and Spectroscopy Studies, dissertation, University of Florida, Gainesville, Florida (1997).
28. V. Sychra, V. Svoboda, I. Rubeska, Atomic Fluorescence Spectroscopy, Von Nostrand Reinhold, London (1975).
29. D.J. Butcher, J.P. Dougherty, J.T. McCaffrey, F.R. Preli, A.P. Walton, G.Wei, and G. Michel, *Prog. Anal. Spectrosc.* **10**, 359 (1987).
30. J.P. Dougherty, F.R. Preli, Jr., and R.G. Michel, *Talanta* **36**, 151 (1989).
31. F.B. Fansworth, B.W. Smith, and N. Omenetto, *Spectrochim. Acta* **45B**, 1151 (1990).
32. N. Omenetto, ed. Analytical Laser Spectroscopy, John Wiley & Sons, New York (1979).
33. K. Dittrich, *Crit. Rev. Anal. Chem.* **16**, 223 (1986).

34. B.W. Smith, P.B. Fansworth, P. Cavalli and N. Omenetto, *Spectrochim. Acta* **45B**, 1369 (1990).
35. L.M. Fraser and J.D. Winefordner, *Anal. Chem.* **44**, 1444 (1972).
36. S.J. Weeks, H. Haraguchi, and J.D. Winefordner, *Anal. Chem.* **50**, 360 (1978).
37. N. Omenetto and H.G.C. Human, *Spectrochim. Acta* **39B**, 1333 (1984).
38. A. Montaser and D.W. Golightly, ed. Inductively Coupled Plasma in Analytical Atomic Spectrometry, VCH Publishers, New York (1992).
39. C.L. Davis, B.W. Smith, M.A. Bolshov, and J.D. Winefordner, *Appl. Spectrosc.* **49**, 907 (1995).
40. B.V. L'vov, Atomic Absorption Spectrochemical Analysis, Hilger, London (1970).
41. I.B. Gornushkin, J.E. Kim, B.W. Smith, S.A. Baker, and J.D. Winefordner, *Appl. Spectrosc.* **51**, 1055 (1997).
42. R.E. Neuhauser, U. Panne, R. Niessnes, G.A. Petrucci, P. Cavalli, and N. Omenetto, *Anal. Chim. Acta* **346**, 37 (1997).
43. W. Slavin, Graphite Furnace AAS a Source Book, Perkin-Elmer Corp., Norwalk (1988).
44. P. Bermejo-Barrera, A. Moreda-Pinero, J. Moreda-Pinero, and A. Bermejo-Barrera, *J. At. Anal. Spectrom.* **10**, 1011 (1995).
45. W. Huettner and C. Bushe, *Fresenius Z. Anal. Chem.* **323**, 674 (1986).
46. W. Slavin, D.C. Manning, and G.R. Carnick, *Anal. Chem.* **53**, 1504 (1981).
47. S.A. Clyburn, T. Kantor, and C. Veillon, *Anal. Chem.* **46**, 2213 (1974).
48. C. Chung, E. Iwamoto and Y. Yamamoto, *Talanta* **34**, 927 (1987).
49. J.P. Matousek, *Prog. Anal. Spectrosc.* **4**, 247 (1981).
50. S.I. Imai, N. Hasegawa, Y. Hayashi, K. Saito, *J. At. Anal. Spectrom.* **11**, 515 (1996).
51. D.L. Tsalev, V.I. Slaveykova, and P.B. Mandjukov, *Spectrochim. Acta Rev.* **13**, 7 (1990).

52. D. Pozebon, V.L. Dressler, and A.J. Curtius, *J. At. Anal. Spectrom.* **13**, 7 (1998).
53. S.I. Imai, M. Harada, Y. Nishiyama, and Y. Hayashi, *Anal. Sci.* **14**, 769 (1998).
54. N. Chekalin and P.B. Mandjukov, *Spectrochim. Acta* **49B**, 1411 (1994).
55. W.C. Campbel and J.M. Ottaway, *Talanta* **21**, 837 (1974).
56. S.J. Cathum, C.L. Chakrabarti, and J.C. Hutton, *Spectrochim. Acta* **46B**, 35 (1991).
57. X. Shan, and D. Wang, *Anal. Chim. Acta* **173**, 315, (1985).
58. S.I. Imai, Y. Nishiyama, T. Tanaka, and Y. Hayashi, *J. At. Anal. Spectrom.* **10**, 439 (1995).
59. D.L. Styris, *Fresenius Z. Anal. Chem.* **323**, 710 (1986).
60. R.E. Sturgeon, C.L. Chakrabarti, and C.H. Langford, *Anal. Chem.* **48**, 1792 (1978).
61. B.V. L'vov, *Spectrochim. Acta* **52B**, 1 (1997).
62. A. Kh. Gilmutdinov, Y. A. Zakharov, V.P. Ivanov, and A.V. Voloshin, *J. At. Anal. Spectrom.* **6**, 505 (1991).
63. W. Slavin, G.R. Carnick, D.C. Manning, and E. Pruskovska, *At. Spectrosc.* **4**, 69 (1993).
64. G.R. Carnick and W. Slavin, *American Lab.* **10** (1988).
65. W. Slavin and D.C. Manning, *Spectrochim. Acta* **35B**, 701 (1980).
66. A.B. Volynsky, *Spectrochim. Acta* **53B**, 139 (1998).
67. B.V. L'Vov, L.A. Pelieva, and A.M.Kh. Sharnopolski, *Prikl. Spectrosk.* **27**, 395 (1977).
68. W. Wendl and G.J. Muller-Vogt, *J. At. Anal. Spectrom.* **3**, 631 (1988).
69. P.B. Madjukov, E.T. Vassilena, and V.D. Simeonov, *Anal. Chem.* **64**, 2596 (1992).
70. Oxford Lasers, Copper Vapor Laser Model CU 15A Operating Manual, Oxford, UK, 1990.
71. R.E. Grove, *Laser Focus World* **18**, 45 (1982).

72. S.R. Hargrove, and T. Kan, *IEEE J. Quantum Electron.* vol **QE-16**, 1108 (1980).
73. Perkim-Elmer, Graphite Furnace model HGA 400 Operating Manual, Norwalk (1984).
74. A. Abu Samra, J.S Morris, and S.R. Koirtyohann, *Anal. Chem.* **47**, 1475 (1975).
75. L.A. Fernando, W.D. Heavner, and C.C Gabrielli, *Anal. Chem.* **58**, 511 (1986).
76. L.B. Fisher, *Anal. Chem.* **58**, 261 (1986).
77. H. Kingston, and L. Jassie, Introduction to Microwave Sample Preparation: Theory and Practice, ACS, Washington, DC (1988).
78. E.D. Neas and M.J. Collins, Introduction to Microwave Sample Preparation, ACS, Washington DC (1988).
79. G. Knapp, *Analytical Proceedings* **27**, 112 (1990).
80. Parr Instrument Company, Operating Instructions for Parr Microwave Acid Digestion Bombs, #243M, Moline, Illinois, (1989).
81. J.R. Davis, Jr., A. Rohatgi, R.H. Hopkins, P.D. Blais, P. Rai-Choudhury, J.R. McCormick, and H.C. Mollenkopf, *IEEE Trans. Electron Devices* **ED-27**, 677 (1980).
82. X.Dong-qun, G.Gang-ping, and S.Han-wen, *J. Anal. At. Spectrom.* **10**, 753 (1995).
83. G.Tao and Z.Fang, *J. Anal. At. Spectrom.* **8**, 577 (1993).
84. T.D. Luckey and B. Venugopal, Metal Toxicity in Mamals, 1st ed., Plenum Press, New York, (1977).
85. A.E. Calverley, D. Rees, R.J. Dowdeswell, P.J. Linnet, and Kielkowski, D., *Occup. and Environ. Med.* **52**, 661 (1995).
86. Farago, M.E., Kavanagh, P., Blanks R., Kelly, J., Kazantizis, G., Thornton, I., Simpson P.R., Cook, J.M., Parry, S., and Hall, G.M., *Fresenius J. Anal. Chem.* **354**, 660 (1996).
87. B. Jan, M.D. Vermorken, W.J.F. van der Vijgh, I. Klein, H.E. Gall, C.J. van Groeningen, G.A.M. Hart, and H.M. Pinedo, *Clin. Pharmacol. Ther.* **39**, 136 (1986).

88. D.T.Burns and D.Dagdar, *Analyst* **105**, 75 (1980).
89. E.M.Donaldson, *Talanta* **31**, 997 (1984).
90. J.Aznaréz, P.Moneo, J.C.Vidad, and F.Palacios, *Analyst* **110**, 747 (1985).
91. C.Schleich and G.Henze, *Fresenius J. Anal. Chem.* **338**, 140 (1990).
92. E.L. Kothny, *Mikrochim. Acta* **1**, 425 (1978).
93. K. Sharma, A.K. Chakkar and L.R. Kakkar, *Annali di Chimica* **85**, 577 (1995).
94. Z. Zhao and H. Freisner, *Anal. Chem.* **58**, 1498 (1986).
95. C.M.G. Van Den Berg and G.S. Jacinto, *Anal.Chim. Acta* **211**, 129 (1988).
96. K. Hoppstock, F. Alt,, K. Cammann, and Weber, G., *Fresenius J. Anal. Chem.* **335**, 813 (1989).
97. J. Messerschmidt, F. Alt, G. Tölg, J. Angerer, and Schaller, K.H., *Fresenius J. Anal.Chem.* **343**, 391 (1992).
98. P. Shearan, M. Smyth, *Analyst* **113**, 609 (1988).
99. C.Schleich and G.Henze, *Fresenius J. Anal. Chem.* **338**, 145 (1990).
100. R. Zeisler and R.R. Greenberg, Trace Element Analytical Chemistry in Medicine and Biology, vol. 5 Walter de Gruyter, Berlin (1988).
101. A.A. Smales, J. van R. Smith and H. Irving, *Analyst* **82**, 539 (1957).
102. P.Baedecker and J.T. Wasson, *Science* **1967**, 503 (1970).
103. D.J.Jonhson, T.S.West, and R.M.Dagnall, *Anal Chim. Acta* **67**, 79 (1973).
104. L. Zhou, T.T. Chao, and A.L. Meier, *Anal. Chim. Acta* **161**, 369 (1984).
105. W.B.Robbins, J.A.Caruso, and F.L.Fricke, *Analyst* **104**, 35 (1974).
106. M.Thompson and B.Pahlavanpour, *Anal. Chim. Acta* **109**, 251 (1979).
107. M.H. Kahn, K.A. Wolnitz, F.L.Fricke, and J.A.Caruso, *Anal. Chem.* **54**,1048 (1984).
108. E.Henden, *Analyst* **107**, 872 (1982).

109. F.L.Fricke, W.D.Robbins, and J.A.Caruso, *J.Assoc. Off. Anal. Chem.* **61**, 1118 (1978).
110. K.J.Mulligan, M.H.Hahn, and J.A.Caruso, *Anal. Chem.* **51**,1935 (1979).
111. C. Dominici, A. Alimonti, S. Caroli, F. Petrucci, and M.A. Castello, *Clin. Chim. Acta* **158**, 207 (1986).
112. V. Di Noto, D. Ni, L.D. Via, F. Scomanzzon, and M. Vidali, *Analyst* **120**, 1669 (1995).
113. M.L Lee, G. Tölg, E. Beinrohr, and P. Tschöpel, *Anal. Chim. Acta* **272**, 193, (1993).
114. S. McLoughlin, D. Bowdler, and N.B. Roberts, *J. Anal. At. Spectrom.* **3**, 273 (1988).
115. J.F. Belliveau, G.M. Matook, G.P. O'Leary, F.J. Cummings, M. Hillstrom, and J. Calabresi, *Anal. Lett.* **19(1&2)**, 135 (1986).
116. W.A.J. de Waal, F.J.M.J. Maessen, and J.C. Kraak, *J. Chromatogr.* **407**, 253, (1987).
117. K.Dittrich, R.Mandry, W.Mothes, and J.G.Judelevic, *Analyst* 1985, **110**, 169.
118. X. Dong-qun, G.Gang-ping, S.Han-wen, *J. Anal. At. Spectrom.***10**, 753 (1995).
119. Y.Mino, S.Shimomura, and N.Ota, *Anal. Chim. Acta* **107**, 253 (1979).
120. A.Kolb, G.Müller-Vogt, W.Wendl, and W.Stöbel, *Spectrochim. Acta* **42B**, 951 (1987).
121. Y.Sohrin, K.Isshiki, T.Kuawamoto, and E.Nakayama, *Talanta***34**, 341 (1987).
122. Y. Hayashibe, M.Kurosaki, F. Takekawa, and R. Kuroda, *Microchim. Acta [Wien]* **II**, 163 (1989).
123. K. Brajter and E. Olbrych-Sleszynska, *Analyst* **111**, 1023, (1986).
124. I. Martinsen and J. Langmyhr, *Anal. Chim. Acta* **135**, 137 (1982).
125. W.H. Evans, P.J. Brooke, and B.E. Lucas, *Anal. Chim. Acta* **148**, 203 (1983).
126. E.M. Donaldson and M. Wang *Talanta* **33**, 233 (1986).

127. J. Coello, J. Gené and H. Iturriaga, *Microchim. Acta* [Wien] **I**, 221 (1986).
128. A.E. Hubert and T.T Chao, *Talanta* **32**, 568 (1985).
129. J. Coello, L-G. Danielson, and S. Hernandez-Cassou, *Anal. Chim. Acta* **201**, 325 (1987).
130. A.F. Leroy, M.L. Wheling, H.L. Sponseller, W.S.R.E. Friauf, R.L. Salomon, and L. Dedrick, *Biochem. Med.* **18**, 184 (1977).
131. D. Priestner, L.A. Sternson, and A.J. Repta, *Anal. Lett.* **14(B15)**, 1255 (1981).
132. M.E. Farago and P.J. Parsons, *Analyst* **107**, 1218 (1982).
133. K. Matsumoto, T. Solin, and K.J. Fuwa, *Spectrochim. Acta* **39B**, 481 (1984).
134. Z.Li, N.Zhe-Ming, and S.Xiao-quan, *Spectrochim. Acta* **44B**, 751 (1989).
135. P.S.Doidge, B.T.Sturman, T.M.Rettberg, *J. Anal. At. Spectrom.* **4**, 251 (1989).
136. G.Tao, and Z.Fang, *J. Anal. At. Spectrom.* **8**, 577 (1993).
137. H.O.Haug and J.Chonghua, *J. Anal. At. Spectrom.* **5**, 215 (1990).
138. N.Zhe-Ming and H.Bin, *J. Anal. At. Spectrom.* **10**, 747 (1995).
139. H.O.Haug, L.Yping, *J. Anal. At. Spectrom.* **10**, 1069 (1995).
140. I.S. Busheina and J.B. Headridge, *Talanta* **29**, 519 (1982).
141. J.R. Castillo, J.M. Mir, and M.T. Gomez, *Microchem. J.* **38**, 387 (1988).
142. L. Liao and A. Li, *J. Anal. At. Spectrom.* **8**, 633 (1993).
143. D. Yan, Z. Yan, G-S. Cheng and A-M Li, *Talanta* **31** 133 (1984).
144. B.Welz, and M.Melcher, *Analyst* **109**, 569 (1984).
145. K.Jin, Y.Shibata and M.Morita, *Anal Chem.* **63**, 986 (1991).
146. P. Schramel, I. Wendler, and S. Lustig, *Fresenius J. Anal. Chem.* **353**, 115 (1995).
147. P. Tothill, L.M. Matheson, and J.F. Smyth, *J. Anal. At. Spectrom.* **5**, 619 (1990).
148. B.J. Perry, and R.E. Balazs, *Anal. Proc.* **31**, 269 (1994).

149. M. Parent, H. Vanhoe, L. Moens, and R. Dams, *Fresenius J. Anal. Chem.* **354**, 664 (1996).
150. D. Pollman, F. Leis, G. Tolg, T Tschopel, J.A.C. Brokaerts, *Spectrochim. Acta* **49B**, 1251 (1994).
151. Y. Kim, H. Kawaguchi, T. Tanaka, and A. Mizuike, *Spectrochim. Acta* **45B**, 333 (1990).
152. D. Goforth and J.D. Winefordner, *Anal. Chem.* **58**, 2598 (1986).
153. E. Masera, P. Mauchien, and Y. Lerat, *Spectrochim. Acta* **51B**, 543 (1996).
154. K. Ditrich and H-J Stark, *J. Anal. At. Spectrom.* **2**, 63 (1987).
155. N.V. Chekalin, I.I. Vlasov, *J. Anal. At. Spectrom.* **7**, 225 (1992).
156. N.V. Chekalin, V.I. Pavlutsкая, and I.I. Vlasov, *Spectrochim. Acta* **46B**, 170 (1991).
157. J.P. Dougherty, F.R. Preli Jr., and R.G. Michel, *J. Anal. At. Spectrom.* **2**, 429 (1987).
158. J.A. Vera, M.B. Leong, C.L. Stevenson, G.A. Petrucci and J.D. Winefordner, *Talanta* **36**, 1291 (1989).
159. B.W. Smith, G.A. Petrucci, R.G. Baldini and J.D. Winefordner, *Anal. Chem.* **65**, 118 (1993).
160. A. Kh. Gilmutdinov, Y. A. Zakharov, V.P. Ivanov, and A.V. Voloshin, *J. At. Anal. Spectrom.* **7**, 675 (1992).
161. D. McAllister, *J. Anal. At. Spectrom.* **5**, 171 (1990).
162. S. Xiao-Quan, N. Zhe-Ming, and Y. Zhi-Neng, *Anal. Chim. Acta* **171**, 269 (1985).
163. K. Oiushi, K. Yasuda, Y. Morshige, and K. Hirokawa, *Fresenius J. Anal. Chem.* **348**, 195 (1994).
164. P.B. Mandjukov and D.L. Tsalev, *Microchem. J.* **42**, 339 (1990).
165. B. Welz, G. Schlemmer, H.M. Ortner, and W. Wegscheider, *Prog. Analyt. Spectrosc.* **12**, 111 (1989).
166. L. Pszonicki and W. Skwara, *Talanta* **36**, 1265 (1989).

167. A.R. Flegal and D.R Smith, *Environ. Res.* **58**, 125 (1992).
168. R. Renner, *Enviro. Science and Tech.* **29B**, 256A (1995).
169. Preventing Lead Poisoning in Young Children-A Statement by the Center of Disease Control; USDHHS/PHS, CDC, Atlanta, GA, USA, October (1991).
170. B.J. Feldman, A. D'Alessandro, J. Osterloh, and H.B. Hata, *Clin. Chem.* **41**, 557 (1995).
171. D. Jagner and Y.D. Wang, *Eletroanalysis* **7**, 614 (1995).
172. P.J. Parsons and W. Slavin, *Spectrochim. Acta.* **48B**, 925 (1995).
173. R.J. Bowins, R.H. McNutt, *J. Anal. At. Spectrom.* **9**, 1233 (1994).
174. F.R. Preli Jr., J.P. Dougherty, and R.G. Michel, *Anal. Chem.* **59**, 1784 (1987).
175. K.Ditrich and H. Stark, *J. Anal. At. Spectrom.* **1**, 237 (1986)
176. J.P. Deavor, E. Becerra, B.W. Smith, and J.D.Winefordner, *Appl. Spectrosc.* **38**, 7 (1993).
177. E.P. Wagner, B.W. Smith and J.D. Winefordner, *Anal. Chem.* **68**, 3199 (1996).
178. D. Priestner., L.A Sternson, and A.J. Repta, *Anal. Lett.* **14(B15)**, 1255 (1981).
179. D.A. Katskov, R.I. McCrindle, R. Schwarzer, and P.J.J.G. Marais, *Spectrochim. Acta* **50B**, 1543 (1995).
180. D.A. Katskov, P.J.J.G. Marais, and P. Tittarelli, *Spectrochim. Acta* **51 B**, 1169 (1996).
181. D.A. Katskov, R. Schwarzer, P.J.J.G. Marais, and R.I. McCrindle, *Spectrochim. Acta* **50B**, 763 (1995).
182. S. Zhang, S. Murachi, T. Imasaka, and M. Watanable, *Anal. Chim. Acta* **314**, 193 (1995).
183. J.L.M. de Boer, W. Verweij, T. van der Velde-Koerts, and W. Mennes, *Wat. Res.* **30**, 190 (1996).
184. A.V. Gorbunov, M.V. Frontasyeva, S.F. Gundorina, T.L. Onischenko, B.B Maksjusta, and C.S. Pal, *Sci. Tot. Environ.* **122**, 337 (1992).
185. T.J. Haley, N. Komesu, A.M. Flesher, and L. Mavis, *Toxicol. Appl. Pharmacol.* **5**,

427 (1963).

186. N. Daskalova, S. Velichkov, and P. Slavova, *Spectrochim Acta*. **51B**, 733 (1996).
187. S.S Biswas, R. Kaimal, A. Sethumadhavan, and P.S. Murty, *Anal. Lett.* **24**, 1885 (1991).
188. J. Kubova, V. Nevorai, and V. Stresko, *J. At. Anal. Spectrom.* **9**, (1994).
189. K. Shinotsuka and M. Ebihara, *Anal. Chim. Acta* **338**, 237 (1997).
190. R. Tsukara and M. Kubota, *Spectrochim Acta*. **45B**, 581 (1990).
191. G.E.M. Hall, J.E. Vaive, and J. Pelchat, *J. At. Anal. Spectrom.* **11**, 779 (1996).
192. S. Augagneur, B. Medina, J. Szupnar and R. Lobinski, *J. At. Anal. Spectrom.* **11**, 713 (1996).
193. J.G. Gupta, *Talanta* **32**, 1 (1985).
194. G. Yungeng and D. Bo, *Spectrochim Acta*. **51B**, 1147 (1996).
195. JG. Gupta, *J. At. Anal. Spectrom.* **8**, 93 (1993).
196. A. Mazzucotteli, M. Galli, and R. Frache, *Analyst* **107**, 104 (1982).
197. B.V. L'vov and L.A. Pelieva, *Can J. Spectrosc.* **23**, 1 (1978).
198. M. Suzuki, K. Otha, T. Yamakita, and T. Katsuno, *Spectrochim Acta*. **36B**, 679 (1981).
199. E. Krakovska, *J. At. Anal. Spectrom.* **5**, 205 (1990).
200. V. Sycha, D. Kolihoiva, O. Vyskocilova, and R. Hlavac, *Anal. Chim. Acta* **105**, 263 (1979).
201. C.D. Wall, *Talanta* **24**, 755 (1977).
202. V. Sychra, J. Dolenzal, R. Hlavac, L. Petros, O. Vykocilova, and D. Kolihoiva, *J. At. Anal. Spectrom.* **6**, 521 (1991).
203. H. Berndt and G. Schaldach, *J. At. Anal. Spectrom.* **3**, 709 (1988).
204. Y. Jiuyu and H. Benli, *Can. J. Spectrosc.* **31**, 77 (1986).
205. M. Yizai and S. Di-jun, *Spectrochim Acta* **47B**, 459 (1992).

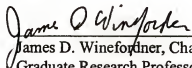
- 206. O. Vyskocilova, V. Sychra, D. Kolihsova, and P. Puchel, *Anal. Chim. Acta* **105**, 271 (1977).
- 207. J. Agget and A.J. Sprott, *Anal. Chim. Acta* **72**, 49 (1974).
- 208. E. Krakovska, *Spectrochim. Acta* **52B**, 1327 (1997).
- 209. M. Suzuki and K. Ohta, *Prog. Anal. At. Spectrosc.* **6**, 49 (1993).
- 210. P. Ljung, N. Nystrom, O. Axner, and W. Frech, *Spectrochim. Acta* **52B**, 703 (1997).

BIOGRAPHICAL SKETCH

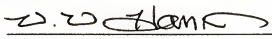
Ricardo Q. Aucélio was born in Brasília, Brazil, on August 28, 1969. He received his Bachelor degree in chemistry in December 1992 from Universidade de Brasília. During the undergraduate course he was granted by Conselho Nacional de Desenvolvimento Científico e Tecnológico (CNPq, Brasil) a fellowship that allowed him to work two years for Dr. David Gevergeese on inorganic research. In March 1995 he received a master's degree from the same university after two years of work under the supervision of Dr. Andrés Campígilia with another fellowship from CNPq. His master's research was on the development of analytical methods based on solid surface room temperature phosphorescence. Shortly after, he worked as a substitute professor at the Universidade de Brasília for six months, just before he was accepted as a Ph.D. candidate in the University of Florida, with a scholarship from Fundação Coordenação de Aperfeiçoamento de Pessoal de Nível Superior (CAPES, Brasil), to work under the direction of Dr. James D. Winefordner.

He is a member of the Sociedade Brasileira de Química (SBQ), International Union and Applied Chemistry (IUPAC), and Society for Applied Spectroscopy (SAS).

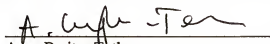
I certify that I have read this study and that in my opinion it conforms to acceptable standards of scholarly presentation and is fully adequate, in scope and quality, as a dissertation for the degree of Doctor of Philosophy.


James D. Winefordner, Chair
Graduate Research Professor of
Chemistry


I certify that I have read this study and that in my opinion it conforms to acceptable standards of scholarly presentation and is fully adequate, in scope and quality, as a dissertation for the degree of Doctor of Philosophy.


Willard W. Harrison
Professor of Chemistry


I certify that I have read this study and that in my opinion it conforms to acceptable standards of scholarly presentation and is fully adequate, in scope and quality, as a dissertation for the degree of Doctor of Philosophy.


Anna Brajter-Toth
Associate Professor of
Chemistry

I certify that I have read this study and that in my opinion it conforms to acceptable standards of scholarly presentation and is fully adequate, in scope and quality, as a dissertation for the degree of Doctor of Philosophy.


Martin T. Vala, Jr.
Professor of Chemistry

I certify that I have read this study and that in my opinion it conforms to acceptable standards of scholarly presentation and is fully adequate, in scope and quality, as a dissertation for the degree of Doctor of Philosophy.



Stephen G. Schulman
Professor of Medicinal Chemistry

This dissertation was submitted to the Graduate Faculty of the Department of Chemistry in the College of Liberal Arts and Sciences and to the Graduate School and was accepted as partial fulfillment of the requirements for the degree of Doctor of Philosophy.

August 1999

Dean, Graduate School